

### 3.8.4 CO<sub>2</sub>, NO<sub>2</sub>, SO<sub>2</sub>, OCS, N<sub>2</sub>O and O<sub>3</sub> on metal surfaces

#### List of abbreviations

AES	Auger electron spectroscopy
ARUPS	angle-resolved ultraviolet photoelectron spectroscopy
BE	binding energy
<i>E</i>	electric field vector
<i>E<sub>d</sub></i>	activation energy for desorption
<i>E<sub>diss</sub></i>	activation energy for dissociation
ELS	energy loss spectroscopy
ESD	electron simulated desorption
FTIR	Fourier transform infrared
HAS	helium atom scattering
HREELS	high-resolution electron-energy loss spectroscopy (EELS)
HR-PES	high-resolution photoelectron spectroscopy (PES)
IRAS	infrared reflection-absorption spectroscopy (RAIRS)
L	Langmuir
LEED	low-energy electron diffraction
MBRS	molecular beam relaxation spectroscopy
ML	monolayer
NEXAFS	near-edge X-ray absorption fine structure (XANES)
<i>S<sub>diss</sub></i>	dissociative sticking coefficient
SEXAFS	surface extended X-ray absorption fine structure
STM	scanning tunneling microscopy
TPD	temperature-programmed desorption spectroscopy (TDS)
TPRS	temperature-programmed reaction spectroscopy
UPS	ultraviolet photoelectron spectroscopy
XAES	X-ray excited Auger electron spectroscopy
XAFS	X-ray absorption fine structure (EXAFS, NEXAFS, SEXAFS)
XPS	X-ray photoelectron spectroscopy

#### 3.8.4.1 Introduction

This chapter discusses adsorption and reaction of six triatomic molecules on metal surfaces: carbon dioxide (CO<sub>2</sub>), nitrogen dioxide (NO<sub>2</sub>), sulfur dioxide (SO<sub>2</sub>), carbonyl sulfide (OCS), nitrous oxide (N<sub>2</sub>O) and ozone (O<sub>3</sub>). All of these molecules have a wide range of interactions with metals and undergo a number of chemical transformations. CO<sub>2</sub>, NO<sub>2</sub> and SO<sub>2</sub> adsorption has been characterized extensively. Only a handful of studies of OCS adsorption are available. Ozone is the most reactive molecule of this collection and its facile dissociative adsorption has been utilized to oxidize several metal and alloy surfaces under mild conditions. However, no information is available about O<sub>3</sub> molecular adsorption.

We have included data on adsorption of these molecules on chemically modified metal surfaces, i.e., surfaces containing preadsorbed or coadsorbed species. Specifically, alkali metal adatoms were considered and reactions of CO<sub>2</sub> and SO<sub>2</sub> with coadsorbed oxygen to form surface carbonate and sulfite or sulfate species, respectively, are discussed. Alkali metal adatoms often serve as promoters, enhancing the reactivity of these molecules at the modified metal surface.

In addition, when available, we have included results from adsorption studies on alloy surfaces. Such chemistry gives insight into reactions on bimetallic heterogeneous catalysts that are ubiquitous in the chemical and petroleum industries. Alloying metal in a catalyst with a second metal can strongly change the activity and selectivity of the catalyst. Even when alloy formation does not occur, the catalytic activity and selectivity are often changed by deposition of one metal on another. For example, adding Cu on Ru supported on silica to form bimetallic clusters gave a catalyst with a dramatically lower capacity for hydrogen chemisorption and improved selectivity for dehydrogenation [76Sin]. In several cases, we have included some information about adsorption of these triatomic molecules on non-metal surfaces for comparison or in order to anticipate what may be found in later studies on metals.

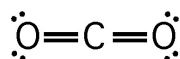
We begin the discussion in each section by a few comments on structure and bonding in the gas-phase molecule [66Her], followed by brief remarks on the coordination chemistry of these molecules as ligands in metal complexes. The literature describing coordination complexes or organometallic cluster compounds provides excellent references for understanding adsorption and reactions on metal surfaces and we refer the interested reader specifically to this material (e.g., see [87Alb, 87Col]).

In summary, carbon dioxide (O=C=O), carbonyl sulfide (O=C=S) and sulfur dioxide can be considered to belong to a class of ligands called cumulenes. CO<sub>2</sub> and OCS are linear triatomic molecules in which an sp-hybridized central atom is bonded to both outer atoms via double bonds. Along with other molecules like allene (CH<sub>2</sub>=C=CH<sub>2</sub>), carbon disulfide (S=C=S) and ketene (CH<sub>2</sub>=C=O) that are not discussed herein, these have coordination bonding in metal complexes and at metal surfaces that is analogous to that of the well-known Dewar-Chat-Duncanson model of ethylene coordination. In this model, electron density from a filled molecular  $\pi$  bond is delocalized into empty orbitals on the metal and electron density from an occupied d orbital on the metal is “back donated” into an empty molecular  $\pi^*$  orbital on the molecule. The extent of this back bonding affects rehybridization of atoms in the molecule and distortion of the molecule from linearity. These molecules can also more weakly bond to metal atoms at the surface through an oxygen or sulfur lone pair and maintain linearity. Nitrous oxide (N $\equiv$ N<sup>+</sup>-O<sup>-</sup>) is also a linear triatomic molecule, but its coordination and surface chemistry is quite different, behaving as a pseudohalogen. NO<sub>2</sub>, SO<sub>2</sub> and O<sub>3</sub> are bent triatomic molecules in the gas phase and are highly reactive molecules that often easily dissociate on metal surfaces to form an oxygen adatom along with a nascent coadsorbed molecular product. No study has yet reported on the molecular chemisorption of O<sub>3</sub> on a metal surface, due to its facile dissociation, but there is a rich literature on NO<sub>2</sub> chemisorption on metals. NO<sub>2</sub> is a radical in the gas phase, and as expected, it exhibits a diversity of bonding modes analogous to the linkage isomerism observed in the coordination of the nitrite anion (NO<sub>2</sub><sup>-</sup>). NO<sub>2</sub> can bond to metal surfaces through either one (monodentate) or both (bidentate in a chelating structure) of the oxygen atoms or through the central N atom, and in bidentate bridging structures involving bonding to N and O atoms.

### 3.8.4.2 CO<sub>2</sub>

#### 3.8.4.2.1 Structure and bonding of CO<sub>2</sub>

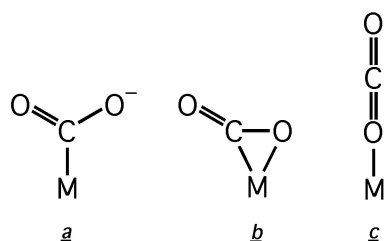
CO<sub>2</sub> in its ground state is a closed-shell, nonpolar, linear molecule, as shown in Scheme I.



Scheme I. Lewis structure for CO<sub>2</sub>.

Undistorted, linear CO<sub>2</sub> molecules can exhibit two bonding modes: (i) dative bond formation via donation of a lone pair on one oxygen atom to an empty orbital on the metal with the molecule in an upright orientation with its axis nearly perpendicular to the surface (as in Scheme II c); or (ii) via  $\pi$  bonds of the CO<sub>2</sub> molecule analogous to ethylene and bonding with the molecular axis oriented parallel to the surface. Both of these are expected to be weak, physisorption interactions. However, charge transfer of an electron from the substrate to CO<sub>2</sub> forms a CO<sub>2</sub><sup>-</sup> anion, which is “bent” and isoelectronic with NO<sub>2</sub>. This additional electronic charge is accommodated by breaking one of the C=O double bonds and forming an

additional oxygen lone-pair orbital. This bond breaking process “opens” the carbon atom and occupies a previously unoccupied  $2\pi_u$  orbital of linear CO<sub>2</sub>, making the molecule a 17-electron system, which tends to avoid a linear geometry [77Are, 83Cal]. Such highly distorted, “bent” CO<sub>2</sub> molecules have several bonding modes possible, and Scheme II illustrates two types: (i) an  $\eta^1$  C-bonded complex (II a); and (ii) an  $\eta^2$  C,O-bonded complex (II b) (the superscript- $\eta$  notation indicates the number of atoms in the molecule that are bonded to the metal). Both linearly adsorbed and bent-CO<sub>2</sub><sup>-</sup> chemisorbed states have been assigned on metal surfaces upon adsorption. Several other molecular orientations and bonding modes, in addition to those given in Scheme II, are feasible.



Scheme II. Types of coordination for CO<sub>2</sub>.

### 3.8.4.2.2 CO<sub>2</sub> adsorption on metal surfaces

CO<sub>2</sub> adsorption on metal surfaces has been extensively studied, and several reviews are available [86Fre, 91Sol1, 96Fre]. The thermodynamics for CO<sub>2</sub> adsorption are given in Table 1. On most metal surfaces, CO<sub>2</sub> adsorbs only weakly. CO<sub>2</sub> does not appear to chemisorb on Pt, Pd, Cu and Ag, although physisorption occurs [91Sol1, 96Fre, 74Nor, 75Nor, 84Seg, 86Ber, 86Sol, 89Rod, 87Sak, 83Bac, 82Stu]. It has been asserted that the metal work function and surface structure, including defects, controls whether or not physisorbed CO<sub>2</sub> can be readily converted to a chemisorbed species. On Fe, Ni, Rh and Re single crystal surfaces, CO<sub>2</sub> dissociates into coadsorbed CO and oxygen adatoms [87Lin, 87Bar1, 88III, 87Pir, 86Beh, 87Fre, 87Beh, 87Bau, 91Wam, 89Pau, 93Nas, 95Hes, 85Sol, 87Pel, 88Ass, 91Rod, 85Beh, 94Mey1, 94Mey2, 98Sey]. Table 2 provides dissociation parameters for adsorbed CO<sub>2</sub>. Vibrational spectroscopy has played a key role in characterizing such surface reactions and adsorption configurations and vibrational data for adsorbed CO<sub>2</sub> is collected in Table 3.

CO<sub>2</sub> interacts on metal surfaces in two states: as a physisorbed, linear CO<sub>2</sub> molecule and as a chemisorbed, non-linear CO<sub>2</sub> molecule, which is bent as in a CO<sub>2</sub><sup>-</sup> species. The chemisorbed bent species is often considered an intrinsic precursor for CO<sub>2</sub> dissociation into CO and O adatoms. Fig. 1 illustrates how a CO<sub>2</sub> molecule might physisorb in a linear configuration as it approaches the surface and, under certain conditions, transform into a bent CO<sub>2</sub><sup>-</sup> species. This molecule resides in a new adsorption well from where it might scatter back into the gas phase or dissociate into two chemisorbed species, coadsorbed CO and O [87Bar1].

Many studies have addressed the adsorption of CO<sub>2</sub> on Fe surfaces and concluded that the adsorption mechanism is face-sensitive [87Pir, 86Beh, 87Fre, 87Beh, 87Bau]. The open Fe(111) surface was much more reactive for CO<sub>2</sub> dissociation than the Fe(110) surface, which was inactive towards CO<sub>2</sub> chemisorption [87Pir, 86Beh, 87Fre, 87Beh, 87Bau]. Introduction of steps and defects into the Fe(110) surface lead to CO<sub>2</sub> chemisorption. Steps on the surface lower the work function and this favors electron transfer from the metal to the adsorbate. This distorts the molecule toward CO<sub>2</sub><sup>-</sup> and chemisorption of CO<sub>2</sub> occurs. The adsorption and reactivity of CO<sub>2</sub> increases for the sequence: Fe(110) < stepped-Fe(110) < Fe(111) < evaporated Fe films [87Pir, 86Beh, 87Fre, 87Beh, 87Bau].

Molecular CO<sub>2</sub> adsorption was observed on an Fe(111) surface at 85 K [87Pir, 86Beh, 87Fre, 87Beh, 87Bau]. Fig. 2 shows UPS spectra of adsorbed CO<sub>2</sub> on Fe(111) at 85 and 140 K, along with calculated one-electron orbital energies of CO<sub>2</sub> and CO<sub>2</sub><sup>-</sup>. The UPS spectra reflected that most of the adsorbed molecules were only slightly distorted upon adsorption at 85 K, but there was a small fraction of the

molecules that were identified as bent, anionic CO<sub>2</sub><sup>-</sup> species [87Pir, 86Beh, 87Fre, 87Beh, 87Bau]. These anionic species were stable up to 160-180 K. Further heating the substrate to room temperature lead to the formation of coadsorbed CO and O on the surface. Thus, on (111) and polycrystalline Fe surfaces, it was concluded that CO<sub>2</sub><sup>-</sup> was a precursor for dissociative adsorption [87Pir, 86Beh, 87Fre, 87Beh, 87Bau]. These data are presented along with other information on the valence electronic structure for adsorbed CO<sub>2</sub> in Table 4. Related electronic excitations for adsorbed CO<sub>2</sub> are summarized in Table 5.

Work function change ( $\Delta\phi$ ) measurements following CO<sub>2</sub> adsorption on Fe(111) and stepped-Fe(110) surfaces [86Beh] are shown in Fig. 3. These data supported the presence of two different species at 77 K. One species caused the work function to increase while the other one lead to a decrease in work function with increasing CO<sub>2</sub> exposures.

HREELS was used to probe the molecular adsorption state of CO<sub>2</sub>, its dissociation to yield coadsorbed CO and O, and possible formation of carbonate (CO<sub>3</sub><sup>-</sup>) species on Fe(111) between 100 and 300 K [95Hes]. A carbonate intermediate was formed from CO<sub>2</sub> exposures on an oxygen-precovered Ag surface [82Stu, 83Bac]. Figs. 4a and b show a series of HREELS spectra probing the effect of pressure and temperature on CO<sub>2</sub> adsorption on Fe(111) [95Hes]. In Fig. 4a, two different groups of energy loss peaks dominate the spectra. Losses at 50, 133 and 145 meV were attributed to a strongly bound CO<sub>2</sub> species because the intensities of these peaks did not increase with increasing CO<sub>2</sub> pressure, while losses at 80 and 290 meV were associated with a weakly bound species. In Fig. 4b, appearance of a new peak at 225 meV, due to a  $\nu_{\text{CO}}$  stretching mode, from heating the layer at 150 K indicates dissociation. In addition, the strong loss peak at 133 meV at 150 K indicates the presence of two different states of strongly bound CO<sub>2</sub> on Fe(111). The behavior and intensity changes of the losses at 145 and 133 meV as the temperature was raised suggested that the two bent CO<sub>2</sub> states were strongly coupled and had two different activation energies for dissociation  $E_{\text{diss}}$ . At 240 K, a new feature appeared at 160 meV, which was associated with a linear CO<sub>2</sub> adsorbed in an upright orientation based on off-specular HREELS spectra, as presented in Fig. 5. The 290 meV loss peak was associated with the  $\nu_{\text{as}}(\text{OCO})$  asymmetric stretching mode of a weakly adsorbed CO<sub>2</sub> molecule in a linear configuration. The appearance of two losses near 160 meV was explained by splitting of the  $\nu_{\text{s}}(\text{OCO})$  symmetric stretching mode due to a Fermi resonance with the first harmonic of the 80 meV mode. The 80 meV loss peak was assigned to the  $\delta(\text{OCO})$  bending mode of an adsorbed linear CO<sub>2</sub> molecule. A vertical geometry of the CO<sub>2</sub> molecules was suggested because the two split modes were excited by impact scattering and the  $\nu_{\text{as}}(\text{OCO})$  mode by dipole scattering. The two modes at 133 and 145 meV and two other modes at 170 and 200 meV were assigned as corresponding to  $\nu_{\text{s}}$  and  $\nu_{\text{as}}$  modes of CO<sub>2</sub> adsorbed in a bent configuration. A definite analysis of the geometry of the bent CO<sub>2</sub><sup>-</sup> on Fe(111) was difficult because the number of observed modes agreed with both C<sub>s</sub> and C<sub>2v</sub> symmetry.

According to UPS, XPS, HREELS and NEXAFS measurements, CO<sub>2</sub> adsorption on Ni(110) [87Lin, 87Bar1, 88III] was very similar to that on Fe(111). Information on core-level binding energies for adsorbed CO<sub>2</sub> in this system and others is given in Table 6. ARUPS and HREELS studies revealed that two species were present on the Ni(110) surface at low temperature: a bent, chemisorbed CO<sub>2</sub><sup>δ-</sup> species and a linear physisorbed CO<sub>2</sub> species. All physisorbed CO<sub>2</sub> desorbed from the surface by heating to 180 K, and CO<sub>2</sub><sup>δ-</sup> species dissociated into coadsorbed CO and O upon heating above 190 K. ARUPS and HREELS results were compatible with C<sub>2v</sub> symmetry of the CO<sub>2</sub><sup>δ-</sup> adsorbate complex. Two possible coordinations satisfy this constraint, C-atom down or O-atoms down, as shown in Fig. 6. An  $\eta^2$  O-coordination of CO<sub>2</sub><sup>δ-</sup> species was proposed by comparison with the bonding of formate ions (HCOO<sup>-</sup>) on Cu(110) [87Lin, 87Bar1], where the molecular plane was aligned along the [110] azimuth and the O atoms were bound to the metal in an  $\eta^2$  configuration.

Further information about the local geometry of CO<sub>2</sub> and CO<sub>2</sub><sup>δ-</sup> species on Ni(110) was available from NEXAFS [88III]. Fig. 7 shows spectra at the oxygen K-edge for a  $\theta_E$  of 90° (normal incidence) and 20° for adsorbed CO<sub>2</sub> at 100 and 180 K. Spectra at 100 K were composed of a mixed phase of linear CO<sub>2</sub> and bent CO<sub>2</sub><sup>-</sup>, whereas the spectra at 180 K only contained the bent CO<sub>2</sub><sup>-</sup> phase. A spectrum for physisorbed CO<sub>2</sub> was derived by subtraction of the bent CO<sub>2</sub><sup>-</sup> spectrum at 180 K from the spectrum of the mixed phase, and this is included in Fig. 7. The sharp features were assigned to a  $\pi$  resonance caused by excitation from the O 1s core level to the 2 $\pi_u$  valence level of linear CO<sub>2</sub> or 2b<sub>2</sub> valence level of bent

CO<sub>2</sub><sup>-</sup>. Because the polarization dependence of the  $\pi$  resonance did not vary strongly with the angle of incidence, it was proposed that the physisorbed species adopts a “lying-down” configuration. If the molecular axis of the physisorbed CO<sub>2</sub> molecule was oriented perpendicular to the surface, then a strong attenuation of the  $\pi^*$  resonance intensity would be expected. This is in contrast to the vertical geometry proposed for physisorbed linear CO<sub>2</sub> on the Fe(111) surface.

Evidence about the orientation of these species from the polarization dependence of NEXAFS spectra has been obtained [88III]. The  $\pi$  resonance was strongly attenuated at  $\theta_E = 20^\circ$  in both azimuth angles, while the intensity of the  $\sigma$  resonance remained almost constant. The interpretation was that the molecular plane of a bent chemisorbed species was most likely oriented perpendicular to the surface plane, but that there was no preferential orientation of the molecular plane along the  $\langle 110 \rangle$  or  $\langle 001 \rangle$  azimuth. The spectra were also compatible with the presence of two different species oriented along each azimuth. A diffuse LEED analysis gave equal numbers of bent molecules adsorbed on atop sites and oriented along the  $\langle 100 \rangle$  and  $\langle 110 \rangle$  directions [82Stu].

The adsorption geometry and dissociation of CO<sub>2</sub> molecules on Re(0001) at 85–135 K was studied by HREELS [88Ass] with results similar to those found on Ni(110). Below 120 K, CO<sub>2</sub> adsorbs as a linear molecule with its axis parallel to the surface. A fraction of the adsorbed molecules desorbed at 120–135 K and the rest transformed into an intermediate identified as bent CO<sub>2</sub> <sup>$\delta^-$</sup> , which then decomposed into coadsorbed CO and O at 135 K.

Initially, CO<sub>2</sub> was thought to dissociate on Rh(111) [79Dub], but this was later attributed to B impurities [85Sol]. This latter result was consistent with a calculation of the dissociative sticking coefficient  $S_{diss}$  for CO<sub>2</sub> on Rh(111) to be about  $10^{-15}$  [83Wei].

### 3.8.4.2.3 CO<sub>2</sub> adsorption on chemically modified metal surfaces

#### 3.8.4.2.3.1 CO<sub>2</sub> adsorption and reaction on metals with coadsorbed O and H adatoms

CO<sub>2</sub> does not adsorb on the Ag(110) surface at 100 K [83Bac, 82Stu]. However, preadsorbed oxygen stabilized a molecular CO<sub>2</sub> state and induced reaction of CO<sub>2</sub> to form surface carbonate (CO<sub>3</sub><sup>2-</sup>) anionic species, as characterized by LEED, TPRS, UPS, XPS and HREELS [83Bac, 83Bar, 82Stu, 83Beh, 91Beh]. Upon heating, CO<sub>3</sub><sup>2-</sup> decomposed into coadsorbed CO<sub>2</sub> and O with a dissociation activation energy of  $E_{diss} = 27$  kcal/mol. UPS showed that the valence levels of adsorbed CO<sub>3</sub><sup>2-</sup> agreed well with those found in bulk K<sub>2</sub>CO<sub>3</sub> and CaCO<sub>3</sub>. This information, coupled with the increase in work function upon formation of adsorbed CO<sub>3</sub><sup>2-</sup>, helped to establish the anionic nature of these species.

C and O K-edge NEXAFS were performed to determine the orientation of the surface carbonate species on Ag(110) at room temperature [88Mad], as shown in Fig. 8. From the dependence of the spectra on the polar and azimuthal angles, it was concluded that the C-O bonds of CO<sub>3</sub><sup>2-</sup> were oriented parallel to the surface within  $10^\circ$ . A single  $\sigma^*$  resonance at 300.5 eV for both azimuths also suggested that all C-O bonds were equivalent. Excellent agreement between the NEXAFS spectra for both azimuths to that from bulk CdCO<sub>3</sub> led to the conclusion that the C-O bond length was 1.29 Å, i.e. the same as that in CdCO<sub>3</sub> [88Mad]. The assignment from NEXAFS of the orientation of the CO<sub>3</sub><sup>2-</sup> species as parallel to the Ag(110) surface contradicted the tilted geometry that was assigned previously based on ARUPS and HREELS [87Sak, 83Bac, 82Stu]. However, it was possible to reinterpret the vibrational spectrum to be consistent with the NEXAFS results and to indicate the C<sub>s</sub> symmetry of the surface-adsorbate complex [88Mad].

CO<sub>2</sub> interacts more weakly with an O-precovered Ni(110) surface than with a clean Ni(110) surface. ARUPS was used to determine that the orientation of CO<sub>2</sub> was parallel ( $\pm 20^\circ$ ) to the surface on O-precovered Ni(110) at 85 K, similar to that on clean Ni(110) at 85 K [87Bar1], as shown in Fig. 9a. The spectrum at 293 K, shown in Fig. 9b, was different from that obtained from the oxygen-free Ni(110) surface. The spectrum could be explained either by the presence of a CO/O coadsorbed phase or by the presence of carbonate species, but these two possibilities were not distinguished.

The reactivity of adsorbed CO<sub>2</sub> with coadsorbed hydrogen on Ni(110) was investigated by using HREELS and high-resolution XPS [91Wam]. HREELS spectra shown in Fig. 10 indicate both linear CO<sub>2</sub>

and bent CO<sub>2</sub><sup>-</sup> species by a  $\delta(\text{OCO})$  peak at 636 cm<sup>-1</sup> and losses at 727, 1103 and 403 cm<sup>-1</sup> attributed to  $\delta(\text{OCO})$ ,  $\nu_s(\text{OCO})$  and  $\nu_{\text{Ni-CO}_2}$  modes of a bent CO<sub>2</sub><sup>-</sup> species, respectively. Upon heating, the band for linear CO<sub>2</sub> disappeared and the losses corresponding to bent CO<sub>2</sub><sup>-</sup> species increased in intensity. Linear CO<sub>2</sub> was apparently converted to bent CO<sub>2</sub><sup>-</sup> species. Above 200 K, the spectra were characterized by three loss peaks at 403, 727, 1353 and a weak peak at 2904 cm<sup>-1</sup>. These vibrational energies compared well with those obtained for adsorbed formate (HCOO<sup>-</sup>) and it was concluded that formate was formed on the surface and was stable to 300 K. Formation of formate species was also supported by XPS [91Wam], as shown in Fig. 11. At low temperatures, peaks due to coadsorbed linear CO<sub>2</sub> (291.2 eV BE) and bent CO<sub>2</sub><sup>δ-</sup> (286.6 eV BE) were found. At 120 K, physisorbed CO<sub>2</sub> desorbed, CO<sub>2</sub><sup>δ-</sup> remained on the surface, and a small peak grew at 285.6 eV BE that corresponded to CO(a). At 200 K, a shift of the 286.6 eV BE peak to 287.0 eV BE indicated formation of formate species along with coadsorbed CO. The inset of the figure provides a spectrum of formate species that were formed by heating formic acid to 200 K, in good agreement with the spectra from CO<sub>2</sub> + H<sub>2</sub>/Ni(110).

### 3.8.4.2.3.2 CO<sub>2</sub> adsorption and reaction on metals with coadsorbed alkali metals

Alkali metals function as promoters for the adsorption and reactivity of CO<sub>2</sub> on metal surfaces [89Pau, 93Nas, 95Hes, 85Sol, 87Pel, 88Ass, 91Rod, 85Beh, 94Mey1, 94Mey2, 98Sey, 96Kra, 89Liu, 91Liu, 87Sol, 88Kis, 87Mat, 89Wam, 94Hof, 94Sol, 90Ehr]. Several examples exist where alkali metals dramatically increased the strength of the interaction between CO<sub>2</sub> and metal surfaces. This was often explained as arising from either direct interaction with the alkali metal or the lowering of the work function of the substrate by adsorption of the alkali metal, because electron transfer to CO<sub>2</sub> to form a more stable CO<sub>2</sub><sup>-</sup> species should be favored in either case. Different species, such as a CO<sub>2</sub> dimer, carbonate and oxalate, were proposed to form on these alkali-precovered metal surfaces depending on the nature of the alkali metals and metal substrates.

Spectroscopic evidence for the presence of CO<sub>2</sub><sup>-</sup> and CO<sub>3</sub><sup>2-</sup> species was presented for the system CO<sub>2</sub>/K/Rh(111) [87Sol, 88Kis, 94Sol] and CO<sub>2</sub>/K/Pt(111) [89Liu, 91Liu].

Interactions of CO<sub>2</sub> with Fe(110) surfaces precovered with K and Cs was studied by UPS, XPS and work function measurements [94Mey1, 94Mey2, 98Sey]. In contrast to the inactivity of CO<sub>2</sub> on Fe(110), a strong interaction between CO<sub>2</sub> and alkali-promoted Fe(110) was found. UPS spectra of CO<sub>2</sub> on Fe(110) at 85 K for two different K precoverages are shown in Fig. 12. At low K coverages and low CO<sub>2</sub> coverages, dissociation occurs to form coadsorbed CO and oxidic oxygen. At higher CO<sub>2</sub> coverages, disproportionation reactions form coadsorbed CO and CO<sub>3</sub><sup>2-</sup> species. Linear CO<sub>2</sub> molecules were found at high CO<sub>2</sub> exposures. Though no stable bent CO<sub>2</sub><sup>-</sup> was identified, its formation as an intermediate was suggested. At higher K coverages ( $\theta_K \geq 0.16$ ), a new adsorbate "species A" was formed. This was proposed to be an oxalate (C<sub>2</sub>O<sub>4</sub><sup>m-</sup>) species, although a C-O-C bridged iso-oxalate or a CO<sub>2</sub><sup>-</sup>·CO<sub>2</sub> adduct could be ruled out. HREELS was used to identify formation of oxalate species upon CO<sub>2</sub> adsorption on K-modified Fe(100) at 85 K [89Pau].

The stability of CO<sub>3</sub><sup>2-</sup> on Fe(110) depends on the K coverage [94Mey2]: small to medium ( $0 < \theta_K \leq 0.20$ ) or high coverages ( $0.26 \leq \theta_K < 0.3$ ). Fig. 13 shows that CO<sub>3</sub><sup>2-</sup> is unstable and decomposes between 200 and 300 K at small to medium  $\theta_K$  values, whereas CO<sub>3</sub><sup>2-</sup> decomposition does not occur until 500 K at high  $\theta_K$  values. Reaction schemes for the CO<sub>2</sub>/K/Fe(110) coadsorbate system for the two different  $\theta_K$  regimes have been proposed [94Mey2].

UPS and XPS were used to determine that the chemistry of CO<sub>2</sub> on Cs/Fe(110) and K/Fe(110) surfaces was similar, despite the larger size and induced work function change of Cs compared to K [98Sey]. Similarity of the chemistry of the CO<sub>2</sub>/K/Cu(110) system to that of CO<sub>2</sub>/K/Fe(110) led to the conclusion that the adsorption behavior of CO<sub>2</sub> was dominated by the adsorbed K and not by the underlying transition metal [96Kra].

IRAS and TPD investigations of the interaction of CO<sub>2</sub> with a ( $\sqrt{3} \times \sqrt{3}$ )R30°-K monolayer and K multilayer on Ru(0001) identified CO<sub>2</sub><sup>-</sup>, CO<sub>2</sub><sup>2-</sup>, oxalate and carbonate formation [94Hof]. On a clean Ru(0001) surface, CO<sub>2</sub> physisorbs in a monolayer that desorbs at 100 K, but interaction of CO<sub>2</sub> with a K

monolayer readily forms oxalate at 85 K. Fig. 14a compares IR spectra after CO<sub>2</sub> adsorption on a K monolayer and multilayer on Ru(0001) with that of bulk K<sub>2</sub>C<sub>2</sub>O<sub>4</sub>. Three bands at 1716, 1342 and 806 cm<sup>-1</sup> were assigned to  $\nu_a(\text{OCO})$ ,  $\nu_s(\text{OCO})$  and  $\delta(\text{OCO})$  modes, respectively, of an oxalate species. Possible structures of this species are shown in Fig. 14b. A study of matrix isolated Li<sup>2+</sup>C<sub>2</sub>O<sub>4</sub><sup>2-</sup> species and theoretical cluster calculations supported structure **AII** in Fig. 14b with D<sub>2h</sub> symmetry for the observed oxalate species [98Zhu]. Application of the surface dipole selection rule determined that the oxalate species was preferentially oriented with its molecular plane perpendicular to the surface and the C-C axis parallel to the surface, because the  $\nu_a(\text{OCO})$  asymmetric stretching mode was much stronger than the other two modes, in contrast to that found in the bulk IR spectrum. After heating above 150 K, oxalate (C<sub>2</sub>O<sub>4</sub><sup>2-</sup>) species on K/Ru(0001) disproportionated into coadsorbed CO<sub>3</sub><sup>2-</sup> and CO.

FTIR spectra of the carbonate species formed from CO<sub>2</sub> adsorption on multilayer, bilayer and monolayer K-covered Ru(0001) are shown in Fig. 15a. For the K monolayer, only one intense band was present at 1467 cm<sup>-1</sup>, which was assigned to  $\nu_a(\text{OCO})$  of CO<sub>3</sub><sup>2-</sup> with D<sub>3h</sub> symmetry. Possible structures for this species are shown in Fig. 15b. The vibrational spectra suggested that structure **CIV** in Fig. 15b, with its molecular plane perpendicular to the surface and C-O bond of the inequivalent, single oxygen atom parallel to the surface, was the most probable structure. Structures **CII** and **CV** were ruled out because these structures with inequivalent oxygen atoms should have given more than one CO stretching mode. Decomposition of CO<sub>3</sub><sup>2-</sup> starts at 700 K and results in simultaneous desorption of K and CO<sub>2</sub>.

#### 3.8.4.2.4 CO<sub>2</sub> adsorption on alloy surfaces

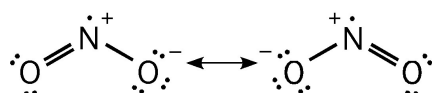
There are two reports concerning adsorption of CO<sub>2</sub> on bimetallic surfaces. One is on the c(2×2) Mn/Pd(100) surface alloy [99San]. No CO<sub>2</sub> adsorption was found on this alloy at any temperature exceeding that required for condensation. Preadsorbed oxygen stabilized adsorbed CO<sub>2</sub>, but oxygen adsorption actually destroys the alloy structure, disorders the surface, and forms MnO<sub>x</sub> complexes before CO<sub>2</sub> adsorption. Fig. 16 shows C(1s) XPS spectra after 20 L CO<sub>2</sub> was dosed on an O<sub>2</sub>-pretreated surface. In addition to the peak at 280 eV BE corresponding to atomic carbon, four other peaks were found and assigned to CO(a) on Pd, CO(a) on Mn, CO<sub>2</sub>(a) and CO<sub>3</sub><sup>2-</sup>(a). Valence photoemission spectra for the same conditions were used to identify adsorbed CO<sub>2</sub> at 110 K and CO<sub>3</sub><sup>2-</sup> after heating the adlayer to 500 K based on comparisons to angle-resolved spectra for CO<sub>2</sub>/Ni(110) [91Wam] and CO<sub>3</sub><sup>2-</sup>/Na/Pd(111) [89Wam] measured at  $h\nu=38$  eV. It was concluded that both of these two latter species were bound to MnO<sub>x</sub> complexes at the surface by comparing the results to those for CO<sub>2</sub> adsorption on oxide surfaces.

In studies on bimetallic Cu/Re(0001) surfaces, it was proposed the observed enhanced activity for CO<sub>2</sub> dissociation over that of pure Cu arose from Cu-Re interactions that enhanced the electron donor capability of Cu atoms supported on Re(0001) [91Rod].

#### 3.8.4.3 NO<sub>2</sub>

##### 3.8.4.3.1 Structure and bonding of NO<sub>2</sub>

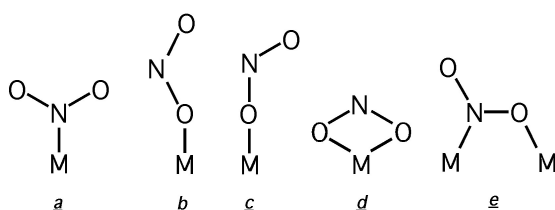
NO<sub>2</sub> is isoelectronic with CO<sub>2</sub><sup>-</sup>, and as such, it is a bent triatomic molecule, as shown in Scheme III. In the gas phase, it has a <sup>2</sup>A<sub>1</sub> ground electronic state, i.e., it is a radical, with the unpaired electron residing on the N atom, and it has an O-N-O angle of 134° and an O-N bond length of 1.2 Å.



Scheme III. Lewis structures for NO<sub>2</sub>.

As expected, adsorbed NO<sub>2</sub> exhibits a diversity of bonding modes analogous to the “linkage isomerism” observed in inorganic transition metal complexes [82Hit, 91Aln]. In these complexes, NO<sub>2</sub> coordinates in the form of nitrite (NO<sub>2</sub><sup>−</sup>) anion. NO<sub>2</sub> and NO<sub>2</sub><sup>−</sup> can bond through either one (monodentate) or both (bidentate in a chelating structure) of the O atoms or through the central N atom, and in bidentate bridging structures involving bonding to N and O atoms. Scheme IV gives some of the possible linkage isomers of NO<sub>2</sub><sup>−</sup> that have been characterized in complexes that are relevant to adsorption on surfaces.

There are four adsorption isomers expected for NO<sub>2</sub> that is bonded upright at the surface, with the molecular plane aligned near the surface normal: nitro or N-bonded (a in Scheme IV); O-nitrito (b and c in Scheme IV); O,O'-nitrito (d in Scheme IV); and μ-N,O-nitrito (the prefix-μ notation indicates the number of metal atoms to which the molecule is bonded) (e in Scheme IV). In complexes, O-nitrito ligands (b and c in Scheme IV) are known to be thermodynamically unstable and usually rearrange to the nitro isomer, so these should be only weakly bound at the surface. In addition, one may find weakly bound adsorption isomers with the molecular plane parallel or slightly inclined to the surface.



Scheme IV. Bonding modes for NO<sub>2</sub>.

### 3.8.4.3.2 NO<sub>2</sub> adsorption on metal surfaces

Thermodynamic values for NO<sub>2</sub> adsorption are given in Table 7. NO<sub>2</sub> is a very reactive molecule and dissociative adsorption occurs on most metal surfaces to form coadsorbed NO and O products at 300 K. Table 8 provides information on dissociation parameters for adsorbed NO<sub>2</sub>. Dissociative adsorption of NO<sub>2</sub> was reported on W(110), Mo(110), Ru(0001), Ag(110) and Ag(111) surfaces even at low temperatures. On W(110), NO<sub>2</sub> almost completely dissociated at 100 K to form coadsorbed N and O adatoms [79Fug, 87Bab]. On Ru(0001) at 80 K, NO<sub>2</sub> initially dissociated to produce coadsorbed NO and O, but higher exposures lead to molecular chemisorption of NO<sub>2</sub> [86Sch1, 86Sch2]. This molecularly adsorbed NO<sub>2</sub> was weakly chemisorbed with an energy of 9 kcal/mol. HREELS was used to conclude that NO<sub>2</sub> bonds through the N atom to Ru(0001) with C<sub>2v</sub> symmetry and the molecular axis oriented essentially perpendicular to the Ru(0001) surface. Vibrational data for adsorbed NO<sub>2</sub> on Ru(0001) and other surfaces is summarized in Table 9.

TPD, LEED, AES and ESD were used to investigate adsorption and decomposition of NO<sub>2</sub> on Pt(100) [85Sch]. It was proposed that molecular adsorption occurred on the reconstructed, hexagonal (5×20) Pt(100) structure of the clean surface at 200 K and the reconstruction was not lifted by NO<sub>2</sub> adsorption at this temperature. Thermal dissociation of NO<sub>2</sub> occurred in a narrow temperature range (<10 K) near 295 K, and a surface structural phase transition occurred to form the unreconstructed (1×1) Pt(100) structure within the same temperature interval. This phase transition lead to highly reactive domains that accelerated NO<sub>2</sub> decomposition and caused an autocatalytic reaction.

NO<sub>2</sub> adsorption on Pt(111) has been investigated by TPD, UPS and HREELS [82Dah, 82Seg, 87Bar2]. Early on, there were some contradictory results concerning the dissociative adsorption of NO<sub>2</sub> on Pt(111) at 120 K. Based on cited unpublished UPS work, it was reported that NO<sub>2</sub> adsorption was completely dissociative on Pt(111) [82Seg], while TPD studies indicated that NO<sub>2</sub> adsorbed molecularly on Pt(111) at 120 K and dissociated at 240 K [82Dah]. Later, it was confirmed that NO<sub>2</sub> adsorption was molecular at all coverages at 100 K [87Bar2]. Fig. 17 summarizes NO<sub>2</sub> adsorption kinetics on Pt(111) at 100 K. At low coverages (<0.25 ML), adsorption was irreversible, and NO<sub>2</sub> dissociated completely during heating in TPD to produce coadsorbed NO and O. At higher coverages, adsorption was partially reversible and desorption of NO<sub>2</sub> occurred with E<sub>d</sub> = 19 kcal/mol. Saturation coverage in the chemisorbed



layer at 100 K was  $\theta_{\text{NO}_2} \approx 0.5$  ML, with about 20 % of the monolayer desorbed as NO<sub>2</sub>. At large exposures, dimerization occurred to form the N-N bonded dimer in a condensed multilayer of N<sub>2</sub>O<sub>4</sub> that desorbed in TPD with an onset near 120 K.

Fig. 18 shows a series of HREELS spectra as a function of NO<sub>2</sub> exposure on Pt(111) at 100 K. Mode assignments were made by comparison to IR data on inorganic cluster compounds that contained NO<sub>2</sub> ligands. The surface-dipole selection rule for specular scattering in HREELS was used to assign C<sub>s</sub> symmetry for the NO<sub>2</sub> surface complex. The large difference in energies (380 cm<sup>-1</sup>) between the  $\nu_s(\text{ONO})$  and  $\nu_a(\text{ONO})$  stretching modes was consistent with a geometry in which NO<sub>2</sub> was strongly bound in a low-symmetry structure. Three isomers could have such a symmetry:  $\mu$ -N,O-nitrito (bridge-bonded NO<sub>2</sub>), O-nitrito and a three-coordinate nitrite (flat-lying). A  $\mu$ -N,O-nitrito species in an upright position ( $\underline{g}$  in Scheme IV) was proposed as the most probable configuration. With the lengthening and weakening of the N-O bond that is nearly parallel to the surface, this species was proposed as a logical precursor for the dissociative adsorption of NO<sub>2</sub> on Pt(111). HREELS spectra taken after annealing small NO<sub>2</sub> coverages ( $\theta_{\text{NO}_2} < 0.25$  ML) on Pt(111) showed that NO<sub>2</sub> dissociated completely to coadsorbed bridge-bonded NO and O from 170-240 K. At higher NO<sub>2</sub> coverages ( $\theta_{\text{NO}_2} > 0.25$  ML), adsorbed NO<sub>2</sub> could be stabilized to above 300 K and NO formed from NO<sub>2</sub> dissociation was adsorbed at atop sites.

NO<sub>2</sub> adsorption in the presence of coadsorbed O adatoms on Pt(111) at 100 K was probed by TPD and HREELS [88Bar]. NO<sub>2</sub> was adsorbed molecularly at all O precoverages, and coadsorption with O decreased the amount of irreversible NO<sub>2</sub> adsorption. Coadsorption inhibited formation of the  $\mu$ -N,O-nitrito species and caused the formation of a new, nitro species that is N-bonded in an upright geometry with C<sub>2v</sub> symmetry. This is shown in Fig. 19. At  $\theta_{\text{O}} = 0.75$  ML, a coverage of 0.15 ML nitro-bonded NO<sub>2</sub> could be formed. All of this NO<sub>2</sub> was reversibly adsorbed, and desorbed in a TPD peak at 155 K, corresponding to a chemisorption bond energy of 11 kcal/mol. An NO<sub>3</sub><sup>-</sup> species was not observed under any conditions.

NO<sub>2</sub> adsorption on Pd(111) was similar to that on Pt(111), as probed by TPD and HREELS [91Wic]. NO<sub>2</sub> chemisorbed as a  $\mu$ -N,O-nitrito isomer with a saturation coverage of 0.5 ML on Pd(111) at 110 K. Decomposition into coadsorbed NO and O occurred upon heating to 180 K, and this initially has a lower activation energy than desorption. NO<sub>2</sub> desorption became competitive with decomposition at higher coverages.

NO<sub>2</sub> is quite reactive at Ag surfaces. The chemistry of NO<sub>2</sub> on Ag(110) and Ag(111) surfaces is complex [87Out, 90Pol1, 90Pol2, 95Bro1, 95Bar]. Many surface species were identified depending upon the adsorption temperature and coverage. Fig. 20 provides IRAS spectra obtained following NO<sub>2</sub> exposure on Ag(111) at 86 K [95Bro1]. The vibrational band assignments were made as follows: 1940 cm<sup>-1</sup>, NO; 1860-1880 cm<sup>-1</sup>, (NO)<sub>2</sub>, N<sub>2</sub>O<sub>3</sub>; 1717/1738/1745/1766 cm<sup>-1</sup>, N<sub>2</sub>O<sub>4</sub>; 1590 cm<sup>-1</sup>, NO<sub>3</sub>, N<sub>2</sub>O<sub>3</sub>; 1265/1285/1305 cm<sup>-1</sup>, NO<sub>3</sub>, N<sub>2</sub>O<sub>3</sub>, N<sub>2</sub>O<sub>4</sub>; 1045 cm<sup>-1</sup>, NO<sub>3</sub>; and 761/774 cm<sup>-1</sup>, NO<sub>3</sub>, N<sub>2</sub>O<sub>3</sub>, N<sub>2</sub>O<sub>4</sub>. Initially, adsorption of NO<sub>2</sub> on Ag(111) at 86 K was dissociative, producing the dimer (NO)<sub>2</sub>, as assigned by the loss peak at 1859 cm<sup>-1</sup>, and adsorbed O. This conclusion was also reached in UPS and XPS studies. Adsorbed NO<sub>3</sub> and N<sub>2</sub>O<sub>3</sub> were formed on Ag(111) by reaction of incoming NO<sub>2</sub> with adsorbed O and (NO)<sub>2</sub>. All of these species coexisted on the surface. A proposed reaction scheme is given in Fig. 21. Available photoelectron spectroscopic data for adsorbed NO<sub>2</sub> is given in Table 10.

Au(111) is the least reactive metal surface that has been studied, and NO<sub>2</sub> adsorption on Au(111) at 100 K was molecular and completely reversible as determined by HREELS, IRAS, AES and TPD [89Bar, 98Wan1]. Fig. 22 shows that chemisorbed NO<sub>2</sub> desorbs from Au(111) in a peak at 230 K, indicating  $E_d = 14$  kcal/mol. After saturation of the NO<sub>2</sub> monolayer ( $\theta_{\text{NO}_2} = 0.4$  ML), an N<sub>2</sub>O<sub>4</sub> multilayer was formed at higher NO<sub>2</sub> exposures and NO<sub>2</sub> from this phase desorbs near 150 K. In the TPD scans shown in Fig. 22, the NO signal reproduced the NO<sub>2</sub> signal as expected for a cracking fragment ion, except for the peak at 170 K which then must be attributed to NO desorption. Because NO does not adsorb on Au(111) under these conditions, this must be NO evolution from the decomposition of an NO-containing surface species, which was shown by HREELS and IRAS to be adsorbed N<sub>2</sub>O<sub>3</sub>. Fig. 23 gives relevant IRAS spectra from Au(111) [98Wan1]. The spectrum obtained by dosing NO<sub>2</sub> at 175 K (to avoid contaminant NO(g) from forming N<sub>2</sub>O<sub>3</sub>) was used to determine the geometry of chemisorbed NO<sub>2</sub> on Au(111). Only two bands were observed because of the C<sub>2v</sub> symmetry of the adsorbed complex. These

were due to the  $\delta(\text{ONO})$  bending mode at  $805\text{ cm}^{-1}$  and  $\nu_s(\text{ONO})$  stretching mode at  $1178\text{ cm}^{-1}$ . There are two possible NO<sub>2</sub> geometries with C<sub>2v</sub> symmetry: O,O'-nitrito (chelating) and nitro (N-bonded) NO<sub>2</sub>. It was concluded that adsorbed NO<sub>2</sub> formed an O,O'-nitro surface chelate with C<sub>2v</sub> symmetry based on the stretching mode vibrations in coordination compounds containing the chelating isomer ( $1171\text{--}1225\text{ cm}^{-1}$ ) and the nitro isomer ( $1306\text{--}1392\text{ cm}^{-1}$ ). Deliberate NO exposure to these species forms adsorbed N<sub>2</sub>O<sub>3</sub> on the surface, as shown in Fig. 23, in an intriguing radical-radical reaction. The IRAS spectrum indicates N<sub>2</sub>O<sub>3</sub> species are adsorbed in an upright geometry with a symmetry of C<sub>s</sub> or lower, in a monodentate O-bonded configuration with the free N=O group oriented nearly perpendicular to the surface. This is a reversible reaction that liberates NO(g) at 170 K in TPD, indicating an N-N bond strength of 10 kcal/mol. While it is not clear whether NO<sub>2</sub> chemisorbs on Au(111) as a radical, its reactivity towards gas-phase NO to produce adsorbed N<sub>2</sub>O<sub>3</sub> shows its capability of undergoing radical-radical type of reactions. Difficulties exist in ESR studies of paramagnetic monolayers on metal surfaces and so information from these experiments is limited [93Bec].

In coadsorption studies with H<sub>2</sub>O on Au(111), NO<sub>2</sub> was shown to react to produce nitrous acid (HONO) and nitric acid (HNO<sub>3</sub>) upon being heated [98Wan1, 98Wan2, 99Wan]. Another reaction channel was observed by exposure of NO<sub>2</sub> on amorphous, condensed H<sub>2</sub>O (ice) films at 85 K (containing free "OH" groups). Heating to 130 K formed the nitrito isomer of N<sub>2</sub>O<sub>4</sub> (ONO-NO<sub>2</sub>), which reacted at 183 K to form nitrosonium nitrate (NO<sup>+</sup>NO<sub>3</sub><sup>-</sup>). This species decomposed at 275 K ultimately to deposit a large concentration ( $\theta_{\text{O}} = 0.4\text{ ML}$ ) of O adatoms on the Au(111) surface. This facile, low-temperature reaction between condensed-phase NO<sub>2</sub> and H<sub>2</sub>O represents a novel route to generate surface oxygen on Au and perhaps on other unreactive surfaces.

One application of the high reactivity of NO<sub>2</sub> with metal surfaces is the use of NO<sub>2</sub> to cleanly, conveniently achieve high, effective O<sub>2</sub>-pressure conditions that enabled new studies of the interaction of oxygen with several transition metal surfaces. This was first utilized on Pt(111) where  $\theta_{\text{O}} = 0.75\text{ ML}$  could be achieved by NO<sub>2</sub> dosing with the substrate at 400 K [88Bar, 89Par, 90Par], in contrast to the value of  $\theta_{\text{O}} = 0.25\text{ ML}$  that is produced by exposures to O<sub>2</sub> in UHV. NO<sub>2</sub> exposures on Pd(111) at 530 K was later used to achieve oxygen coverages of up to 3.1 ML under UHV conditions [90Ban, 90Par]. NO<sub>2</sub> dosing has been used extensively on Ru(0001) to create high atomic oxygen coverages, novel high-density ordered structures, subsurface oxygen and RuO<sub>x</sub> layers [91Mal, 92Mal, 95Hrb, 96Mit, 97He, 97Kos, 99Böt]. Decomposition of NO<sub>2</sub> was used for the oxidation of Ag, Zn and Cu films [94Rod] and to study the O/Rh(111) system [95Pet]. At high temperatures ( $\sim 1000\text{ K}$ ), pure films of polycrystalline MoO<sub>2</sub> that were 20-Å thick were produced from NO<sub>2</sub> exposures on Mo(110) [00Jir].

### 3.8.4.3.3 NO<sub>2</sub> adsorption on alloy surfaces

There are a few reports on the interaction of NO<sub>2</sub> with bimetallic surfaces. NO<sub>2</sub> was found to dissociate on a supported Zn monolayer on Ru(0001) similar to that on polycrystalline Zn [93Rod]. On Zn<sub>1.0</sub>/Ru(0001) at 80 K, initial NO<sub>2</sub> adsorption was dissociative to produce adsorbed O and NO(g), but subsequent NO<sub>2</sub> adsorption was molecular due to passivation of the surface by adsorbed O. This chemisorbed NO<sub>2</sub> decomposed at 160-250 K. At 300 K, the dissociation probability for NO<sub>2</sub> on Zn surfaces was 100 times that of O<sub>2</sub>.

On Pd/Rh(111) bimetallic surfaces ( $\theta_{\text{Pd}} = 0.6\text{--}1.2\text{ ML}$ ) formed by deposition of Pd overlayers on Rh(111), NO<sub>2</sub> exhibited a reactivity that was substantially lower than on Rh(111) or Pd(111) [99Jir1]. Pd atoms supported on Rh(111) were able to dissociate NO<sub>2</sub> at low temperature, but the NO and O products desorbed or diffused away from the Pd islands below 400 K, spilling over to bare Rh(111) patches.

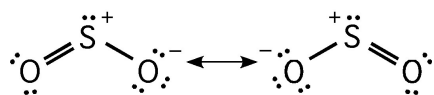
Adsorption of NO<sub>2</sub> on a ( $\sqrt{3}\times\sqrt{3}$ )R30°-Sn/Pt(111) surface alloy was investigated using TPD, AES, HREELS and LEED [04Vos]. At 120 K, NO<sub>2</sub> dimerizes at the surface to form the N,N-bonded dimer, N<sub>2</sub>O<sub>4</sub>, in the chemisorbed monolayer. This species bonds to the surface through a single O atom in an upright but tilted geometry. However, no N<sub>2</sub>O<sub>4</sub> or NO<sub>2</sub> desorbs molecularly from the monolayer. The dimer completely dissociates at 300 K, leaving coadsorbed NO<sub>2</sub>, NO and O on the surface. Adsorbed NO<sub>2</sub> further dissociates to coadsorbed NO and O at 300-400 K. The maximum oxygen atom coverage obtained by heating the N<sub>2</sub>O<sub>4</sub> monolayer was  $\theta_{\text{O}} = 0.4\text{ ML}$ , but this could be increased to  $\theta_{\text{O}} = 1.1\text{ ML}$  by NO<sub>2</sub>

dosing on the alloy surface at 600 K to remove inhibition by coadsorbed NO. Under these latter conditions, adsorbed oxygen desorbs as O<sub>2</sub> in three clear desorption states, the lowest of which is associated with O<sub>2</sub> desorption from Pt sites and the other two are from decomposition of reduced tin oxide phase(s), SnO<sub>x</sub>.

### 3.8.4.4 SO<sub>2</sub>

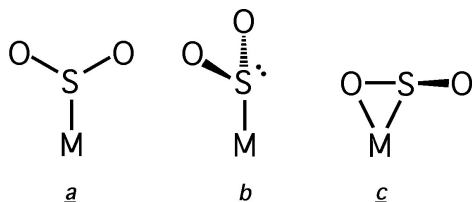
#### 3.8.4.4.1 Structure and bonding of SO<sub>2</sub>

SO<sub>2</sub> is a bent, polar triatomic molecule, as shown in Scheme V. It is isoelectronic with NO<sub>2</sub><sup>-</sup>, one of the most versatile oxyanion ligands in metal complexes, as explained above. As usual, the coordination chemistry of SO<sub>2</sub> is determined by the nature of its highest occupied (HOMO) and lowest unoccupied molecular orbital (LUMO) that act as electron donor and acceptor levels, respectively. For SO<sub>2</sub>, the HOMO is the 8a<sub>1</sub> orbital and the LUMO is the 3b<sub>1</sub> orbital, which lies about 2 eV above the 8a<sub>1</sub> level [71Roo]. These orbitals are shown in Fig. 24. The empty d orbitals do not participate in the bonding and SO<sub>2</sub> can act as both a σ-donor and π-acceptor [81Rya]. When the π-acceptor aspect dominates, π bonds between the SO<sub>2</sub> and metal are formed and the molecule lies flat on the surface. On the other hand, in cases where σ-bonding is preferred, the molecule adsorbs with its molecular plane perpendicular to the surface.



Scheme V. Lewis structures for SO<sub>2</sub>.

The structure and bonding of SO<sub>2</sub> containing metal complexes has been reviewed [78Min]. In complexes with terminal SO<sub>2</sub> ligands, there are three distinct bonding modes, as shown in Scheme VI: η<sup>1</sup>-planar (**a**), η<sup>1</sup>-pyramidal (**b**) and η<sup>2</sup> (**c**), each having a metal-S bond [74Ang, 85Sak].



Scheme VI. Bonding modes for terminal SO<sub>2</sub>.

Bridging SO<sub>2</sub> ligands are also found in polynuclear compounds [79Kub]. The angle between the SO<sub>2</sub> plane and metal-S axis is close to 180° in η<sup>1</sup>-planar complexes and close to 120° in the η<sup>1</sup>-pyramidal complexes.

The infrared active S-O stretching frequencies are diagnostic of different bonding modes in SO<sub>2</sub> complexes [81Rya, 85Sak]. Various bonding modes of SO<sub>2</sub> can be distinguished by frequency shifts of ν(SO) as shown in Fig. 25. The η<sup>2</sup> mode can be easily distinguished because the ν<sub>s</sub>(OSO) stretching mode drops to a value of 850-950 cm<sup>-1</sup>, far below that for any other modes, and this results in a large splitting of (ν<sub>as</sub> - ν<sub>s</sub>) ~230 cm<sup>-1</sup>. For η<sup>1</sup>-planar complexes, (ν<sub>as</sub> - ν<sub>a</sub>) is always less than 180 cm<sup>-1</sup> and this characterizes SO<sub>2</sub> bonding through the S atom only. Use of the surface-cluster analogy aids identification of the coordination of SO<sub>2</sub> on surfaces using the known structures that are available for SO<sub>2</sub> ligand in complexes, but one should always proceed with caution because of differences in bonding of the molecules in the two cases.

Adsorption behavior of SO<sub>2</sub> on metal surfaces in some ways resembles the adsorption of CO on metals because σ donor, π acceptor interactions are important for both molecules. However, the orbital

energy of the  $\pi^*$  orbital in SO<sub>2</sub> is much lower than that in CO, suggesting that SO<sub>2</sub> should be a stronger  $\pi$  acceptor in metal-SO<sub>2</sub> complexes. Charge donation from the substrate into the  $\pi^*$  orbital of SO<sub>2</sub> is expected if the substrate orbitals have proper symmetry, energy and location to overlap the  $\pi^*$  orbital.

#### 3.8.4.4.2 SO<sub>2</sub> adsorption on metal surfaces

SO<sub>2</sub> adsorption on metal surfaces has been extensively studied. Some of this literature has been reviewed [97Haa]. On Ag surfaces, SO<sub>2</sub> was molecularly and reversibly adsorbed; it was desorbed with no evidence of decomposition [72Las, 81Rov, 84Out, 86Out1, 86Out2, 93Pre, 90Ahn, 90Rod, 91Sol2, 92Höf, 93Höf, 93Was, 96Gut2, 91Cas]. SO<sub>2</sub> decomposed on Fe, Mo, Ni, Cu, Ru, Pd and Pt, surfaces [78Fur, 88Hor, 81Ku, 82Köh, 82Kat, 82Ast, 83Köh, 90Höf, 94Sun1, 97Wil, 97Pol, 95Wil, 85Köl, 88Bur1, 88Bur2, 97Ter, 99Lee, 89Leu, 92Ahn, 93Ahn, 93Pan, 96Pol, 97Nak1, 97Pan, 97Nak2, 98Pol, 93Zeb, 95Yok1, 95Yok2, 95Ter, 96Yok, 97Jac, 98Wil, 99Jir2]. However, the S-O bond in SO<sub>2</sub> was weakened more on Ag(110) than on Pd(100), as indicated by a comparison of the  $\nu_s(\text{OSO})$  frequencies for adsorbed SO<sub>2</sub> on the two surfaces, i.e., 985 cm<sup>-1</sup> on Ag(110) and 1035 cm<sup>-1</sup> on Pd(100). If so, bond strength arguments alone cannot explain the decomposition behavior of SO<sub>2</sub> on these surfaces. SO<sub>2</sub> was molecularly adsorbed on Ni surfaces at 150 K, which places a lower limit on the barrier to decomposition  $E_{\text{diss}}$  of SO<sub>2</sub> on Ni of 10-12 kcal/mol.  $E_{\text{diss}}$  for SO<sub>2</sub> on Ag(110) was larger than that on Pd(100), Pt(111) or Ni surfaces. In addition, on Ag(110), SO<sub>2</sub> is bonded through the S atom only at atop sites. It has been suggested that the participation of more directional d orbitals in bonding leads to lowering of  $E_{\text{diss}}$ .

SO<sub>2</sub> adsorption thermodynamics data and dissociation parameters are summarized in Tables 11 and 12, respectively.

At low temperatures, SO<sub>2</sub> adsorbed molecularly on most transition metals. SO<sub>2</sub> was more reactive on Ru(0001) than on Pt(111) or Pd(100) surfaces [98Jir, 97Wil, 88Bur2], and SO<sub>2</sub> dissociatively adsorbed on Ru(0001) at 100 K to form sulfite SO<sub>3</sub><sup>-</sup> and sulfate SO<sub>4</sub><sup>2-</sup> species [98Jir]. Decomposition of SO<sub>3</sub><sup>-</sup> and SO<sub>4</sub><sup>2-</sup> occurred below 380 K on Ru(0001), but at temperatures higher than 400 K on Pt(111) or Pd(100) surfaces.

Several different adsorption geometries for adsorbed molecular SO<sub>2</sub> have been observed, with the configuration and site for SO<sub>2</sub> adsorption depending on the electronic structure and geometry of the substrate. These species have been characterized by photoelectron spectroscopy, NEXAFS, SEXAFS and vibrational spectroscopy. Tables 13-16 summarize the available measurements for SO<sub>2</sub> adsorption, respectively.

On Pt(111), Pd(100) and Cu surfaces, SO<sub>2</sub> adopted a geometry in which the molecular plane was perpendicular to the surface and the S atom and one O atom directly interacted with the surface [82Köh, 82Kat, 82Ast, 83Köh, 90Höf, 94Sun1, 97Wil, 97Pol, 95Wil, 85Köl, 88Bur1, 88Bur2, 97Pan]. On the other hand, SO<sub>2</sub> adsorbed on Ni surfaces with its molecular plane parallel to the surface [93Zeb, 95Yok1, 95Yok2, 95Ter, 96Yok, 97Jac, 98Wil]. A bonding geometry involving only the S atom was found on Ag(110) [86Out2, 93Pre, 90Ahn, 90Rod, 91Sol2, 92Höf, 93Höf, 93Was, 96Gut]. It was suggested that the different behavior of SO<sub>2</sub> may be derived from different energies of the metal d bands. For Ag, the metal d bands lie nearly 4 eV below the Fermi level and are too low in energy to bond effectively to SO<sub>2</sub>. Instead, the s and p orbitals are involved in making a Ag-SO<sub>2</sub>  $\sigma$  bond. For Ni, the d orbitals lie at Fermi level and this leads to strong interactions with the  $\pi^*$  orbitals in SO<sub>2</sub> and results in a flat-lying orientation. It has been argued that the deeper d bands for Cu, Pd and Pt interact less significantly with the SO<sub>2</sub>  $\pi^*$  orbital and allow a SO<sub>2</sub> geometry with the molecular plane perpendicular to the surface.

##### 3.8.4.4.2.1 Molecular adsorption and desorption of SO<sub>2</sub>

SO<sub>2</sub> adsorbs and desorbs molecularly on Ag surfaces [72Las, 81Rov, 84Out, 86Out1, 86Out2, 93Pre, 90Ahn, 90Rod, 91Sol2, 92Höf, 93Höf, 93Was, 96Gut, 91Cas]. The adsorption of SO<sub>2</sub> on Ag(110) has been characterized by several techniques, including TPD, UPS, HREELS, XPS and NEXAFS [72Las, 81Rov, 84Out, 86Out1, 86Out2, 93Pre, 90Ahn, 90Rod, 91Sol2, 92Höf, 93Höf, 93Was, 96Gut].

Molecular adsorption and desorption of SO<sub>2</sub> appear to occur without decomposition or dissociation on the clean Ag(110) surface. At a surface temperature of 100 K, multilayers of SO<sub>2</sub> are formed, and this leads to desorption in a sharp peak near 120 K in TPD. Three different desorption states labeled as  $\alpha_1$ ,  $\alpha_2$  and  $\alpha_3$  were observed at 170, 225 and 275 K, respectively, and these have been assigned to desorption from bilayer, monolayer and submonolayer coverages of SO<sub>2</sub>. Desorption energies in these peaks are 41, 53 and 64 kJ/mol, respectively, indicating that the binding energy of SO<sub>2</sub> molecules at the Ag(110) surface is energetically in between that expected for physisorption and chemisorption.

UPS, HREELS and NEXAFS provide evidence that the bonding geometry was unchanged between two chemisorbed phases on Ag(110) [72Las, 81Rov, 86Out2]. HREELS measurements suggested that chemisorbed SO<sub>2</sub> was bound via a Ag-S bond, with the O atoms not involved in surface bonding, based on the similarity in the frequencies of the  $\nu_s(\text{OSO})$  mode for SO<sub>2</sub> bound to the surface and in S-bonded SO<sub>2</sub> complexes. Based on the presence of a SO<sub>2</sub>-Ag out-of-plane wagging mode, a geometry in which SO<sub>2</sub> was tilted towards the surface with the O atoms parallel to the surface was proposed. Sulfur K-edge NEXAFS measurements provided evidence that the SO<sub>2</sub> molecular plane on Ag(110) was not strongly tilted, but nearly (within 15°) perpendicular to the plane of the surface [96Gut]. The apparent contradiction between the two assignments might be explained by the uncertainty (~10°) in the NEXAFS measurements that could accommodate a small tilt that would allow the wagging modes to be dipole-active in HREELS measurements, or by an important influence of impact scattering in HREELS that could make it appear that the out-of-plane wagging mode of surface bound SO<sub>2</sub> was dipole active.

The coverage dependence of the adsorption geometry of SO<sub>2</sub> on Ag(110) was probed with S K-edge NEXAFS measurements [96Gut2]. Figs. 26a and b show NEXAFS spectra for coverages of 0.3 and 0.6 ML SO<sub>2</sub> adsorbed on Ag(110). The insets give the azimuthal dependence of the  $\pi^*$ -resonance intensity. The bonding geometry of SO<sub>2</sub> on Ag(110) was obtained from this data using the dipole selection rule and group theory. The  $\pi^*(b_1^*)$  resonance is excited by a component of the  $E$  vector perpendicular to the plane of the molecule while the  $\sigma^*(a_1^*+b_1^*)$  resonance is excited by a component of the  $E$  vector parallel to the plane of the molecule. In the low coverage spectra, the  $\pi^*$  resonance has a maximum intensity at normal incidence of the X-rays with the  $E$  vector along the [110] azimuth. The  $\pi^*$ -resonance intensity is very weak with the  $E$  vector along the [001] azimuth and independent of the X-ray incident angle. This, along with the polarization dependence of the  $\sigma^*$  resonance, suggested that SO<sub>2</sub> molecules at low coverage adopt an upright geometry with the molecular plane along the [001] azimuth. The best fit to the data, based on an azimuthally aligned molecules, corresponded to the molecular plane tilting only  $2\pm 5^\circ$  from the surface normal.

In the 0.6 ML SO<sub>2</sub> layer, Fig. 26b shows that the maximum-to-minimum  $\pi^*$ -intensity ratio is dependent on the azimuthal angle, indicating an azimuthal alignment at higher coverage. Best-fit results correspond to a tilt angle of  $13\pm 5^\circ$  for the molecular plane with respect to the surface normal and a twist angle of  $55\pm 5^\circ$  from [001]. This allows a higher packing density on the surface. Using the surface-cluster analogy, an on-top adsorption site was favored [88Hor] and this lead to the structural model shown in Fig. 27.

#### 3.8.4.4.2.2 Molecular adsorption and decomposition of SO<sub>2</sub>

SO<sub>2</sub> adsorption on Pt and Pd surfaces was studied in several laboratories, and it was found that dissociation occurs to a small extent [81Ku, 82Köh, 82Kat, 82Ast, 83Köh, 90Höf, 94Sun1, 97Wil, 97Pol, 95Wil, 85Köl, 88Bur1, 88Bur2, 97Ter]. TPD, AES, work function measurements, UPS, XPS and HREELS were used to characterize adsorption of SO<sub>2</sub> on Pt(111) [82Kat, 82Ast, 83Köh, 90Höf, 94Sun1, 97Wil, 97Pol, 95Wil]. Typically, it was observed that SO<sub>2</sub> adsorbed molecularly on Pt(111) below 120 K. SO<sub>2</sub> desorption from the multilayer occurred at 130 K and from the chemisorbed layer at 285 K in TPD. Following SO<sub>2</sub> adsorption at room temperature, both SO and SO<sub>4</sub> species were identified on the surface. Studies using TPD have reported molecular and dissociative adsorption states of SO<sub>2</sub> on Pt(111) at 160 K at low coverages, along with recombinative SO<sub>2</sub> desorption at 280 K [83Köh, 90Höf].

The adsorption geometry and reaction paths of adsorbed SO<sub>2</sub> on Pt(111) have been examined by HREELS and XPS [94Sun1, 97Pol]. HREELS spectra are shown in Fig. 28. The inset shows TPD spectra

with peaks at 127 and 285 K corresponding to SO<sub>2</sub> desorption from the multilayer and monolayer, respectively. The HREELS spectra indicate that SO<sub>2</sub> adsorbs molecularly on Pt(111) at 110 K. An adsorption geometry in which SO<sub>2</sub> bonds to Pt in the monolayer through the S atom and at least one O atom was proposed based on the  $\nu(\text{Pt-SO}_2)$  and  $\nu(\text{Pt-O})$  stretching loss peaks at 266 and 430 cm<sup>-1</sup>, respectively. The relatively low energy  $\nu_s(\text{OSO})$  peak at 940 cm<sup>-1</sup> and the large difference of 312 cm<sup>-1</sup> between the  $\nu_s(\text{OSO})$  and  $\nu_a(\text{OSO})$  modes support an  $\eta^2\text{-SO}_2$  geometry, bonding through both S and O atoms. In addition, both XPS and UPS results reveal electron back-donation from the substrate to the SO<sub>2</sub> antibonding orbital [94Sun1, 97Wil, 97Pol]. The absence of a  $\delta(\text{OSO})$  wagging mode, typically near 680 cm<sup>-1</sup>, suggested that the SO<sub>2</sub> molecular plane was normal to the surface and that SO<sub>2</sub> was bonded through one of the O atoms. In addition, it was suggested that the O-O axis of SO<sub>2</sub> was tilted with respect to the surface normal because of the presence of dipole-active loss peaks for both  $\nu_s(\text{OSO})$  and  $\nu_a(\text{OSO})$  modes of SO<sub>2</sub>. In a similar study on Pd(100), a 9° in-plane tilt was proposed based on a  $\nu_a/\nu_s$  intensity ratio of 0.44 [88Bur1]. A larger in-plane tilt for SO<sub>2</sub> on Pt(111) compared to Pd(100) was suggested because  $\nu_a/\nu_s = 2$  on Pt(111).

The adsorption geometry for SO<sub>2</sub> on Pt(111) is shown in Fig. 29. For the  $\eta^2\text{-SO}_2$  configuration, both S and O are bonded to the surface, and both  $\pi$  and  $\sigma$  bonds can be formed. Formation of a  $\pi$  bond appears to occur between the 3b<sub>1</sub> orbital of SO<sub>2</sub> and the d<sub>xz</sub> or d<sub>yz</sub> orbitals of Pt, whereas  $\sigma$  bonds are formed between the 8a<sub>1</sub> orbital of SO<sub>2</sub> and d<sub>z2</sub> orbital of Pt. It was suggested that atop (Fig. 29a) and two-fold sites (Fig. 29c and d) were energetically accessible for SO<sub>2</sub> adsorption, but that two-fold sites were more favorable.

SO and SO<sub>4</sub><sup>2-</sup> species were identified after SO<sub>2</sub> adsorption on Pt(111) at room temperature [83Köh, 90Höf, 94Sun1, 97Wil, 97Pol, 95Wil]. The formation of SO<sub>4</sub><sup>2-</sup> is of interest because it was reported to be responsible for the poisoning of Pt-catalyzed oxidation of CO and alkenes, and on the other hand, responsible for the promotion of alkane oxidation [99Lee]. XPS indicated some Pt sulfide formation, but no atomic oxygen was found. The following surface reactions were proposed:



The characteristic S (2p) doublet and corresponding O (1s) spectra from high-resolution core-level photoemission are shown in Fig. 30 for adsorption and decomposition of SO<sub>2</sub> on Pt(111) [97Pol]. Two different kinds of SO<sub>2</sub> species forming the monolayer phase at 150 K were indicated by different binding energies. NEXAFS also indicates different molecular orientations for these two species [97Pol]. Quantitative analysis of this data yields an orientation for the molecular plane of 31±10° with respect to the surface normal for the SO<sub>2</sub> phase at 212 K. The phase consisting of both SO<sub>2</sub> species in the monolayer at 148 K was characterized by a tilt angle of 42°, which indicates that the second SO<sub>2</sub> species was more flat lying. At 300 K, an SO<sub>4</sub><sup>2-</sup> species was formed.

The adsorption and the surface geometry of SO<sub>2</sub> on Pd(100) as probed by TPD, HREELS and NEXAFS [85Köl, 88Bur1, 88Bur2, 97Ter], was similar to that on Pt(111). SO<sub>2</sub> was molecularly adsorbed on Pd(100) below 120 K and the SO<sub>2</sub> multilayer could be desorbed at 135 K to leave behind the chemisorbed monolayer. Fig. 31 shows that decomposition of SO<sub>2</sub> occurred above 420 K to leave coadsorbed O and SO, which in turn dissociated at higher temperature. An SO<sub>4</sub><sup>2-</sup> species was formed above 300 K by reaction of SO<sub>2</sub> with O adatoms from SO<sub>2</sub> dissociation. The ( $\nu_s - \nu_a$ ) difference of 215 cm<sup>-1</sup> indicated some bonding occurred through the O atom in addition to S bonding, and so, based on the HREELS data, an  $\eta^2\text{-SO}_2$  bonding geometry was proposed with the molecular plane perpendicular to the surface.

The S K-edge NEXAFS spectra and the Fourier transform of the S K-edge SEXAFS functions  $k^2\chi(k)$  are shown in Fig. 32 for SO<sub>2</sub> adsorbed on Pd(100). Analysis of the S-O shell indicates that the S-O distance was elongated to 1.48 Å from 1.43 Å in SO<sub>2</sub>(g), due to charge transfer into the antibonding  $\pi^*$  orbital. The polarization dependence of the S-O effective coordination number also lead to the conclusion that the C<sub>2</sub> axis of the molecule was tilted by 34° from the surface normal. Thus, one O atom directly interacts with the surface. Comparison of the ratio of the S-Pd effective coordination number,

$N^*(\theta = 90^\circ)/N^*(\theta = 55^\circ) = 0.52 \pm 0.06$ , with the calculated values of 0.57 for bridge, 1.12 for hollow, and 0.00 for atop sites suggested that the S atom in SO<sub>2</sub> was in a bridge site, as shown in Fig. 32c.

Adsorption of SO<sub>2</sub> on Cu single crystal surfaces [89Leu, 92Ahn, 93Ahn, 93Pan, 96Pol, 97Nak1, 97Pan, 97Nak2, 98Pol] has been studied extensively. TPD and fast, high-resolution XPS [93Ahn, 96Pol] revealed that SO<sub>2</sub> decomposition on Cu(100) results in a coadsorbed SO<sub>2</sub> + O phase, with a negligible amount of additional coadsorbed SO and S on the surface. Upon heating to room temperature, a coadsorbed SO + 2O phase formed that exhibited a weak (2×2) LEED pattern. Below 400 K, SO + O recombination appeared to occur to form SO<sub>2</sub> that then desorbed from the surface, leaving S and O adatoms on the surface. An earlier HREELS study [89Leu] had reported the presence of SO<sub>3</sub><sup>-</sup>, suggesting a disproportionation reaction on the surface at room temperature, but this was inconsistent with this conclusion.

NEXAFS and SEXAFS measurements [97Nak1, 97Pan, 97Nak2] provided evidence that SO<sub>2</sub> on Cu(100) was adsorbed with its molecular plane parallel to the surface normal in the coadsorbed SO<sub>2</sub> + O phase formed after heating a condensed SO<sub>2</sub> layer to 180 K. The coadsorbed O adatoms were located in bridge sites. SO species were lying flat on the surface and bound to Cu through both S and O atoms for the coadsorbed SO + 2O phase formed by heating a SO<sub>2</sub> multilayer to 280 K. The S atom in SO was located in hollow sites and the coadsorbed O adatoms were located in bridge sites. Decomposition of SO<sub>2</sub> during TPD resulted in the formation of SO. If no additional SO<sub>2</sub> was delivered from the gas phase during heating of adsorbed SO<sub>2</sub>, the decomposition product SO remained on the surface until it recombined with coadsorbed O adatoms and desorbed as SO<sub>2</sub>; no SO<sub>3</sub><sup>-</sup> was formed. But, in the presence of SO<sub>2</sub>(g), such as occurs for room-temperature SO<sub>2</sub> adsorption, SO<sub>3</sub><sup>-</sup> formation occurs according to



A consistent picture of formation of adsorbed SO<sub>3</sub><sup>-</sup> from adsorption and reaction of SO<sub>2</sub> on Cu(100) at room temperature has now been given [97Nak1]. An example of polarization-dependent S K-edge NEXAFS spectra of SO<sub>3</sub><sup>-</sup> on Cu(100) is presented in Fig. 33. Peaks at 2477.4 and 2479.3 eV were assigned to adsorbed SO<sub>3</sub><sup>-</sup> species by comparing the data to S K-edge spectra of SO<sub>3</sub><sup>-</sup> salts. Curve-fitting analysis of the e\* and a<sub>1</sub>\* peaks determined that the orientation of SO<sub>3</sub><sup>-</sup> species was nearly perpendicular to the surface. In addition, Fig. 33 shows that the calculated spectrum for Model 1 with SO<sub>3</sub><sup>-</sup> in an upright orientation with the S aimed away from the surface was in good agreement with the Fourier transforms of the SEXAFS spectra at  $\theta = 15^\circ$  and  $90^\circ$ . The configuration in Model 1 with the S atoms located above the bridge site and two O atoms occupying the adjacent bridge sites was judged the most probable one.

STM images of SO<sub>2</sub> on Cu(100) revealed two domains, one forming a (2×2) square lattice and the other forming a rhombic c(4×6) structure [97Nak1]. AES, XPS and NEXAFS studies lead to the conclusion that only two types of species, SO<sub>3</sub><sup>-</sup> and S, were present on the surface in a stoichiometric ratio of 2:1 [97Nak1]. All of the bright spots in the (2×2) and c(4×6) domains were assigned to SO<sub>3</sub><sup>-</sup> species and the dim spots appearing in the c(4×6) domain were assigned to S adatoms. Because only SO<sub>3</sub><sup>-</sup> existed in the (2×2) domains, the c(4×6) domains must have a S/SO<sub>3</sub><sup>-</sup> population ratio equal to two.

There are some discrepancies about molecular versus dissociative chemisorption in reports on the adsorption of SO<sub>2</sub> on Ni surfaces and about the orientation of adsorbed SO<sub>2</sub> on Ni(110) [93Zeb, 95Yok1, 95Yok2, 95Ter, 96Yok, 97Jac, 98Wil]. ARUPS and XPS results for SO<sub>2</sub> on Ni(110) suggested that SO<sub>2</sub> adsorption was molecular for temperatures below 150 K, independent of coverage [93Zeb]. The saturated monolayer formed a c(2×2) structure corresponding to an absolute coverage of 0.5 ML. Initial coverages below 0.25 ML dissociated completely upon heating. For higher initial coverages, SO<sub>2</sub> desorption occurred in a single peak between 300 and 400 K. ARUPS was used to assign an orientation of SO<sub>2</sub> such that the molecular plane was tilted and perpendicular to the densely packed substrate rows. This was attributed to Ni-O interactions, as was reported on Pt(111) and Pd(100) surfaces.

A later study of SO<sub>2</sub> chemisorption on Ni(110) by XPS and XAFS indicated partial decomposition of adsorbed SO<sub>2</sub> at 160 K to leave SO<sub>3</sub>(a) and S(a) on the surface [98Wil]. Fig. 34 presents S(2p) and O(1s) spectra obtained at 160 K during annealing a saturation exposure of SO<sub>2</sub> on the Ni(110) surface at 160 K [98Wil]. Two different SO<sub>2</sub> species are apparently formed upon SO<sub>2</sub> adsorption on Ni(110) at 160 K that might correspond to two different adsorption sites. In addition, even at 160 K, SO<sub>2</sub> partially decomposed

to form coadsorbed SO<sub>3</sub><sup>-</sup> and S. Heating the surface at 800 K leaves only S adatoms on the surface, which gives rise to a c(2×2) LEED pattern.

Fig. 35 shows S K-edge NEXAFS spectra obtained after a saturation exposure of SO<sub>2</sub> on Ni(110) at 160 K and after subsequent heating to room temperature and 800 K. The structures in the spectra obtained at 160 K consisted predominately of overlapping  $\pi^*$  and  $\sigma^*$  resonances of adsorbed SO<sub>2</sub>, along with e\* and a<sub>1</sub>\* resonances of SO<sub>3</sub><sup>-</sup>. This was more evident after heating to room temperature where XPS showed only the presence of coadsorbed SO<sub>3</sub><sup>-</sup> and S. The polarization dependence of the spectra suggests that SO<sub>3</sub><sup>-</sup> exists as a trigonal pyramid with the C<sub>3</sub> axis oriented perpendicular to the surface, because the electric dipoles associated with the e\* and a<sub>1</sub>\* transitions are oriented perpendicular and parallel to the molecular axis, respectively. This orientation is like that on Cu(100) [97Pan]. The orientation of SO<sub>2</sub> in the coadsorbed SO<sub>2</sub> + SO<sub>3</sub><sup>-</sup> phase formed by adsorption at 160 K was approximately flat lying because the  $\pi^*$  resonance nearly vanished at normal incidence. Comparison of these experiments with values calculated assuming a two-fold substrate symmetry yielded a tilt angle  $\alpha$  of  $13 \pm 15^\circ$  between the molecular plane of SO<sub>3</sub><sup>-</sup> and the substrate. A flat-lying geometry of adsorbed SO<sub>2</sub> was also found by a similar NEXAFS study on a dilute SO<sub>2</sub> layer on Ni(110) [95Ter].

SEXAFS studies of the phase obtained after SO<sub>2</sub> exposure on Ni(110) at 160 K were performed to determine the adsorption sites of SO<sub>2</sub> and its decomposition products [98Wil]. XPS showed that the phase consisted of coadsorbed SO<sub>2</sub>, SO<sub>3</sub><sup>-</sup> and S with relative coverages of 1, 0.37 and 0.21, respectively. Adsorption sites for different species were determined by comparing measured SEXAFS amplitude ratios with those calculated for different high symmetry sites assuming a S-Ni bond length of 2.30 Å. The simulations also used a SO<sub>2</sub> tilt-angle of  $13^\circ$  between the molecular plane and the surface, as determined by NEXAFS, as well as an S-O-S bond angle of  $106^\circ$  and an upright orientation of the C<sub>3</sub> axis.

The proposed model shown in Fig. 36 includes two different SO<sub>2</sub> species adsorbed in both short- and long-bridged sites, SO<sub>3</sub><sup>-</sup> species that have the S atom located on the short-bridge sites, and S adatoms that occupy two-fold hollow sites [98Wil]. After determining the S sites of the SO<sub>2</sub> and SO<sub>3</sub><sup>-</sup> species by SEXAFS, the corresponding O sites were guessed from the fact that SO<sub>2</sub> lies flat on the surface, as shown in Fig. 36a. For SO<sub>3</sub><sup>-</sup>, two possible symmetric structures were suggested, as shown in Fig. 36b.

NEXAFS was used to show that SO<sub>2</sub> on Ni(111) and Ni(100) at 170 K adopts a very similar geometry as on Ni(110) with the molecular plane parallel to the surface [95Yok1].

#### 3.8.4.4.2.3 Dissociative adsorption of SO<sub>2</sub>

SO<sub>2</sub> adsorption and surface chemistry on Ru(0001) at 100 and 300 K was probed, and S(2p) XPS spectra after sequential exposure of SO<sub>2</sub> on Ru(0001) at 100 K are presented in Fig. 37a [98Jir]. Even at low coverages, multiple S-containing species were present. The final dose of 1 L SO<sub>2</sub> produced a strong peak at 167.9 eV that corresponded to a physisorbed SO<sub>2</sub> multilayer. As shown in Fig. 37b, heating to 160 K caused peaks corresponding to adsorbed S, SO<sub>2</sub>, SO<sub>3</sub><sup>-</sup> and SO<sub>4</sub><sup>2-</sup>. SO<sub>4</sub><sup>2-</sup> was the dominant species above 260 K and annealing to 350 K lead to complete decomposition of SO<sub>2</sub> to leave S adatoms. Small SO<sub>2</sub> exposures on Ru(0001) at 300 K [98Jir] lead to complete decomposition and produced coadsorbed O and two different kinds of S adatoms. SO<sub>3</sub><sup>-</sup> and SO<sub>4</sub><sup>2-</sup> species eventually appeared after high exposures when the number of empty sites was limited. INDO/S and BOC-MP methods predicted that O<sub>3</sub>O- or S,O-coordinated SO<sub>2</sub> species were the most probable precursors for dissociation [98Jir].

#### 3.8.4.4.3 SO<sub>2</sub> adsorption on metals with coadsorbed alkali metals

Adsorption of SO<sub>2</sub> on a Cs-precovered Ag(100) surface at 80 K was investigated using and AES, LEED, TPD, work function measurements and molecular beam back scattering [92Höf, 93Höf]. SO<sub>2</sub> TPD spectra from such a surface are reproduced in Fig. 38a. SO<sub>2</sub> was molecularly adsorbed and desorbed intact from both the clean and modified Ag(100) surface, but coadsorbed Cs shifted the SO<sub>2</sub> desorption peak to higher temperature. This indicated a short-range interaction between SO<sub>2</sub> and Cs that increased the SO<sub>2</sub>



adsorption energy. SO<sub>2</sub> adsorption caused a sharp increase in the work function, as shown in Fig. 38b. This was thought to be consistent with a strong interaction between SO<sub>2</sub> and Cs that would cause neutralization of the Cs-induced charge transfer with the substrate.

High-resolution, synchrotron-based XPS was used to investigate the chemistry of SO<sub>2</sub> on Cs/Mo(110) surfaces, along with that on Mo(110) and MoO<sub>2</sub>/Mo(110), specifically probing the effects of Cs and O on the formation of SO<sub>3</sub><sup>-</sup> and SO<sub>4</sub><sup>2-</sup> species [99Jir2]. Cs addition to the Mo(110) surface enhanced substantially its reactivity with SO<sub>2</sub>, forming SO<sub>3</sub><sup>-</sup> and SO<sub>4</sub><sup>2-</sup> on the surface at 300 K, in contrast to the chemistry on Mo(110). Cs coadsorption also increased the thermal stability of SO<sub>4</sub><sup>2-</sup> compared to that on Mo(110).

#### 3.8.4.3.4 SO<sub>2</sub> adsorption on alloy surfaces

The interaction of SO<sub>2</sub> with several bimetallic surfaces has been studied: ( $\sqrt{3}\times\sqrt{3}$ )R30°-Sn/Pt(111) surface alloy [98Rod], c(2×2)-Mn/Cu(100) surface alloy [98Lu] and Pd/Rh(111) bimetallic surface formed by deposition of a Pd adlayer on Rh(111) [99Rod]. XPS studies of SO<sub>2</sub> on the ( $\sqrt{3}\times\sqrt{3}$ )R30°-Sn/Pt(111) surface alloy revealed that this surface was much less reactive towards SO<sub>2</sub> decomposition than either pure, metallic Sn or the clean Pt(111) surface [98Rod]. On this alloy, SO<sub>2</sub> adsorbed molecularly at 100 K and most of the adsorbed SO<sub>2</sub> desorbed molecularly between 250 and 300 K. Only a small amount of decomposition occurred during TPD to form S and O adatoms. A pure Sn film and the clean Pt(111) surface decomposed SO<sub>2</sub> to form many sulfur-containing species, such as SO<sub>4</sub><sup>2-</sup>, SO<sub>3</sub><sup>-</sup>, SO<sub>2</sub> and S on the surface. The large reduction in the reactivity of Sn in the alloy surface was explained by a combination of ensemble and electronic effects, but it was proposed that electronic effects were the main contributors for the decreased reactivity of Pt in the alloy. This was suggested to arise from a reduction in the electron donor ability of Pt atoms due to rehybridization.

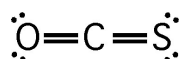
High-resolution XPS indicated that adsorption of SO<sub>2</sub> on the c(2×2)-Mn/Cu(100) surface alloy at room temperature was dissociative, oxidized alloyed Mn atoms to Mn<sup>2+</sup>, and formed adsorbed O and S adatoms on the surface [98Lu]. High exposures also lead to the formation of SO<sub>3</sub><sup>-</sup> and SO<sub>4</sub><sup>2-</sup> complexes on the surface.

For the Pd/Rh(111) bimetallic surface, the Pd<sub>1.0</sub>/Rh(111) surface was less reactive than either pure Pd or Rh(111) [99Rod].

#### 3.8.4.5 OCS

##### 3.8.4.5.1 Structure and bonding of OCS

OCS is isoelectronic with CO<sub>2</sub>, and like CO<sub>2</sub>, it is a linear triatomic molecule in which the central C atom is sp-hybridized and bonded by double bonds to both outer atoms that each have sp<sup>2</sup>-hybridization. However, the presence of O and S atoms breaks the symmetry inherent in CO<sub>2</sub> so that OCS has a dipole moment and unequal bonding in the C=O and C=S bonds. The coordination chemistry literature reveals that OCS is much more reactive than CO<sub>2</sub>, almost exclusively cleaving the C=S bond in dissociation reactions to yield a CO product.



Scheme VII. Lewis structure for OCS.

##### 3.8.4.5.2 OCS adsorption on metal surfaces

There are only a few reports about the interaction of OCS with metal surfaces. OCS adsorption was explored on evaporated Ni and W films over the temperature range of 195-450 K [85Sal]. OCS was

reported to adsorb molecularly at 195 K on both Ni and W films, but to dissociate at higher temperatures into CO and S adatoms. However, a later study on polycrystalline Ni foil using XPS, UPS and AES concluded that chemisorption of OCS was dissociative at all temperatures in the range 77-293 K, yielding adsorbed S and gaseous CO [88Sas]. Tables 17-19 provide the available data on OCS adsorption on metals.

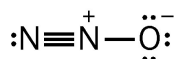
The thermal and photochemical behavior of adsorbed OCS on Ag(111) was investigated [90Zho]. OCS TPD curves after adsorption of OCS on Ag(111) at 128 K are presented in Fig. 39. OCS adsorbed completely reversibly and only desorption of OCS was found in TPD for all exposures. AES spectra recorded after desorption gave supporting evidence and showed no detectable O, C or S left on the surface. The absolute coverage of OCS on Ag(111) was determined by XPS to be  $5.3 \pm 0.5 \times 10^{14}$  molecules/cm<sup>2</sup>. The UPS spectrum shown in Fig. 40 indicates that OCS adsorbs on Ag(111) with very little distortion from its gas-phase structure.

There are a few surface photochemistry studies of OCS adsorbed on Ag(111) [90Zho, 99Kid, 00Kid] and on non-metal surfaces such as LiF(001) [90Leg, 90Dix, 90Pol3], NaCl(001) [97Pic] and GaAs(100) [97Hua]. However, not much is known in this work about the structure and bonding of chemisorbed OCS species or thermal reaction pathways and energetics on these surfaces. The structure and dynamics of an OCS monolayer on NaCl(001) has been investigated by IRAS, helium atom scattering (HAS) and LEED [96Gle, 96Doh].

### 3.8.4.6 N<sub>2</sub>O

#### 3.8.4.6.1 Structure and bonding of N<sub>2</sub>O

Nitrous oxide (N<sub>2</sub>O) is a linear triatomic molecule, like CO<sub>2</sub> and OCS, but its bonding at metal surfaces and surface chemistry is different. The Lewis structure shown in Scheme VIII which schematically shows bonding in the gas-phase molecule indicates why this is so, and also helps to explain the large differences in barriers to cleavage of the two bonds in the molecule; the N≡N bond energy is 113.7 kcal/mol, while the much weaker N–O bond has a bond energy of only 38.7 kcal/mol.



Scheme VIII. Lewis structure for N<sub>2</sub>O.

Knowledge about the coordination chemistry of N<sub>2</sub>O is relatively limited, but N<sub>2</sub>O in coordination compounds behaves as a pseudohalogen, i.e., forming dimers and strong acids with hydrogen. In this respect, its surface chemistry should resemble that of the isoelectronic anion ligands such as cyanate (OCN<sup>−</sup>) and thiocyanate (SCN<sup>−</sup>).

#### 3.8.4.6.2 Adsorption of N<sub>2</sub>O on metal surfaces

On most transition metal surfaces, N<sub>2</sub>O adsorbs via the terminal N atom to form a weak, donor bond through the lone-pair electrons in the 7σ orbital. Such an assignment was made in many studies on the basis that the N–N stretching vibrational band was blue-shifted (shifted to higher energy) while the energy of the N–O stretching band was nearly unchanged from the respective gas-phase values.

Metals can be divided into two groups based on their reactivity toward N<sub>2</sub>O. For example, molecular adsorption of N<sub>2</sub>O occurred on Pt(111), Ir(111) and Ag(111) surfaces [72Wes, 73Wei, 83Ave, 91Kis, 92Saw, 90Cor, 90Gri, 96Sch1], which are less reactive and located in the lower right-hand side of the periodic table, and dissociative adsorption of N<sub>2</sub>O occurred on Ni(100), Ni(110), Ru(0001) and Al(100), desorbing N<sub>2</sub> and leaving O on the surface [81Umb, 82Kim, 83Mad, 96Hua, 81Sau, 87Hof, 89Pas]. While charge transfer from the substrate to N<sub>2</sub>O obviously affects the chemisorption bond strength and reactivity, several papers have suggested that the reactivity of metal surfaces can be qualitatively

determined by the work function ( $\phi$ ) of the substrate: surfaces are more reactive if they have  $\phi < 5.4$  eV and are less reactive if  $\phi > 5.4$  eV. Ag(111) is an exception to such a simple idea, where  $\phi = 4.74$  eV predicts a high reactivity of the surface, but only molecular adsorption and desorption was found. Table 20 presents thermodynamic data for N<sub>2</sub>O adsorption and dissociation parameters are given in Table 21.

#### 3.8.4.6.2.1 Molecular adsorption of N<sub>2</sub>O

Although N<sub>2</sub>O is often considered an effective oxidant under high-pressure conditions, kinetic limitations often inhibit this reaction under UHV conditions. Thus, N<sub>2</sub>O was not observed to dissociate under UHV conditions on Pt(111) [73Wei, 83Ave, 91Kis, 92Saw], Pt(100) [72Wes], Ir(111) [90Cor] and Ag(111) [96Sch1]. Only molecular desorption of N<sub>2</sub>O was seen in TPD. As a useful reference point, N<sub>2</sub>O desorbed at 30 K from condensed N<sub>2</sub>O multilayers on Ag(111) [90Gri].

Several studies have addressed the adsorption of N<sub>2</sub>O on Pt(111) [83Ave, 91Kis, 92Saw]. N<sub>2</sub>O from the multilayer and monolayer phases on Pt(111) desorbs at very low temperatures of 86 and 90-100 K, respectively [83Ave]. Leading edge analysis of the zero order desorption peak from the monolayer gave an initial value for  $E_d = 5.6$  kcal/mol that increased to 6.05 kcal/mol at saturation coverage. This indicates a small adsorption energy and weak bonding interactions between N<sub>2</sub>O and Pt. A similar shift of the N<sub>2</sub>O desorption peak to higher temperatures with increasing coverage was found in later work, along with a (3×3) LEED pattern for the N<sub>2</sub>O monolayer on Pt(111) [92Saw]. Opposite behavior of the N<sub>2</sub>O TPD peak with coverage on Pt(111) was observed too [91Kis], and a similar shift of the N<sub>2</sub>O desorption peak to lower temperatures with increasing coverage was reported on Ir(111) [90Cor]. No evidence of decomposition was found in HREELS. On a Pt(100) surface, N<sub>2</sub>O was reported to decompose at temperatures greater than 1000 K [72Wes].

HREELS was used to determine the nature and geometry of N<sub>2</sub>O adsorption in a monolayer and multilayer on Pt(111) at 78 K, as shown in Fig. 41 [83Ave]. A blue shift of the  $\nu_{N-N}$  stretching mode by 80 cm<sup>-1</sup> was used to conclude that N<sub>2</sub>O bonded to the surface via the terminal N atom. This blue shift arises from kinematic coupling between the molecule and a massive metal atom. This may seem surprising, because in adsorbates such as CO,  $\nu_{CO}$  is red-shifted upon adsorption. For CO, this kinematic blue shift is overshadowed by the reduction in the CO bond strength due to back donation into the CO 2 $\pi^*$  orbital. However, since the corresponding unfilled orbital in the N<sub>2</sub>O molecule, i.e., the 3 $\pi^*$ , is so strongly antibonding, no back donation occurred.

N<sub>2</sub>O is a soft Lewis acid and can bond to the surface by donating charge from either (or both) of the filled non-bonding 7 $\sigma$  or bonding 2 $\pi$  molecular orbitals. Donation from the 7 $\sigma$  orbital is favored because it is located on the terminal N atom, while the 2 $\pi$  orbital is evenly distributed between the terminal N and O atoms, which would imply some oxygen bonding. Because all of the molecular modes,  $\Sigma^+(\nu_{N-N}, \nu_{N-O})$  and  $\Pi(\delta_{NNO})$ , have large intensities in specular scattering in HREELS spectra of chemisorbed N<sub>2</sub>O, configurations with the molecular axis parallel or perpendicular to the surface can be ruled out. This reflects that the molecule must be inclined at the surface. This angle was estimated to be ~35° based on a comparison of the measured, screened intensities of the  $\Sigma^+$  and  $\Pi$  modes in the adsorbate relative to their gas phase IR intensities.

Furthermore, it was assumed that the N-N-O axis of the N<sub>2</sub>O molecule remained linear in the adsorbed species because neither the 7 $\sigma$  or 2 $\pi$  molecular orbital has central N character and so the weak donor bond formed to the surface was unlikely to affect the N-N or N-O bond strength. Two models were proposed for the structure of N<sub>2</sub>O on Pt(111), as shown in Fig. 42, with configuration (b) in Fig. 42 preferred because the more tightly bound 7 $\sigma$  orbital should lead to a linear configuration. Additional evidence that N<sub>2</sub>O bonds via the 7 $\sigma$  orbital on the terminal N atom in the molecule comes from He II UPS spectra for N<sub>2</sub>O on Pt(111) at 50 K. The strong attenuation of the 7 $\sigma$  orbital intensity in spectra from submonolayer and monolayer coverages indicated that the 7 $\sigma$  orbital of N<sub>2</sub>O is more strongly coupled to the surface than other N<sub>2</sub>O valence orbitals.

The strong intensity of the  $\delta_{\text{NNO}}$  bending peak at 590 cm<sup>-1</sup> in HREELS spectra from an N<sub>2</sub>O multilayer, as shown in the bottom trace of Fig. 41, indicated that the physisorbed N<sub>2</sub>O in the multilayer has its molecular axis oriented parallel to the surface.

In a XPS and SIMS study on Ag(111), N<sub>2</sub>O was reported to thermally decompose to form coadsorbed NO<sub>3</sub><sup>-</sup>, NO and O, which were stable up to 426 K [90Gri]. A reinvestigation of the same system later by TPD and AES found no N<sub>2</sub>O dissociation [96Sch1]. These authors proposed that the previous results of N<sub>2</sub>O dissociation on Ag(111) may have been due to the effects of secondary electrons produced by the X-rays used in XPS. They showed that N<sub>2</sub>O in the multilayer was dissociated by 50 and 2500 eV electrons to produce mainly coadsorbed N<sub>2</sub> and O and a small amount of unidentified N<sub>x</sub>O<sub>y</sub> species.

Tables 22 and 23 provide the available data for N<sub>2</sub>O adsorption from UPS and XPS and from vibrational spectroscopy, respectively.

#### 3.8.4.6.2.2 Dissociative adsorption of N<sub>2</sub>O

N<sub>2</sub>O dissociatively adsorbs on reactive metal surfaces such as Ru(0001) [81Umb, 82Kim, 83Mad, 96Hua], Ni(110) [81Sau], Ni(100) [87Hof] and Al(100) [89Pas] to deposit O adatoms on the surface, and on W(110) [81Umb, 79Fug], Rh(100) [96Li], Rh(110) [81Dan] and Ru(10 $\bar{1}$ 0) [80Kle] to deposit both O and N adatoms.

Adsorption and decomposition of N<sub>2</sub>O on Ru(0001) was studied with TPD, XPS, UPS and HREELS [81Umb, 82Kim, 83Mad, 96Hua]. N<sub>2</sub>O adsorption was partly dissociative initially on Ru(0001) at 100 K, but molecular adsorption predominated with increasing exposures. Upon heating, some adsorbed N<sub>2</sub>O dissociated to form N<sub>2</sub>(g) and adsorbed O, and some N<sub>2</sub>O desorbed molecularly in TPD peaks at 120 and 160 K [82Kim, 83Mad]. In another study, three desorption peaks were identified at 116-123, 145 and 160-165 K [96Hua].

HREELS, UPS and ARUPS studies were performed to determine the N<sub>2</sub>O bonding mode on Ru(0001) [81Umb, 82Kim, 83Mad, 96Hua]. HREELS spectra indicated N<sub>2</sub>O coordination to the surface through the terminal N atom in the molecule because there was a blue shift of the  $\nu_{\text{N-N}}$  band from 2224 to 2290 cm<sup>-1</sup> and no change in the  $\nu_{\text{N-O}}$  band, similar to results on Pt(111). At low coverage, very weak intensity of the  $\delta_{\text{NNO}}$  peak at 470 cm<sup>-1</sup> indicated that N<sub>2</sub>O was terminally bonded in a nearly vertical position [83Mad]. At higher coverage, an inclined linear configuration dominated, as observed at all coverages on Pt(111). UPS and ARUPS gave a consistent picture for N<sub>2</sub>O bonding on Ru(0001) via the 7 $\sigma$  orbital localized on the terminal N atom in N<sub>2</sub>O [81Umb, 82Kim]. A physisorbed N<sub>2</sub>O state oriented parallel to the surface was reported to coexist with vertically chemisorbed N<sub>2</sub>O in the same adlayer at high coverages [81Umb]. In HREELS data at high coverages, the intensity of the bending mode at 560 cm<sup>-1</sup> increased, indicating increased tilting of the N<sub>2</sub>O molecular axis away from the surface normal or an additional flat-lying state. Only adsorbed O was found from decomposition of N<sub>2</sub>O on Ru(0001), but both O and N adatoms were observed from decomposition of N<sub>2</sub>O on the more open Ru(10 $\bar{1}$ 0) surface [80Kle].

On Cu single crystals, the more open Cu(110) surface [84Spi] was much more active for N<sub>2</sub>O dissociation than Cu(100) or Cu(111) surfaces. No adsorption or dissociation of N<sub>2</sub>O was observed on Cu(100) or Cu(111) over the temperature range of 90 to 300 K. On Cu(110) at 90 K, adsorption of N<sub>2</sub>O was dissociative at low coverages to produce O adatoms on the surface. Molecular adsorption of N<sub>2</sub>O was observed after an initial coverage of 0.25 ML. ELS of N<sub>2</sub>O on Cu(100) showed a 9.5 eV peak associated with the  $\pi$ - $\pi^*$  transition. Because the dipole moment associated with this transition is oriented parallel to the molecular axis, it was suggested that adsorbed N<sub>2</sub>O was oriented nearly perpendicular to the surface.

On most of the transition metal single crystal surfaces discussed above, N<sub>2</sub>O decomposes to give N<sub>2</sub> and leave O adatoms on the surface. On W(110), both O and N adatoms were found following N<sub>2</sub>O adsorption and dissociation, as investigated using XPS, UPS and XAES at 100 and 300 K [81Umb, 79Fug]. N<sub>2</sub>O adsorption on W(110) at 300 K was completely dissociative, while on W(110) at 100 K, initial dissociation of N<sub>2</sub>O was followed by condensed layers of N<sub>2</sub>O. Heating of the condensed N<sub>2</sub>O layers lead to further dissociation as well as desorption of molecular N<sub>2</sub>O.

XPS spectra of adsorbed N<sub>2</sub>O on W(110) at 100 K [79Fug] are shown in Fig. 43. At low coverage, only one N(1s) peak at 396.8 eV BE and one O(1s) peak at 530.3 eV BE appeared from N<sub>2</sub>O dissociation,

corresponding to N and O adatoms, respectively. With increasing coverages, two new N(1s) peaks at 401.8 and 405.9 eV BE were observed with a splitting (separation) close to that in N<sub>2</sub>O gas. This molecularly adsorbed N<sub>2</sub>O can be readily desorbed by heating to 100 K and can be recondensed on top of the dissociated adlayer produced by heating to 160 K.

Valence band photoemission was used to determine the orientation of adsorbed N<sub>2</sub>O molecules coadsorbed with O and N adatoms from N<sub>2</sub>O dissociation on W(110) [81Umb], as shown in Fig. 44. Spectra taken at polar angles of 83° and 62° with respect to the surface normal were similar, but spectra taken at 41° showed decreased intensities of the two  $\sigma$  orbitals relative to the  $\pi$  orbitals. Because  $\sigma$  states couple strongly with  $E$  parallel to the molecular axis, it was suggested that N<sub>2</sub>O was lying flat, i.e. oriented parallel to the surface.

### 3.8.4.6.3 N<sub>2</sub>O adsorption on alloy surfaces

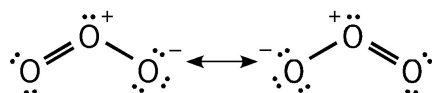
Adsorption of N<sub>2</sub>O on a Cu/Ru(0001) bimetallic surface obtained by depositing Cu on a Ru(0001) substrate was investigated by TPD and AES [81Shi]. A small amount of Cu (<0.02 ML) deposited on Ru(0001) lowered the dissociative sticking probability  $S^{diss}$  of N<sub>2</sub>O by 40%, but only slightly decreased the monolayer saturation coverage. Two possible origins of the large drop in  $S^{diss}$  were suggested [81Shi]. First, Cu could decrease the precursor-state lifetime. Because adsorption of N<sub>2</sub>O on Ru(100) is controlled by precursor kinetics, if Cu atoms at the Ru(100) surface promoted the desorption of N<sub>2</sub>O from this molecular precursor state, this would decrease the precursor lifetime and decrease the dissociation probability. The second possibility was that a restrictive geometric or energetic requirement existed for N<sub>2</sub>O dissociation. It was suggested that a configuration of N<sub>2</sub>O with the molecular axis parallel to the surface was required for dissociation. If there was only a weak interaction of N<sub>2</sub>O on Cu, as predicted from the very small sticking coefficient ( $10^{-5}$ ) of N<sub>2</sub>O on Cu(111), then an N<sub>2</sub>O configuration with the molecular axis parallel to the surface would not occur easily on a Cu-covered Ru(0001) surface. However, no data exists at present to test these molecular level details.

In studies of N<sub>2</sub>O on a Ag/Rh(100) bimetallic surface obtained by depositing Ag on a Rh(100) substrate, the effect of Ag on N<sub>2</sub>O chemisorption was similar to that found for Cu in the Cu/Ru(0001) system [81Dan]. A simple site-blocking model was used to adequately describe the influence of Ag on N<sub>2</sub>O chemisorption on Rh(100).

### 3.8.4.7 O<sub>3</sub>

#### 3.8.4.7.1 Structure and bonding of O<sub>3</sub>

Ozone is a polar triatomic molecule that is isoelectronic with NO<sub>2</sub><sup>-</sup>. It has equal O-O bond distances of 1.28 Å and is bent with an angle of 116° [00Oya]. It has a singlet ground state (no unpaired electrons), with partial double-bond character between each of the oxygen atoms. Scheme IX shows a localized electron picture of the bonding in O<sub>3</sub> along with the resonance structures that are needed. A valence bond view would more clearly illustrate that there are four electrons in the  $\pi$  orbitals of O<sub>3</sub>. A final state effect that arises because of the stability of O<sub>2</sub> creates a very small bond dissociation energy in O<sub>3</sub> with D(O<sub>2</sub>-O) = 25.5 kcal/mol. This causes ozone to be a very reactive oxidant.



Scheme IX. Lewis structures for O<sub>3</sub>.

### 3.8.4.7.2 O<sub>3</sub> adsorption on metal surfaces

No study has yet reported on the molecular chemisorption of O<sub>3</sub> on a well-defined metal surface. The facile dissociation of this molecule, even on a Au(111) surface at 90 K [98Sal], is responsible for this situation, but low-temperature adsorption experiments in the future may be able to trap the molecular precursor to dissociation.

Studies of ozone adsorption on metals that have been reported find dissociative adsorption. Indeed, the high reactivity of ozone compared to O<sub>2</sub> [78Ele, 80Leg, 84Pir, 84Can, 86Sau, 82Nor] or even NO<sub>2</sub>, has been utilized to produce high concentrations of oxygen adatoms on metal surfaces and even to oxidize the surface under mild, UHV conditions. An Ag<sub>2</sub>O film up to 20 µm thick can be created by exposing O<sub>3</sub> to a polycrystalline silver film [01Wat]. In addition, while a number of studies on Au surfaces determined that no dissociative adsorption of O<sub>2</sub> occurred under UHV conditions [78Ele, 80Leg, 84Pir, 84Can], O<sub>3</sub> can be used as a clean source (with no H<sub>2</sub>O or OH contamination) of atomic oxygen on the Au(111) surface [98Sal].

TPD spectra for O<sub>2</sub> desorption after O<sub>3</sub> exposures on Au(111) at 300 K are presented in Fig. 45. Similar results were obtained on Au(111) at 100 K, no lower temperature O<sub>2</sub> or O<sub>3</sub> desorption was observed. The saturation coverage of oxygen on the surface under these conditions corresponds to  $\theta_{\text{O}} = 1.2$  ML. Such experiments give information on the O-Au bond strength and temperatures required for oxygen desorption from the surface. The O<sub>2</sub> desorption activation energy was determined to be 23 kcal/mol, increasing rapidly at low coverages up to 30 kcal/mol near saturation coverage.

Similarly, surface oxygen concentrations of up to  $\theta_{\text{O}} = 2.4$  ML were obtained by exposing O<sub>3</sub> on Pt(111) [99Sal1]. For  $\theta_{\text{O}} \leq 1$  ML, the O<sub>2</sub> TPD peak is due to desorption from chemisorbed oxygen adatoms and shifts to lower temperature with increasing  $\theta_{\text{O}}$  due to lateral repulsions in the adlayer. For  $\theta_{\text{O}} \geq 1$  ML, O<sub>2</sub> desorption is from decomposition of oxidic species in a sharp and narrow TPD peak and the peak temperature shifts higher with increasing  $\theta_{\text{O}}$ .

It may be useful to comment on some related studies of ozone condensation. O<sub>3</sub> deposition on a gold cube substrate at various temperatures utilizing direct deposition or using helium as a carrier gas have been reported [00Cha1]. Ozone forms an amorphous phase for deposition below 11 K, a crystalline phase above 55 K and a mixed phase over the range 11 - 55 K. IRAS was employed to study these phases of solid ozone. The  $\nu_{\text{as}}$  ( $\nu_3$ ) stretching and  $\delta$  ( $\nu_2$ ) bending modes are often used to characterize ozone phases. Fig. 46 shows the  $\nu_{\text{as}}$  and  $\delta$  regions in IRAS spectra of ozone deposited on the substrate under various condition. The spectrum of O<sub>3</sub> deposited at 11 K showed a broad  $\nu_{\text{as}}$  band at 1037 cm<sup>-1</sup>. This band became broader with deposition at 20 and 40 K, which indicated mixed phases. For deposition at 55 K, the  $\nu_{\text{as}}$  band developed into a very narrow line at 1026.9 cm<sup>-1</sup> independent of deposition methods. Ozone desorbed (sublimed) at higher temperatures between 61 and 68 K, with  $E_d = 23 \pm 2$  kJ mol<sup>-1</sup>. The available thermodynamic data for O<sub>3</sub> adsorption is given in Table 24. In addition, Table 25 provides a summary of the vibrational data for O<sub>3</sub> adsorption.

In addition, ozone adsorption was investigated on amorphous and crystalline phases of water (ice) [00Cha1, 01Bor]. If ozone is dosed on amorphous ice at 55 K, it exists as crystalline phase. Two bands appear at 1027.8 and 1033.7 cm<sup>-1</sup> in the region of the  $\nu_{\text{as}}$  band. The band at 1027.8 cm<sup>-1</sup> corresponds to ozone physisorbed on ice and the band at 1033.7 cm<sup>-1</sup> to ozone chemisorbed to free OH in ice pores. Chemisorbed ozone desorbed at slightly higher temperature than physisorbed one indicating that additional activation energy is needed to break the O<sub>3</sub>-HO bond.

### 3.8.4.7.3 O<sub>3</sub> adsorption on alloy surfaces

Dissociative ozone adsorption was found on two alloy surfaces, the (2×2)-Sn/Pt(111) and ( $\sqrt{3} \times \sqrt{3}$ )R30°-Sn/Pt(111) surface alloys [99Sal2]. Both of these two alloys were less reactive towards O<sub>3</sub> than clean Pt(111) at 300 K, but dissociative O<sub>3</sub> adsorption still caused extensive oxygen uptake and oxidation of these alloys. The saturation oxygen coverage after modest O<sub>3</sub> exposures on these surfaces at 300 K was 1.2 and 0.87 ML on the (2×2)- and ( $\sqrt{3} \times \sqrt{3}$ )R30°-Sn/Pt(111) alloys, respectively. This was decreased from  $\theta_{\text{O}} = 2.4$  ML on Pt(111). Dissociative ozone adsorption disorders the surface, dealloying and

extracting Sn into the adlayer. Fig. 47 shows the O<sub>2</sub> TPD spectra obtained after O<sub>3</sub> exposure on the ( $\sqrt{3}\times\sqrt{3}$ )R30°-Sn/Pt(111) surface alloy at 300 K, for example. Initially, only a high temperature peak at 1000 - 1100 K occurs due to O<sub>2</sub> desorption from SnO<sub>x</sub> decomposition. At higher oxygen coverages, a low temperature desorption peak at 700 - 834 K occurs that is similar to that on Pt(111), which is due to O<sub>2</sub> desorption from PtO<sub>x</sub> decomposition.

#### 3.8.4.7.4 O<sub>3</sub> adsorption on metal oxide surfaces

While no studies have been reported on molecular adsorption of ozone on metal surfaces, molecular adsorption of O<sub>3</sub> has been observed on metal oxide surfaces. This work is briefly discussed here to provide some insight into the nature of ozone molecular adsorption. Ozone adsorption has been studied on CaO [97Bul], CeO<sub>2</sub> [98Bul], MgO(poly) [02Ber], SiO<sub>2</sub> [94Bul] and TiO<sub>2</sub>(anatase) [95Bul] powders pressed into pellets. For TiO<sub>2</sub> (anatase) at 77 K with water present on the surface, vibrational bands of O<sub>3</sub> measured by FTIR spectroscopy were at  $\nu_s = 1108$  and  $\nu_{as} = 1034$  cm<sup>-1</sup> indicating that ozone was mostly weakly bound on the surface [95Bul]. Removing the water caused shifts such that  $\nu_s = 1145$  ( $\Delta\nu = + 27$  cm<sup>-1</sup>) and  $\nu_{as} = 990$  cm<sup>-1</sup> ( $\Delta\nu = - 44$  cm<sup>-1</sup>). These relatively large band shifts indicated a large distortion of the O<sub>3</sub> molecule adsorbed on TiO<sub>2</sub> dehydrated at 773 K. O<sub>3</sub> adsorbs on SiO<sub>2</sub> through hydrogen bonding interactions with Si-OH groups at 77 K [94Bul]. In contrast to TiO<sub>2</sub>, most of vibrational modes of O<sub>3</sub> adsorbed on SiO<sub>2</sub> were close to those in solid O<sub>3</sub>, indicating less distortion of the adsorbed O<sub>3</sub> molecules. While O<sub>3</sub> adsorbed on hydrated CaO was only a weak complex, bonding via surface OH groups, FTIR studies of O<sub>3</sub> on dehydrated CaO showed a more distorted geometry of chemisorbed O<sub>3</sub>, suggested to be ozonide ion, O<sub>3</sub><sup>-</sup> [97Bul]. This ozonide species, along with superoxide, O<sub>2</sub><sup>-</sup>, was also detected when O<sub>3</sub> was adsorbed on dehydrated CeO<sub>2</sub> at 973 K [98Bul]. These species appeared to be intermediates of ozone decomposition. FTIR spectra from O<sub>3</sub> deposited on polycrystalline MgO showed two different types of ozone bonding geometries, attributed to two different bonding sites [02Ber]. Fig 48a shows FTIR spectra in the region of the  $\nu_s$  and  $\nu_{as}$  stretching bands. Schematic drawings of adsorbed O<sub>3</sub> geometries are shown in Fig. 48b. Bands **A1** and **A3** in Fig. 48a were assigned to O<sub>3</sub> adsorbed on 5-coordinated Mg<sup>2+</sup> on MgO, as shown in Scheme 1 in Fig. 48b and bands **B1** and **B3** in Fig. 48a were assigned to O<sub>3</sub> adsorbed on defect sites on MgO, as shown in Scheme 2 in Fig. 48b.

#### Acknowledgments

We acknowledge support by the Chemical Sciences, Geosciences and Biosciences Division, Office of Basic Energy Sciences, Office of Science, U.S. Department of Energy.

#### 3.8.4.8 Tables for 3.8.4

##### Organisation of tables

- Table 1.** Thermodynamics of CO<sub>2</sub> adsorption
- Table 2.** Dissociation parameters for adsorbed CO<sub>2</sub>
- Table 3.** Vibrational data for adsorbed CO<sub>2</sub>
- Table 4.** Valence electronic structure for adsorbed CO<sub>2</sub>
- Table 5.** Electronic excitations for adsorbed CO<sub>2</sub>
- Table 6.** Core-level binding energies for adsorbed CO<sub>2</sub>
- Table 7.** Thermodynamics of NO<sub>2</sub> adsorption
- Table 8.** Dissociation parameters for adsorbed NO<sub>2</sub>
- Table 9.** Vibrational data for adsorbed NO<sub>2</sub>
- Table 10.** Photoelectron spectroscopic data for adsorbed NO<sub>2</sub>
- Table 11.** Thermodynamics of SO<sub>2</sub> adsorption
- Table 12.** Dissociation parameters for adsorbed SO<sub>2</sub>
- Table 13.** Photoelectron spectroscopic data for adsorbed SO<sub>2</sub>

**Table 14.** NEXAFS data for adsorbed SO<sub>2</sub>**Table 15.** K-edge SEXAFS spectroscopic data for adsorbed SO<sub>2</sub>**Table 16.** Vibrational data for adsorbed SO<sub>2</sub>**Table 17.** Thermodynamics of OCS adsorption**Table 18.** Photoelectron spectroscopic data for adsorbed OCS**Table 19.** Vibrational data for adsorbed OCS**Table 20.** Thermodynamics of N<sub>2</sub>O adsorption**Table 21.** Dissociation parameters for adsorbed N<sub>2</sub>O**Table 22.** Photoelectron spectroscopic data for adsorbed N<sub>2</sub>O**Table 23.** Vibrational data for adsorbed N<sub>2</sub>O**Table 24.** Thermodynamics of O<sub>3</sub> adsorption**Table 25.** Vibrational data for adsorbed O<sub>3</sub>**Table 1.** Thermodynamics of CO<sub>2</sub> adsorption

Substrate	$T_s$ [K]	Chemi- sorption	Coverage	$T_{des}$ [K]	$E_d$ [kJ/mol]	Technique	Ref.
Ag(111)	40	No				TPD	91Sol1, 87Sak
Ag(110)	300	No	0.25			TPD	83Bac
	100	No				TPD	82Stu
O/Ag(110)							
$\theta_O = 0.1$	100	Yes		480	84-102	TPD	91Sol1, 82Stu
$\theta_O = 0.25$	100	Yes		420	113	TPD	83Bac
Al foil	80	Yes		<295		XPS	87Car
Al(100)	100	No				TPD	91Sol1
Na/Al(100)	100	Yes		285		TPD	91Sol1
Bi(0001)	80	No				XPS, HREELS	91Bro
Cu film	90	Yes (weak)		<200		XPS	98Poh
Cu(110)	80	No				TPD	89Rod
	130	No				TPD	96Kra
Cu(100)	100	No				XPS, HREELS	91Bro
Cs/Cu(110)							
$\theta_{Cs} = 1$	80	Yes	0.25	500-600		TPD	94Car, 01God
	80	Yes	0.25	370, 500		TPD	89Rod
K/Cu(110)							
$\theta_K = 0.5$	100	Yes		<175		HREELS	95Ons
$\theta_K = 0.75$	130	Yes	Satn.	<160		UPS, XPS	96Kra
O/Cu(110)	80	Yes		<295		XPS, HREELS	94Car
O/Cu(211)	80	Yes (weak)		<130		XPS	88Cop
Fe(poly)	80	Yes (weak)		<110		XPS, UPS	87Pir
Fe(111)	77	Yes (weak)		<160		ARUPS, HREELS	86Beh, 87Fre, 87Beh, 87Bau
	100	Yes (weak)		<130	40	HREELS	95Hes
Fe(110)	77	No				ARUPS, HREELS	86Beh, 87Beh, 87Bau
Fe(100)	110	Yes		162		TPD	93Nas
K/Fe(100)	100	Yes	1	590		TPD	89Pau
$\theta_K = 0.83$							
Mg(0001)	88	Yes		<130		XPS, HREELS	91Sol1, 86Cam
Ni(110)	135	Yes (weak)	0.25	<220		HREELS	87Lin
	150	No				NEXAFS, XPS	88Ill
	80	Yes (weak)		<230		ARUPS, HREELS	87Bar1
	300	No				TPD	73McC



Substrate	$T_s$ [K]	Chemi- sorption	Coverage	$T_{des}$ [K]	$E_d$ [kJ/mol]	Technique	Ref.
Ni(100)	150	Yes (weak)		250		TPD	79Ben
O/Ni(110) $\theta_O = 0.3$	80	Yes (weak)		<300		ARUPS, HREELS	87Bar1
Pd(100)	100 130	No	Monolayer	135 200	34	TPD	86Ber 86Ega
Pd(111)	85	No	Monolayer	135	34	ARUPS	89Wam, 90Ehr
K/Pd(100) $\theta_K = 0.05$ $\theta_K = 0.10$ $\theta_K = 0.26$ $\theta_K = 0.42$	100	Yes	0.03	185 215 432 556		TPD	86Ber
Mn-Pd(100)	110	No				UPS	99San
O/Mn-Pd(100)	110	Yes		170		UPS	99San
Na/Pd(100) $\theta_{Na} = 1$ ML	130	Yes	Monolayer	380, 550, 650		TPD	86Ega
Na/Pd(111) $\theta_{Na} = 0.25$ $\theta_{Na} = 0.25$ $\theta_{Na} = 0.25$	85 90 85	Yes (weak)	Monolayer	<125 <120 <120		ARUPS HREELS HREELS	89Wam 90Ehr 89Woh
Pt(111)	112	No				TPD	89Liu, 91Liu
K/Pt(111) $\theta_K = 0.5$	112	Yes		674		TPD	89Liu, 91Liu
Re(0001)	80	Yes	0.5	130	35.5	TPD	87Pel
Rh(111)	300 110 90	Yes (weak) Yes (weak) Yes (weak)	Monolayer	490 244 250	42.7	TPD TPD TPD	78Cas, 79Dub, 80Dub 85Sol 94Sol
B/Rh(111)	300	Yes		502		TPD	84Sol
K/Rh(111) $\theta_K = 1$ $\theta_K = 0.36$	90 90	Yes Yes	Monolayer Monolayer	724 740		TPD TPD	87Sol 94Sol
Ru(0001)	85	Yes	1	100		TPD	94Hof
K/Ru(0001) $\theta_K = 0.33$ ML	85	Yes	1	434, 710		TPD	94Hof
CeO <sub>2</sub>	323	Yes		413, 713		TPD	97Luo
Cr <sub>2</sub> O <sub>3</sub> (0001)	90	Yes		180, 330		TPD	99Sci

**Table 2.** Dissociation parameters for adsorbed CO<sub>2</sub>

Substrate	$T_s$ [K]	Coverage	$T_{dis}$ [K]	Reference
Fe(111)	77		140	87Fre
	100		150	95Hes
Fe(100)	110		300	93Nas
K/Fe(110)	85		140	94Mey2
Cs/Fe(110)	85		140	98Sey
Mg(0001)	88		100	86Cam
K/Pd(100)	100			86Ber
$\theta_K=0.26$			573	
$\theta_K=0.42$			663	
Na/Pd(111)	85	$\frac{\sqrt{7}}{3} \times \frac{\sqrt{7}}{3}$ R10.9°-Na; $\theta_{CO_2}=0.5$	153	90Ehr
$\theta_{Na}=0.25$				
K/Pt(111)	112	Monolayer		89Liu
$\theta_K=0.16$			200	
$\theta_K=1$			640	
Re(0001)	80	$S_{diss}=0.85$ at $\theta \leq 0.1$ $S_{diss}=0.35$ at $\theta=1$ (2×2) structure	135	91Rod
Rh(111)	300	$S_{diss}=10^{-15}$ at $10^{-6}$ torr and 300 K $S_{diss}=10^{-11}$ at 1 atm. and 300 K		83Wei
B/Rh(111)	110		500	84Sol
$\theta_B=0.36$				
K/Rh(111)	90		130	87Sol, 94Sol
$\theta_K=0.36$				

**Table 3.** Vibrational data for adsorbed CO<sub>2</sub>

Substrate	$T_s$ [K]	Coverage	Vibrational frequencies [cm <sup>-1</sup> ]				Adsorption site / Configuration	Technique	Reference
			$\nu_{(M-O)}$	$\delta_{(OCO)}$	$\nu_{s(OCO)}$	$\nu_{a(OCO)}$			
CO <sub>2</sub> (gas)			672		1351	2396		IR	96Fre
Ag(111)	40 50	Satn.			670 645	1320 1307	2360 2380	linear	87Sak 90May
O/Ag(110) $\theta_O=0.1$	100 200		270 660	850, 1050 830, 1050	1280 1360		bent	HREELS	82Stu
$\theta_O=0.25$	100 300	Satn. (2×1) Satn. (4×1)	260 653	830, 1050 847, 1057	1360 1355		bent bent	HREELS HREELS	91Sol1 83Bac
K/Ag(111) $\theta_K=0.26$	50	Satn.		760	1260	1600		HREELS	90May
Cs/Ag(111) $\theta_{Cs}=0.13$	50	Satn.		770	1220	1600		HREELS	90May
Na/Al(foil)	100		460		1310	1480		HREELS	91Sol1
Bi(0001)	80		670		1360	2360		HREELS	91Bro
Cu(100)	160		340	800	1500			HREELS	89Rob
K/Cu(110) $\theta_K=0.4$	107 173 233	Satn.		627 362 1045	1375, 1440 1512 1512	1704 1704 2050		HREELS	95Oms
Cs/Cu(110)	110 298		295 350	660 1060	1460 1510	1660 1660	linear bent	HREELS	94Car
Fe(111)	100 100 150	Satn.		645 766 403	1250 1170 1072, 1170	1370 1370	linear bent bent	HREELS	95Hes, 57Eis
Fe(100)	110 300				1232 1246	1634 1639		HREELS	93Nas
K/Fe(100) $\theta_K=0.83$	100 200	Satn.		650 800, 950	1200	1450	linear bent	HREELS	89Pau
Mg(0001)	131			850, 1090	1390	1630	bent	HREELS	91Sol1, 86Cam

Substrate	$T_s$ [K]	Coverage	Vibrational frequencies [cm <sup>-1</sup> ]				Adsorption site / Configuration	Technique	Reference
			$\nu_{(\text{M-O})}$	$\delta_{(\text{OCO})}$	$\nu_{s(\text{OCO})}$	$\nu_{a(\text{OCO})}$			
Ni(110)	135		387	726	1113		bent	HREELS	87Lin 87Bar1
	140		410	670, 750	1130, 1390	1620			
	200		405	745	1130				
	270		470			1895			
H/Ni(110) $\theta_{\text{H}}=0.1$	90			636			linear	HREELS	91Wam
	90		403	727	1103				
	200		403	727	1353				
						2337			
O/Ni(110)	145			653	1274		2355		87Lin
	220			831	1307	1564			
Na/Pd(111) $\theta_{\text{Na}}=0.25$	100	Satn.	282	645	1298	1452	linear	HREELS	90Ehr, 89Woh
				744	1210	1530			
							bent		
Pt(111)	112	Satn.				1855	2100	HREELS	91Sol1
K/Pt(111) $\theta_{\text{K}}=0.15$ $\theta_{\text{K}}=0.5$	112		430	640, 780	1220	1520	bent	HREELS	91Sol1, 84Seg, 89Liu, 91Liu
	112			660, 870	1240	1610			
							bent	HREELS	91Liu
K/Rh(111) $\theta_{\text{K}}=0.09$ $\theta_{\text{K}}=0.36$ $\theta_{\text{K}}=1.0$	90	Satn.		640	1490		linear	HREELS	91Sol1, 94Sol
						2350			
				646, 840	1440	1630			
				640, 840	1340	1630			
Re(0001)	85	Satn.		650		1600	2350	HREELS	91Sol1, 88Ass
O/Re(0001)	85			650	1290	1650			
Ru(001)	85	Satn.		653		2352	linear	IRAS	88Ass
K/Ru(001)	85	Satn.		666	1342	2357			
$\theta_{\text{K}}=0.33$		$(\sqrt{3}\times\sqrt{3})\text{R}30^\circ$					linear	IRAS	94Hof
Cr <sub>2</sub> O <sub>3</sub> (0001)	90	Satn.			1289		linear	IRAS	99Sei
	200				1301, 1342				
NiO(111)	123	Satn.		910	1263		bent	IRAS	99Mat

**Table 4.** Valence electronic structure for adsorbed CO<sub>2</sub><sup>1</sup>

Substrate	$T_s$ [K]	Structure	Coverage/ adsorbed state	Valence levels [eV]			Technique	Reference
				$1\pi_g$	$1\pi_u / 3\sigma_u$	$4\sigma_g$		
CO <sub>2</sub> (gas)				13.8	17.6 / 18.1	19.4	UPS	87Bar1
CO <sub>2</sub> (solid)				13.0	16.7 / 17.6	18.8	UPS	87Bar1, 84Foc
Cu(poly)	77		Satn.	7.4	11.6	12.9	UPS	76Nor
Cs/Cu(110)	160		Satn.	9.2	13.4	15.0	UPS	01God
$\theta_{Cs}=1.0$								
H/Cs/Cu(110)	160		Satn.	8.9	13.1	14.7	UPS	01God
$\theta_{Cs}=1.0$								
K/Cu(110)			Satn.					
$\theta_K=0.5$	107			8.5	12.6	14.2	UPS	95Ons
$\theta_K=0.75$	130			9.0	13.3	14.8	UPS	96Kra
$\theta_K=1.1$	107			9.0	11.5	18.0	UPS	95Ons
Fe(poly)	80		Satn.	7.9	12.1	13.6	UPS	87Pir
	110			5.8	9.2	11.0		
Fe(111)	77			7.3	11.2	12.8	UPS	86Beh, 87Fre, 87Beh
Cs/Fe(110)	85			8.8	12.6 / 13.2	14.8	UPS	98Sey
$\theta_{Cs}=0.13$								
K/Fe(110)	85		Satn.					
$\theta_K=0.06$				8.8	13.0	14.5	UPS	94Mey1
$\theta_K=0.30$				9.3	13.5	15.0	UPS	98Sey
Ni(110)	80		Submono.	7.3	11.1 / 11.7	13.0	ARUPS	87Bar1
	293		Monolayer	7.0	10.9 / 11.4	12.8	ARUPS	
O/Ni(110)	85		Monolayer	6.8	10.2 / 10.6	12.4	ARUPS	87Bar1
$\theta_O=0.3$	253		Monolayer	7.1	9.0/10.7	12.4		
Na/Pd(111)	85						ARUPS	89Wam
$\theta_{Na}=0.25$				7.8	11.6	13.5		
$\theta_{Na}=2$				10.1	14.1	15.8		
Pt(poly)	77		Satn.	6.9	10.9	12.5	UPS	75Nor, 76Nor
Rh(111)	110			6.6	10.7	12.1	UPS	91Sol1, 88Kis
K/Rh(111)	90	bent		5.2	8.7	10.9	UPS	91Sol1, 88Kis
$\theta_K=0.33$								
K/Rh(111)	90	linear					UPS	88Kis
$\theta_K=0.1$				8.0	12.0	13.6		
$\theta_K=0.3$				8.8	13.0	14.5		
Ca/Si(111)	300		Monolayer	7.6	12.2	14.5	UPS	98Och
$\theta_{Ca}$ =thick film								

<sup>1</sup> Electron binding energies for adsorbed layer are referenced to the Fermi level, with  $E_F = 0$  eV BE.

**Table 5.** Electronic excitations for adsorbed CO<sub>2</sub>

Substrate	$T_s$ [K]	Coverage	Energy loss peaks [eV]					Configuration	Reference
Fe(111)	77	Satn.	6.0	8.5	12.0	15.3			87Beh
Fe(100)	110	Satn.		8.1	11.9				93Nas
	220		3.2	8.7	11.3				
	350		3.2	7.9	11.6				
Pd(100)	100	Satn.	4.0	6.6	14.7		22.3	via O, $\perp$ surface	86Sol
K/Pd(100)	100	Satn.						bent, $\parallel$ surface	86Sol
$\theta_k=0.21$			3.7	11.8	15.6	19.3	24.6		
$\theta_k=0.42$			3.7	11.9	15.4	18.8	24.7		
Rh(111)	100	Satn.			14.0			linear, $\parallel$ surface	85Sol, 94Sol
B/Rh(111)	300			9.4	13.0				84Sol
K/Rh(111)	90	Satn.		8.1	11.9	15.0		bent, bidentate (C <sub>2</sub> O)	91Sol1, 94Sol

**Table 6.** Core-level binding energies for adsorbed CO<sub>2</sub> <sup>1</sup>

Substrate	$T_s$ [K]	Coverage	Adsorption configuration	Core level energies [eV]		Reference
				C 1s	O 1s	
CO <sub>2</sub> (gas)				297.5	541.1	72All
O/Ag(110)	170	Multilayer	bent	287.7	529.9	83Bar
Bi(0001)	80			291.5	535.0	91Bro
Cu(film)	90	Satn.	linear	289.8	532.6	91Sol1, 98Poh
			linear	291.8	535.4	76Nor
Cs/Cu(110)	110	Satn.				89Rod
$\theta_{Cs}=0.48$			linear	292.5	536.3	
K/Cu(110)						
$\theta_k=0.4$	139	Satn.	bent	293.2	531.0	98Llo
	139	Satn.	bent	286.4	531.0	96Kra
O/Cu(211)	130			293.0	533.0	88Cop
Fe(poly)	80	Satn.	linear	291.5	534.8	88Ill, 87Pir
			bent	286.0	531.0	
Fe(100)	110	Monolayer	linear		534.9	93Nas
			bent		531.1	
Fe(111)	77		linear	291.5	534.8	87Bau
			bent	286.0	531.0	
Cs/Fe(110)	85	Monolayer				98Sey
$\theta_{Cs}=0.11$				291.9	535.6	
$\theta_{Cs}=0.30$				292.3	535.9	
K/Fe(110)	85	Monolayer				98Sey
$\theta_k=0.08$			linear	292.3	535.6	
$\theta_k=0.34$			linear	292.3	535.9	
Al(poly)	120			291.3	531.8	87Car
Mg(0001)	88		linear	292.0	533.0	86Cam
Ni(110)	150	Satn.	linear	291.2	534.7	88Ill
			bent	286.4	531.1	
O/Ni(110)	85			283.0	531.2	91Sol1

Substrate	$T_s$ [K]	Coverage	Adsorption configuration	Core level energies [eV]		Reference
				C 1s	O 1s	
Pt(poly)	110	0.5 ML	linear	291.1	534.5	74Nor
	80		linear	291.1	534.5	76Nor
Rh(111)	90	Satn.				91Sol1, 88Kis
			linear	292.0	534.7	
K/Rh(111)	90		linear	292.0	534.0	91Sol1, 88Kis
			bent	290.5	532.8	
Re(0001)	120	Multilayer			530.5	91Rod
Ca/Si(111)	300	Monolayer	bent		532.0	98Och

<sup>1</sup> Electron binding energies for adsorbed layer are referenced to the Fermi level, with  $E_F = 0$  eV BE.

**Table 7.** Thermodynamics of NO<sub>2</sub> adsorption

Substrate	$T_s$ [K]	Dissociative adsorption	Coverage	$E_d$ [kJ/mol]	$T_{des}$ [K]	Technique	Reference
Ag(111)	300	Yes	Satn.			TPD	90Pol1
	500	Yes				TPD	95Bar
Ag(110)	298	Yes	Satn.	75.3	280	TPD	95Bar
	95	No				TPD	87Out
O/Ag(110) $\theta_o = 0.5$ ML	140	No				TPD	87Out
Au(111)	100	No	0.4	58.5	230	TPD	89Bar
	35	No	1.0		230	TPD	93Bec
	85	No	~1	58	220		98Wan1
Pd(111)	530	Yes	< 1.0			TPD	90Ban
	110	No	1.0			TPD	91Wic
Pt(111)	300	Yes		79.5	320	TPD	82Seg
	120	No				TPD	82Dah
	100	No				TPD	87Bar2
	400	Yes				TPD	89Par
Pt(100)	200	Yes			285	TPD	85Sch
O/Pt(111)							
$\theta_o = 0.25$	300	Yes	Satn.		155	TPD	82Seg
$\theta_o = 0.75$	100	No				TPD	88Bar
	300	Yes				TPD	90Par
$\theta_o = 1.0$	120					TPD	82Dah
Sn/Pt(111) ( $\sqrt{3} \times \sqrt{3}$ )R30°	120	Yes	1			TPD	04Vos
Rh(111)	300	Yes	0.5			TPD	95Pet, 99Jir
Ru(0001)	80	No	1	37.7	140	TPD	86Sch1, 86Sch2
	400	Yes				TPD	91Mal
	600	Yes				TPD	91Mal, 92Mal
	800	Yes				TPD	91Mal, 95Hrb
	600	Yes				TPD	96Mit
Ag/Ru(0001) $\theta_{Ag} = 10$ ML	600	Yes				TPD	94Rod
Zn/Ru(0001) $\theta_{Zn} = 1$ ML	80	Yes	Monolayer		245	TPD	93Rod
HOPG	90	No	1	38.5	150	TPD	90Sjö

**Table 8.** Dissociation parameters for adsorbed NO<sub>2</sub>

Substrate	$T_s$ [K]	Coverage/ Adsorbed state	$T_{dis}$ [K]	$E_{diss}$ [kJ/mol]	Reference
Ag(111)	300	Satn.	300		90Pol1
Ag(110)	95	Monolayer	280		87Out
Mo(110)	100		300		00Jir
Pd(111)	110	0.5 ML-(2×2)	180		91Wic
Pt(111)	120	Monolayer	240		82Dah
	100	0.5 (Satn.)	285	79.5	87Bar2
Pt(100)	200	(5×20)	290		85Sch
Rh(111)	110		150		99Jir1
Ru(0001)	80	Monolayer	140		86Sch1
Zn/Ru(0001)	80	Monolayer	80		93Rod
$\theta_{Zn}=1$ ML					
Sn/Pt(111)	120	(4×1)	400		04Vos
$(\sqrt{3}\times\sqrt{3})R30^\circ$					

**Table 9.** Vibrational data for adsorbed NO<sub>2</sub>

Substrate	$T_s$ [K]	Coverage	Vibrational frequency [cm <sup>-1</sup> ]				Technique	Reference
			$\nu_{M-mol}$	$\delta_{(ONO)}$	$\nu_{sym}$	$\nu_{asym}$		
NO <sub>2</sub> (gas phase)				750	1318	1610	FTIR	65Stl
Ag(111)	86			780	1291	1742	IRAS	95Bro1
Ag(110)	95		270	795	1280	1390	HREELS	87Out
Au(111)	100	0.4	250	800	1180		HREELS	89Bar
	85	1.0		805	1178		IRAS	98Wan1
Pd(111)	110		600	790	1170	1545	HREELS	91Wic
	230		465			1575		
Pt(111)	100	Low coverage	300	780	1180	1550	HREELS	87Bar2
	100	High coverage	460	780	1180	1560		
	240	High coverage		795	1190			
O/Pt(111) $\theta_o=0.75$	170	Monolayer	460	795	1270		HREELS	88Bar
		Multilayer	460	795	1270	1750		
Sn/Pt(111) ( $\sqrt{3}\times\sqrt{3}$ )R30°	120	1.0	280	780	1273	1792	HREELS	04Vos
	300			588	1278	1648		
Ru(0001)	80	1.0	440	780	1300	1600	HREELS	86Sch1
	280		440	580		1600		
O/Ru(0001)								
$\theta_o=0.5$	80	1.0	420	810	1220	1580	HREELS	86Sch2
	600	Multilayer	530	820		1795		96Mit
$\theta_o=1.0$	300	Satn.	280	675				97He
HOPG	90	1.0		782	1290	1760	HREELS	90Sjö
GaAs(100)	110			782	1255	1760	IRAS	90vom
O/GaAs(100) $\theta_o$ =thick film	110			850	1670	2235	IRAS	90vom



**Table 10.** Photoelectron spectroscopic data for adsorbed NO<sub>2</sub><sup>1</sup>

Substrate	$T_s$ [K]	Coverage	Valence levels [eV]				Core levels [eV]		Technique	Ref.
			$2\pi_g$	$4\sigma_g$	$1\pi_g$	$3\sigma_g$	N (1s)	O (1s)		
NO <sub>2</sub> (gas)			11.2	14.0	17.6	19.0	412.4	541.3	UPS, XPS	76Bru
Ag (111)	300	Saturation		5.5	10.0	14.0	401.6	531.0	UPS, XPS	90Pol1
	25	Saturation					401.6	531.0		90Pol2
	145	Multilayer					405.8	531.4		
Mo(110)	80	Saturation					404.0		XPS	00Jir
	100	Saturation					398.0	530.5		
Ni (poly)	77	Multilayer	3.2	5.2	9.6	11.3	400.8	531.9	UPS	76Bru
Pd(111)	530	1.0						529.6	XPS	90Ban
O/Pt(111)	400	Saturation								89Par
$\theta_o=0.25$ $\theta_o=0.75$				6.8						
				6.8						
Rh(111)	300	0.5					402.0	532.0		99Jir1
O/Rh(111)	300	0.5					401.3	531.7		99Jir1
$\theta_o=0.6$										
Ru(0001)	800	Multilayer		7.0					UPS	95Hrb
O/Ru(0001)										
$\theta_o=0.4$	600	Multilayer						529.8		92Mal
$\theta_o=0.5$	800	Saturation						529.9		95Hrb
Zn/Ru(0001)	80	1.0					403.8	530.0		93Rod
$\theta_{zn}=1$ ML										
W(110)	100	Saturation		5.8	10.2	15.0	398.0	530.4	UPS	79Fug
	300	Saturation					397.6	530.5		

<sup>1</sup> Electron binding energies for adsorbed layer are referenced to the Fermi level, with  $E_F = 0$  eV BE.**Table 17.** Thermodynamics of OCS adsorption

Substrate	Adsorbate structure	Coverage/ Adsorbed state	$T_{des}$ [K]	$E_d$ [kJ/mol]	Technique	Ref.
Ag(111)		Molecular	128 115		TPD TPD	90Zho 00Kid
Ni film		OCS <sub>ads</sub> : associative at 195 K OCS <sub>g</sub> → OCS <sub>ads</sub> → S <sub>ads</sub> + CO <sub>ads</sub> → S <sub>inc</sub> + CO <sub>g</sub> at ≥293 K		97	TPD	85Sal
Ni(poly)		OCS <sub>g</sub> → OCS <sub>ads</sub> → S <sub>ads</sub> + CO <sub>g</sub> at 77 ~ 293K			UPS, XPS	88Sas
W film		OCS <sub>ads</sub> : associative at 195 K		150	TPD	85Sal
NaCl(001) (2×1)			95		HAS, LEED	97Pic
				25	HAS	96Gle
GaAs(100)			160	39 <sup>1</sup>	TPD	97Hua

<sup>1</sup> Calculated value from Redhead analysis assuming first order desorption and 10<sup>13</sup> s<sup>-1</sup> for preexponential factor.

**Table 11.** Thermodynamics of SO<sub>2</sub> adsorption

Substrate	$T_s$ [K]	Adsorbate Structure	Coverage/adsorbed state	$T_{des}$ [K] (heating rate)	Preexponential factor [s <sup>-1</sup> ]	$E_d$ [kJ/mol]	Technique	Reference	
Ag(111)	105		Multilayer	130	$10^{13}$		TPD	91Cas	
			Compressed Monolayer	145 (2.1 K/s)		37 <sup>1</sup>			
			Monolayer	180		46 <sup>1</sup>			
	77		Multilayer	130	$10^{13}$		MBS, TPD	90Ahn	
			$\alpha$	145					
$\alpha_1$			170	41					
$\alpha_2$			220	54					
Ag(110)	130	p(1×1) c(4×2) p(1×2)	$\alpha_3$	245	61				
			$\alpha_4$	275	69				
			Bilayer / $\alpha_1$	170	$10^{13}$	41	TPD, LEED	84Out	
			Monolayer / $\alpha_2$	225	53				
	77		0.50(±0.05) / $\alpha_3$	275	64				
Multilayer			122	$10^{(16\pm0.5)}$	36	MBS, TPD	90Ahn		
$\alpha_1$			170	$10^{(12.6\pm0.2)}$	41				
$\alpha_4$			277	$10^{(12.6\pm0.2)}$	64				
Multilayer			110			MBS, TPD	81Rov, 92Höf		
Ag(100)	80	(3×1) c(2√2×3√2)R45°	$\alpha_1$	146	$10^{15}$	42			
			$\alpha_2$	240	67				
			$\alpha_3$	330 (2 K/s)	$10^{13}$	86 <sup>1</sup>	TPD	92Höf, 93Höf	
	$\theta_{Cs}=0.3$	80	c(2√2×4√2)R45°	$\alpha_4$ ( $\theta_{Cs}\geq 1.5$ ML)	380		100 <sup>1</sup>		
				$\alpha_5$	660		176 <sup>1</sup>		
$\alpha_6$ ( $\theta_{Cs}\geq 1.5$ ML)				780		209 <sup>1</sup>			
Cu(111)	80		$\alpha_7$	860		231 <sup>1</sup>			
			Multilayer / $\alpha_1$	130			TPD	92Ahn, 93Ahn	
			0.34 ML / $\alpha_2$	280		61.7~64.6			
	Ni(110)	100		Multilayer	112			TPD	93Zeb
	Pd(100)	120		Multilayer	135			TPD	88Bur1
Pt(111)	110		~3 ML	127 (5 K/s)	$10^{13}$		TPD	94Sun1	
			Recombinative desorption	285		72			

<sup>1</sup> Calculated value from Redhead analysis assuming first order desorption and  $10^{13}$  s<sup>-1</sup> for preexponential factor.

**Table 12.** Dissociation parameters for adsorbed SO<sub>2</sub>

Substrate	$T_s$ [K]	Adsorbate structure	Coverage/adsorbed state	$T_{des}$ [K]	$E_d$ [kJ/mol]	Technique	Reference
Cu(111)	80		Dec. on defect sites	480		TPD	93Ahn
Ni(110)	100	c(2×2)	0.5 ML dec. < 0.25 ML	360		TPD, LEED	93Zeb, 95Ter, 98Wil
Pd(111)	160	disordered	$\theta=0.3$ at Satn.	240 330-370	59.6 55.9	TPD, LEED	85Köl
Pd(100)	120		Molecular & dissociative ads.	240 270 465	59 66 116	TPD	88Bur <sup>1</sup> , 88Bur2
Pt(111)	160 160		Molecular + dissociative ads. 0.15 ML	285 275-290		TPD TDMS	97Wil 83Köh

**Table 13.** Photoelectron spectroscopic data for adsorbed SO<sub>2</sub> <sup>1</sup>

Substrate	$T_s$ [K]	Coverage	Valence levels [eV]			Core levels [eV]		Adsorption geometry / Adsorbed species	Technique	Reference
			8a <sub>1</sub>	1a <sub>2</sub> +5b <sub>2</sub>	2b <sub>1</sub> +7a <sub>1</sub>	S (2p <sub>3/2</sub> )	O (1s)			
Gas phase			12.5	13.4	16.5	174.8	539.6		UPS, XPS	75Bru
Ag(110)	125		3.8	-	7.7, 9.0	165.4	530.6	Tilted by 13(±5)°, rotated from [001] at high $\theta$ Upright (within 2°±5°), along the [001] at low $\theta$	XPS, UPS	84Out
Au(111)	77	Multilayer	5.6	6.7	10.1	168.4	532.5		XPS, UPS	75Bru
Cd(poly)		Satn.		6.7	9.1				UPS	95Tou
Cu(100)	178 303	Satn.				164.3, 165.3 165.3, 160.9	531.6, 530.9 531.6, 530.9, 530.2	SO <sub>2, ads</sub> → SO <sub>ads</sub> +O <sub>ads</sub> +S <sub>ads</sub>	XPS	96Pol
Cu(111)	170 285 450	0.24 ML				164.1, 165.3 165.2, 166.4 160.2, 161.3	530.2 530.2 530.2	Less SO <sub>ads</sub> formed than Cu(100)	XPS	96Pol, 98Pol

Substrate	$T_s$ [K]	Coverage	Valence levels [eV]			Core levels [eV]		Adsorption geometry / Adsorbed species	Technique	Reference
			8a <sub>1</sub>	1a <sub>2</sub> +5b <sub>2</sub>	2b <sub>1</sub> +7a <sub>1</sub>	S (2p <sub>3/2</sub> )	O (1s)			
Mn/Cu(100) c(2×2)	300	1/2-satn.				161.5	529.7, 531.9	SO <sub>2,ads</sub> → 2O <sub>ads</sub> + S <sub>ads</sub> (<0.5 L)	HR-PES	98Lu
							529.7, 531.8	SO <sub>2,ads</sub> +2O <sub>ads</sub> → SO <sub>4,ads</sub>		
		Multilayer				161.1, 161.5, 167.3, 166.9, 166.4, 165.9		SO <sub>2,ads</sub> +O <sub>ads</sub> → SO <sub>3,ads</sub> (>1 L)		
Fe(poly)	80	Satn.				166.7	531.2		XPS	78Fur
FeS						161.3			XPS	78Fur
FeSO <sub>4</sub>						168.9	532.5		XPS	78Fur
Ni(poly)	77	Cond.	5.4	6.4	9.8	168.0	532.5		UPS	75Bru
Ni(110)	100	0.24 ML				163.8, 165.0		SO <sub>2</sub> adsorbed molecularly	XPS	93Zeb
	160	0.25 ML				163.4, 164.1, 165.2	531.2, 533	No molecular adsorption at 160 K, formed SO <sub>3</sub> , S, SO <sub>x</sub>	XPS	98Wil
	90	Multilayer	7.3		10.6	169.0	169.0	SO <sub>2</sub> adsorbed molecularly with 0.03 ML S <sub>ads</sub>	XPS, UPS	95Yok2
	170	0.4 ML	6.0		8.9	165.7	165.7			
Pd(poly)	100	Monolayer				165.8		SO <sub>2</sub> adsorbed molecularly at 100 K, no dissociation.	HR-PES	99Rod
		Multilayer				165.8, 168.6		SO <sub>2,ads</sub> → 2O <sub>ads</sub> + S <sub>ads</sub> or		
	300	Multilayer				162.7, 165.7, 167.0		SO <sub>2,ads</sub> +2O <sub>ads</sub> → SO <sub>4,ads</sub> 300 K	XPS, UPS	94Sun1
								Non-dissoc. at 100 K Dissoc. at 300 K		
Pt(111)	100	5 ML				167.6	532.3		XPS,	94Sun1
	130					165.3	530.1			
	60	3 ML	4.7	5.8	9.0				UPS	
	160				8.3					
	160	Satn.				171		η <sup>2</sup> -SO <sub>2</sub> (S,O)	XPS	97Wil
	90	Multilayer				166.4, 167.5, 164.0, 164.8	532.4		XPS	97Pol
						164.0, 164.8				
	148	1 ML				164, 164.8, 166	530.8			
	212	0.43 ML				164.8, 166.0	530.8	Tilted by 31±10°		
Sn(poly)/ Pt(111)	100	0.05 ML				161.6, 164.7 + add'l 166.2	530.5	2SO <sub>2,ads</sub> → SO <sub>g</sub> + SO <sub>3,ads</sub> 100 K	HR-PES	98Rod
		1.5 ML				166.2, 168.8	~531			
		Multilayer				162.2, 166.9, 165.8	533	SO <sub>2,ads</sub> → SO <sub>4,ads</sub> +S <sub>ads</sub> +O <sub>ads</sub> after annealed to 300 K		
	300	Multilayer					530, 531.6			

Substrate	$T_s$ [K]	Coverage	Valence levels [eV]		Core levels [eV]		Adsorption geometry / Adsorbed species	Technique	Reference
			8a <sub>1</sub>	1a <sub>2</sub> +5b <sub>2</sub>	2b <sub>1</sub> +7a <sub>1</sub>	S (2p <sub>3/2</sub> )	O (1s)		
Sn/Pt(111) ( $\sqrt{3}\times\sqrt{3}$ )R30°	100	0.1 ML				164.9, 165.7		HR-PES	98Rod
		2.5 ML				+ add'l 168.0			
	150	Multilayer				168	533		
	350	Monolayer				165.7	530.5		
Rh(111)		Satn.				162.2	530	HR-PES	99Rod
	100	Submono				162, 165.5			
		Multilayer				165.5, 168.5			
	300	Multilayer				162, 165.5, 166.3			
Pd/Rh(111) $\theta_{Pd}=0.5$	100	Submono				162.5, 165.8		HR-PES	99Rod
		Multilayer				165.8, 168.2			
	300	Multilayer				162.5, 165.5,			
						166.0, 167.0			
Ru(0001)	100	Half satn.				161.8, 162.4,		XPS	98Jir
						164.9, 165.4			
		Satn.				168.2			
	300	1/4 satn.				161.8, 162.4	530.8		
Zn(poly)		Satn.				+ add'l 166	530.8, 533	XPS	98Cha
	100	1/5 ML				165.5, 166.9	531.5, 533.4		
		Monolayer				166.9			
	300	Multilayer				166.4, 169.2	~532		
		1/3 ML				161.5, 163.5		UPS	95Tou
		Multilayer				162.5, 165.8,			
						166.8, 167.7			
	300	Multilayer				7.9	9.9		

<sup>1</sup> Electron binding energies for adsorbed layer are referenced to the Fermi level, with  $E_F = 0$  eV BE.

**Table 14.** NEXAFS data for adsorbed SO<sub>2</sub>

Substrate	$T_s$ [K]	Coverage	X-ray incident angle [°]	Azimuth of substrate	O K-edge		S K-edge		Adsorption geometry / Adsorbed species	Reference
					$b_1^*$	$a_1^*, b_2^*$	$b_1^*$	$a_1^*, b_2^*$		
Ag(110)	100	Multilayer			530.7/5.0	535.8/1.6			For 1/3 ML, C <sub>2</sub> axis $\perp$ surface (within 2 $\pm$ 5°) & $\sigma^1 \perp [110]$	91Sol2, 96Gut2
	185	Mono L (~0.3 ML)	90	[110]		531.9/3.6	535.2/0.7	2473.6/1.0	2477.6	
			90	[001]		531.9/0.6	535.2/3.9	2473.6/0.05	2477.6	
			20	[110]		531.9/0.4	534.3/4.1	2473.6/0.1	2477.6	
			20	[001]		531.9/0.6	534.3/4.0	2473.6/0.01	2477.6	
Cu(111)	170	0.24 ML	90		532.5	-	2473.5/1.0 <sup>3</sup>	2478/0.2 <sup>3</sup>	C <sub>2</sub> axis $\perp$ surface (within 12° $\pm$ 10°)	98Pol
			20		-	536				
			30				2473.5/0.4	2478/0.4		
Cu(100)	300	0.15 ML	90					2477.4	3SO <sub>2,ads</sub> $\rightarrow$	97Nak1,
			55					2477.4	2SO <sub>3,ads</sub> +S <sub>ads</sub> at r.t.	97Nak2
			15					2479.3	SO <sub>3,ads</sub> t.p. (C <sub>3v</sub> ) <sup>2</sup>	
	100	Cond.			531.5	536.5	2473.4	2478.6	SO <sub>2,ads</sub> $\rightarrow$ SO <sub>2,g</sub> +O <sub>ads</sub>	97Pan
	180	0.25 ML	90		532.0/1.0	535.6/0.6	2474.2/1.0 <sup>3</sup>	2470.0/0.4 <sup>3</sup>	C <sub>2</sub> (SO <sub>2</sub> )axis $\perp$ surface	
Ni(111)			20				2474.2/0.1	2470.0/1.0	SO <sub>2,ads</sub> $\rightarrow$ SO <sub>2,g</sub> +O <sub>ads</sub>	
			5		535.6/0.3	535.6/1.0			at 280 K	
	92	Cond.					2473.2	2478.4		95Yok1
		0.35 ML	90				2473.3/1.0 <sup>3</sup>	2477/0.1 <sup>3</sup>	Flat-lying; C <sub>2</sub> $\parallel$ surface	
			55				2473.3/0.4	2477/0.5		
Ni(100)			15				2473.3/0.03	2477/1.0		
	150	0.5 ML					2473/1.0 <sup>3</sup>	2477/0.1 <sup>3</sup>	Flat-lying; C <sub>2</sub> $\parallel$ surface	97Jac
							2473/0.4	2477/0.6	S & O are in off-atop	
							2473/0.03	2477/1.0		
	92	Cond.					2473.2	2478.4		95Yok1
Ni(100)	170	0.41 ML	90				2473.3/1.0 <sup>3</sup>	2476.7/0.1 <sup>3</sup>	Flat-lying; C <sub>2</sub> $\parallel$ surface	
			55				2473.3/0.4	2476.7/0.5		
			15				2473.3/0.03	2476.7/1.0		
	92	Multilayer	55		530.7	535.9				95Yok2
	170	~0.4 ML	90		530.7/1.0	534.9/0.2			Flat-lying; C <sub>2</sub> $\parallel$ surface	
			55		530.7/0.4	534.9/0.5				
			15		530.7/0.1	534.9/0.5				

Substrate	$T_s$ [K]	Coverage	X-ray incident angle [°]	Azimuth of substrate	O <i>K</i> -edge		S <i>K</i> -edge		Adsorption geometry / Adsorbed species	Reference
					$b_1^*$	$a_1^*, b_2^*$	$b_1^*$	Position/Area $a_1^*, b_2^*$		
Ni(110)	92	Cond.					2473.2	2478.4	SO <sub>2</sub> is randomly oriented to azimuth.	95Ter
	170	0.24 ML	90				2473.3/1.0 <sup>3</sup>	~2477/0.2 <sup>3</sup>	SO <sub>2</sub> is lying flat on long- & short-bridge site	
			55				2473.3/0.4	~2477/0.7		
			15				2473.3/0.03	~2477/1.0		
	90	Multilayer		<110>			2473.2	2478.4	SO <sub>2</sub>	98Wil
	160	0.25 ML	90				2473.2/0.01 <sup>3</sup>	2477.5/2.0 <sup>3</sup>	SO <sub>2</sub> +SO <sub>3</sub> ; 2.5:1	
			20				2473.2/1.0	2477.5/0.4	Two types of SO <sub>2</sub> : flat-lying (13°) and S in short- & long-bridge sites.	
Pd(100)	170	0.35 ML	90				2473.5/1.0 <sup>3</sup>	2479	C <sub>2</sub> axis tilted by 34°	97Ter
			55				2473.5/0.4	2478		
			15				2473.5/0.1	2478		
Pt(111)	160-270		90				2473.7	2478.2		97Wil
	148	1 ML	90		530.8	535.3			Tilt angle of 42°	
	212	0.43 ML	10		531.6	536.0				
			90		530.8	535.3			Tilt angle of 31±10°	
			10		531.6	536.0				

<sup>1</sup>  $\sigma$  denotes the molecular S-O-S plane that contains all three atoms.

<sup>2</sup> Trigonal pyramid structure is labeled by *t.p.*

<sup>3</sup> Calculation based on figures contained in cited references.

**Table 15.** K-edge SEXAFS spectroscopic data for adsorbed SO<sub>2</sub>

Substrate	$T_s$ [K]	Coverage/ Adsorbate state	X-ray incident angle [°]	Azimuth of substrate	FT peak of S-O bond [Å]	S-O distance [Å]	M-S [Å]	M-O [Å]	Elongation of bond [Å]	Reference
Gas phase										
Cu(100)	100	Multilayer			1.03	1.43				93Pan
					1.03	1.43±0.02			-	93Pan
					1.0	1.48±0.03			0.05	
300		0.15 ML	90, 15		1.0	1.49±0.03	2.30±0.02		0.06	97Nak1
					90	1.48	2.3	2.0	0.06	97Pan
					20	1.42				
280						1.43±0.03	2.34±0.05	2.15±0.05		
						1.43±0.03	2.33±0.05	2.14±0.05	-	98Pol
						1.48±0.03			0.05	
Ni(111)	170	0.35 ML	90		1.1	1.48±0.03	2.16±0.05		0.05	95Yok1
					1.1	1.51±0.03	2.18±0.05		0.08	95Yok1
					1.1	1.49±0.03	2.20±0.03		0.06	95Ter
160		0.25 ML	90	<100>		1.50±0.05	2.30±0.04			
					20		2.28±0.04			
					90		2.31±0.04			
					20		2.29±0.04			
Pd(100)	170	0.35 ML			1.0	1.48			0.05	97Ter

**Table 16.** Vibrational data for adsorbed SO<sub>2</sub>

Substrate	$T_s$ [K]	Coverage/ Adsorbed state	Vibrational frequencies [cm <sup>-1</sup> ]					Adsorption site/ Configuration	Technique	Reference
			$\nu(\text{M-SO}_2)$	$\nu(\text{M-O})$	$\delta(\text{SO}_2)$	$\nu_s(\text{SO})$	$\nu_{as}(\text{SO})$			
Gas					517.7	1151.4	1361.8		IR	72Shi
Solid					521	1147	1308, 1330		IR	54Pol
Ag(110)	100	Multilayer	200	-	530	1145	1320	Monolayer: on-top or 2- fold bridging site/ tilted	HREELS	86Out1
	100	Monolayer				1005				
	100	Monolayer	210	360	505, 660	985	-			
									HREELS	91Sol2





**Table 19.** Vibrational data for adsorbed OCS

Substrate	$T_s$ [K]	Vibrational Frequencies [cm <sup>-1</sup> ]			Technique	Reference
		$\delta(\text{OCS})$	$\nu(\text{CS})$	$\nu(\text{CO})$		
Gas phase		520	859	2062	IR	77Shi
In Ar liquid	84.4	519.77	858.93	2052.50	IR	91Zit
NaCl(001)	77			2058.3	s FTIR	96Doh
				2065.2	m	
				2070.1	sh	
				2071.3	s	
				2074.2	sh	
				2076.3	s	

**Table 20.** Thermodynamics of N<sub>2</sub>O adsorption

Substrate	$T_s$ [K]	Coverage/ adsorbed state	$T_{des}$ [K]	$E_d$ [kJ/mol] <sup>1</sup>	Technique	Reference
Ag(111)	83	Multilayer 0.44 ML / Monolayer	86 (1 K/s) 94-102		TPD	96Sch1
	45	Multilayer Monolayer	78-83 83-86		IRAS	95Bro2
Cu(111)	90	No ads. & dec. at 100 K			UPS, ELS, XPS	84Spi
Cu(100)	90	No ads. & dec. at 100 K			UPS, ELS, XPS	84Spi
Ir(111)	84	No dissoc.	93 (1 K/s) 102		TPD	90Cor
Pt(111)	50	Multilayer	86 (0.8 K/s)	21.9	TPD	83Ave, 91Kis, 92Saw
		0.44 ML - (3×3)	90-100	23.4-25.3		
Ru(0001)	75	Multilayer	95		TPD	96Hua

<sup>1</sup> Calculated value from Redhead analysis assuming first order desorption and 10<sup>13</sup> s<sup>-1</sup> for preexponential factor.

**Table 21.** Dissociation parameters for adsorbed N<sub>2</sub>O

Substrate	$T_s$ [K]	Coverage/ Adsorbed state	$T_{dis}$ [K]	$E_d$ [kJ/mol]	Products by dissociation	Initial reaction probability, $P$	Technique	Reference
Al(100)	80	0.11 ( $\pm 0.03$ ) ML			N <sub>2</sub> (g) + O <sub>ads</sub>	0.0016 at 80 K	XPS	89Pas
Cu(110)	90	$\theta > 0.25$ ML: N <sub>2</sub> O ads $\theta < 0.25$ ML: Dec.	400		N <sub>2</sub> (g) + O <sub>ads</sub>	$\sim 0.7$ at 100K	UPS, ELS, XPS, MBS	84Spi, 96Bro
Ni(110)	323-873				N <sub>2</sub> (g) + O <sub>ads</sub>		MBRS, AES	81Sau
Ni(100)	170-500			26.1 $\pm$ 1.5	N <sub>2</sub> (g) + O <sub>ads</sub>		MBRS, AES	87Hof
Rh(111)	200-573	Inert to N <sub>2</sub> O Ads. & dec. on defects			N <sub>2,ads</sub> + O <sub>ads</sub>		MBRS, XPS	96Li
Rh(110)	200-573	Dec.			N <sub>2,ads</sub> + O <sub>ads</sub>	0.55 at 198 K	MBRS, XPS	96Li
Rh(100)	530-680					0.48 at 530 K	AES	81Dan
Rh(100) + 0.5 ML Ag	530-680	Ag block sites for N <sub>2</sub> O dissociation				$\sim 0$ at 530 K	AES	81Dan
Ru(0001)	75	Multilayer Molecular and dissociative ads.	95 116-123 145 160-165		N <sub>2</sub> (g) + O <sub>ads</sub>	0.46	TPD, XPS, UPS	81Umb, 82Kim, 83Mad, 96Hua
Ru(10 $\bar{1}$ 0)	150	dec. at 150 K	150		<sup>15</sup> N <sub>2,ads</sub> + O <sub>ads</sub>		TPD	80Kle
Ru(0001) + 0.14 ML Cu	300-900					Decreased initial reaction probability by 75% at 520 K		81Shi
W(110)	100	Condensed layer at high expos. Dec. at low expos.			N <sub>2,ads</sub> + O <sub>ads</sub>		XPS, UPS	81Umb, 79Fug
Si(100)	90	Multilayer $\alpha$ -N <sub>2</sub> O $\beta$ -N <sub>2</sub> O	110 150	26.4 36.4	N <sub>2</sub> (g) + O <sub>ads</sub>		TPD	97Kub
	60	1.3 ML	80	20	N <sub>2</sub> (g) + O <sub>ads</sub>		TPD	96Kat

**Table 22.** Photoelectron spectroscopic data for adsorbed N<sub>2</sub>O<sup>1</sup>

Substrate	$T_s$ [K]	Coverage/ Adsorbed state	$\Delta\phi$ [eV]	Valence levels [eV]			Core levels [eV]			Technique	Reference
				$2\pi$	$7\sigma$	$1\pi$	$6\sigma$	N(1s)	O(1s)		
Gas phase				12.9	16.4	18.2	20.1	408.5, 412.5	541.2		70Tur, 74Rob
Ag(111)	32	Multilayer						402.5, 406.3	535.1	XPS	90Gri
		1 ML						402.3, 406.3	535.1		
Al(100)	80	Satn.						403.5, 407.1	532.0	XPS	89Pas
Au(111)	77	condensed		6.1	9.5	11.3	13.3	401.6, 405.6	534.5	XPS, UPS	75Bru
Cu(111)				6	9.5	11.5	13.3	402, 406	535	XPS, UPS	79Joh
Cu(100)	80	0.08 ML						402, 406	534.9	XPS	79Joh
Cu(110)	90	Monolayer	0.27 at 0.5 L N <sub>2</sub> O	6.2	9.6	11.6	13.5			UPS	84Spi
Ni film	77	Condensed		6.3	9.7	11.5	13.4	402.0, 406.0	534.6, 531.5	XPS, UPS	76Bru, 75Bru
	300								530.5		
Pt(111)	50	2 ML		6.7	10.0	11.8	13.6	401.4, 405.6	534.1	XPS, UPS	91Kis
		1 ML	-0.8 at 3 ML	5.9	9.3	11.0	12.8	401.0, 405.0	533.9		
		0.15 ML		~5.9		~11.0	~12.8	401.6, 405.0	~533.9		
Ru(0001)	100	$\gamma$ , $\theta_{\text{low}}$ , Flat lying		6.3	9.9	11.6	13.6	401.6, 405.6	534.3	XPS, UPS	81Umb
		$\alpha$ , $\theta_{\text{high}}$ , Flat lying		5.2	8.9	10.6	12.6	400.5, 404.5	533.2		
		$\nu$ , $\theta_{\text{high}}$ , Vertical		6.0	7.7	11.0	13.2	400.9, 403.6	533.5		
		$\theta_{\text{low}}$						399-409 (broad)	~534	XPS	82Kim
		$\theta_{\text{high}}$						401.8, 405.7	534.2		
W(110)	100	Flat lying at $\theta_{\text{low}}$						400.6, 404.4	533.6	XPS, UPS	81Umb,
		At saturation		6.1	9.6	11.4	13.4	401.8, 405.9	534.3		79Fug
Si(100)	60	1.2 ML						403, 407	536	XPS	96Kat

<sup>1</sup> Electron binding energies for adsorbed layer are referenced to the Fermi level, with  $E_F = 0$  eV BE.

**Table 23.** Vibrational data for adsorbed N<sub>2</sub>O

Substrate	$T_s$ [K]	Coverage/ Adsorbed state	Vibrational frequencies [cm <sup>-1</sup> ]					Technique		Reference
			$\nu$ (M-N <sub>2</sub> O)	$\delta$ (NNO)	$2\delta$ (NNO)	$\nu$ (NO)	$\nu$ (NN)	$2\nu$ (NO)		
Gas phase		<sup>14</sup> N <sup>14</sup> N <sup>16</sup> O	588.7		1284.9	2223.7		IR		72Shi
		<sup>14</sup> N <sup>15</sup> N <sup>16</sup> O	585.3		1269.9	2201.6				
		<sup>15</sup> N <sup>15</sup> N <sup>16</sup> O	571.9		1265.3	2154.7				
Solid phase	65		589		1293	2235		IR		64Yam
[Ru(NH <sub>3</sub> ) <sub>5</sub> N <sub>2</sub> O]Br <sub>2</sub>	298	Linear NNO			1157	2236		2312	IR	74Dia, 72Bot
Ag(111)	67	Multilayer			1296	2223, 2249	2580		IRAS	95Bro2
		Monolayer			1279	2227				
		Submonolayer			1277	2228				
Cu(110)	85	Multilayer			1273, 1308	2225, 2267			IRAS	96Bro
		Monolayer			1308	2250				
		Submonolayer			1310	2249				
Ir(111)	84	Multilayer	330	570	1280	2320		HREELS	90Cor	
Pt(111)	78	Multilayer:    to surf.		590	1180	1300	2230	2590	HREELS	83Ave
		Monolayer: end-on, inclined 35° to surf.	325	575	1300	2310				
Ru(0001)	75	$\theta_{\text{high}}$ =coexisted with horizontal physisorbed	230	540~560	1290	2290	2570		HREELS	83Mad
		$\theta_{\text{low}}$ =vertical chemisorbed		470		2224				
Si(100)	90	Multilayer		589	1282	2242			EELS	97Kub
		$\alpha$ -N <sub>2</sub> O: unclear	363		1411	2323				
		$\beta$ -N <sub>2</sub> O: bonded via <i>z</i> -N				1637				

**Table 24:** Thermodynamics of O<sub>3</sub> adsorption

Substrate	<i>T<sub>s</sub></i> [K]	Coverage/ Adsorbed state	<i>T<sub>des</sub></i> [K]	<i>E<sub>d</sub></i> [kJ/mol]	Technique	Reference
Au cube	11	Amorphous	61 - 68	23 ±2	FTIR	00Cha1
	50	Crystalline				
H <sub>2</sub> O: Ice	50		70 - 90	20 ±3	FTIR, TPD	01Bor
Au(111)	300	decomposed to give 1.2 ML O			TPD, UPS, LEED	98Sal
Pt(111)	300	decomposed to give 2.4 ML O			TPD, LEED	99Sal1
Sn/Pt(111) (2×2)	300	decomposed to give 1.2-ML O			AES, TPD	99Sal2
Sn/Pt(111) (√3×√3)R30°	300	decomposed to give 0.87-ML O			AES, TPD	99Sal2

**Table 25:** Vibrational data for adsorbed O<sub>3</sub>

Substrate	$T_s$ [K]	Adsorbed state	Vibrational frequencies [cm <sup>-1</sup> ]					Technique		Reference
			$\delta(\text{O}_3)$	$\nu_{\text{as}}$	$\nu_s$	$\nu_{\text{as}} + \nu_s$	$3\nu_{\text{as}}$			
Gas phase			700.9 w	1042.1 s	1103.1 vw	2110.7	3046.1	IR		68MacC, 77Shi
	4		704	1050	1120	2110	3060	IR		58Har
	5		703.9	1037	1108.8	2108.1	3033.6	IR		93Bro
Ar matrix	20		703.6, 704.2	1039.7, 1041.2	1105.1			FTIR		96Sch2 93Bro
	16		701	1038	1104			Raman		72And
Kr matrix	30		701.66	1036.05	1103.2	2103.7		FTIR		93Bro
Ne matrix	5		699.63	1039.87, 1038.7	1104.4	2109.7, 2107.6	3041.5, 3041.0	FTIR		93Bro
	17		704.2	1042.8	1108.3	2117.1	3051.4	FTIR		96Sch2, 93Bro
N <sub>2</sub> matrix	35		699.1	1043.14	1097.31	2090.3, 2091.1		FTIR		93Bro
Au plated Cube	11	Amorphous	703.5	1037.1	1106.1	2110.1				00Chal
	50	Crystalline	707.6	1026.9	1107.1	2108.6	3033.9			

Substrate	$T_s$ [K]	Adsorbed state	Vibrational frequencies [cm <sup>-1</sup> ]				Technique	Reference
			$\delta$ (O <sub>3</sub> )	$\nu_{as}$	$\nu_s$	$\nu_{as} + \nu_s$		
CaO powder	77	Physisorbed Chemisorbed		1035	1106	2106	FTIR	97Bul
				1034.5	1109	2113		
CeO <sub>2</sub> powder	77		705	1035	1104		FTIR	98Bul
H <sub>2</sub> O: amorphous ice	55	Physisorbed + Chemisorbed		1027.8			IRAS	00Cha1
				1033.7				
	25 45	Solid aggregates		1029 1036			FTIR	01Bor
H <sub>2</sub> O: crystalline ice	55	Physisorbed		1027.8			IRAS	00Cha1
MgO(poly)				1024, 1038	1105, 1140		FTIR	02Ber
SiO <sub>2</sub>	80	<sup>18</sup> O <sub>3</sub>	703	1037	1104 <sup>1</sup>	2106.4	FTIR	94Bul
	80		664	978.8	1044.7 <sup>1</sup>	1992.1 2867		
TiO <sub>2</sub> (anatase)	77	O <sub>3</sub> on hydrated		1034	1108		FTIR	95Bul
		O <sub>3</sub> on dehydrated		990	1145			

<sup>1</sup> Predicted value.

## 3.8.4.9 Figures for 3.8.4

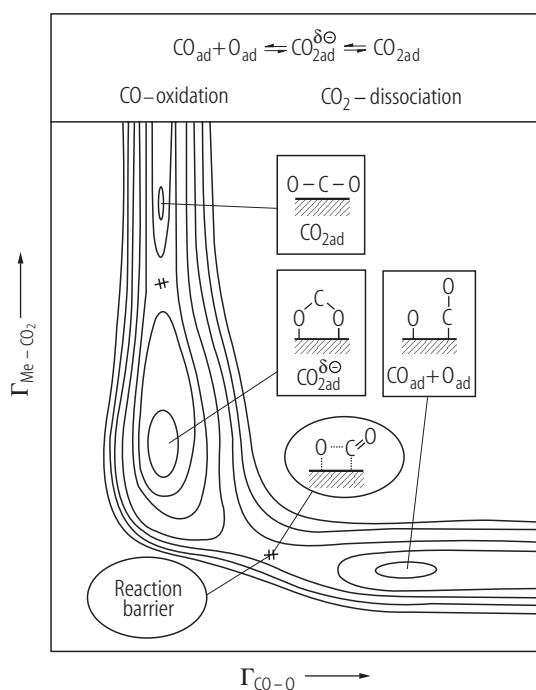


**Fig. 1.** Schematic two-dimensional potential energy diagram for metal-CO<sub>2</sub> interaction (vertical axis) and CO-O-dissociation (horizontal axis). [87Bar1]

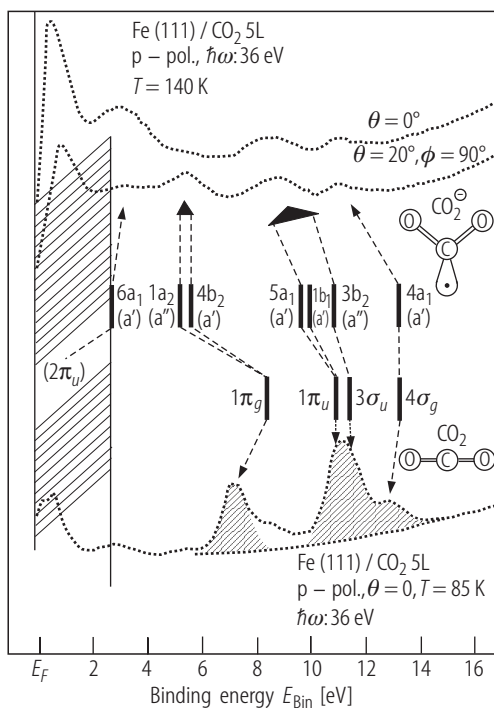


**Fig. 2.** Assignment of the photoelectron spectra at 85 K (lower curve) and 140 K (normal emission  $\theta = 0^\circ$ , and off normal emission  $\theta = 20^\circ$ ,  $\phi = 90^\circ$ ) to undisturbed molecular CO<sub>2</sub> and adsorbed CO<sub>2</sub><sup>δ</sup> based on *ab initio* calculations [87Fre].

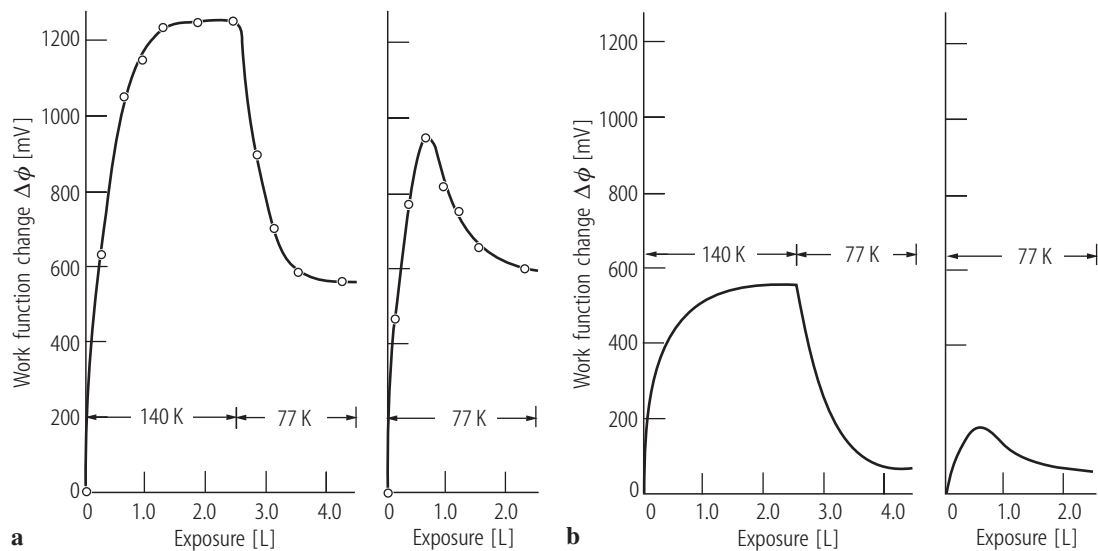


**Fig. 3** Change in work function due to adsorption of CO<sub>2</sub> on Fe(111) (a) and stepped Fe(110) (b) at 140 and 77 K [86Beh].



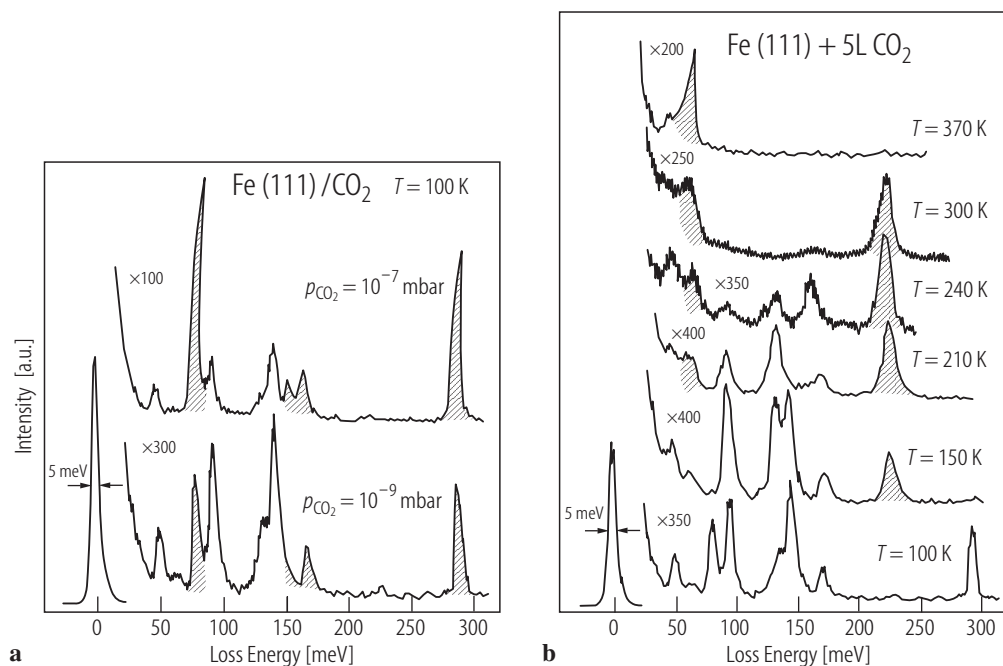


**Fig. 4** (a) HREELS spectra taken from Fe(111) under permanent CO<sub>2</sub> pressure ( $10^{-9}$  mbar, lower spectrum), ( $10^{-7}$  mbar, upper spectrum) and 100 K surface temperature. The shaded areas denote loss peaks that grew with increased pressure. (b) Series of HREELS spectra taken from Fe(111) under permanent CO<sub>2</sub> pressure of  $10^{-9}$  mbar and different temperatures as indicated. The shaded areas correspond to loss peaks of the CO<sub>2</sub> dissociation products of CO, O and C [95Hes].

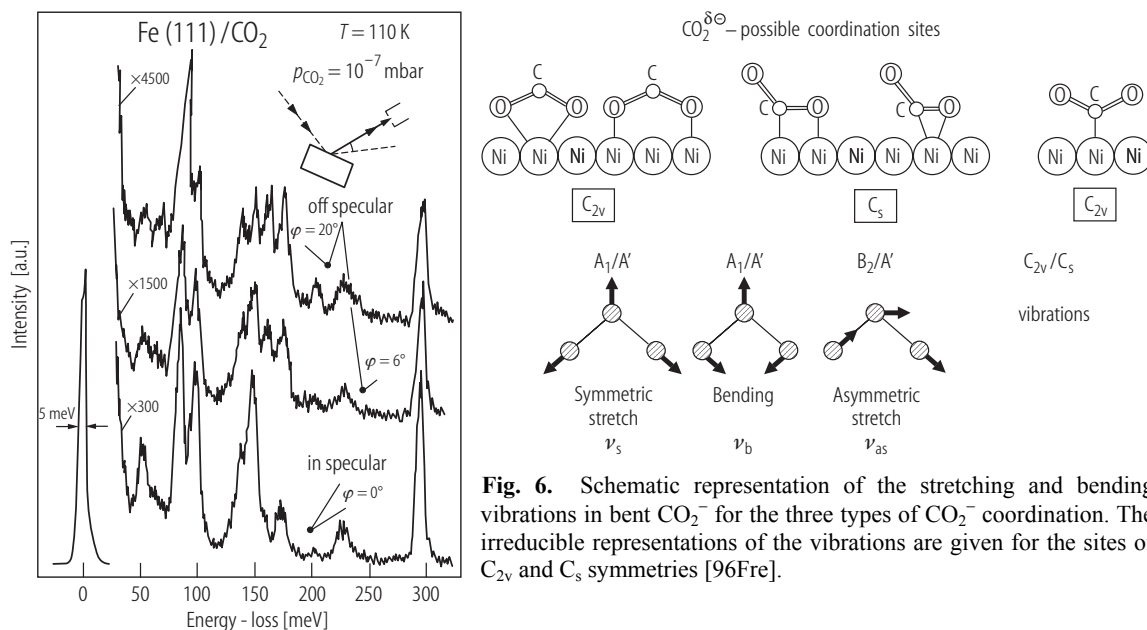


**Fig. 5** Series of HREELS spectra taken from Fe(111) under permanent CO<sub>2</sub> pressure of  $10^{-7}$  mbar and different off-specular angles as indicated. [95Hes].

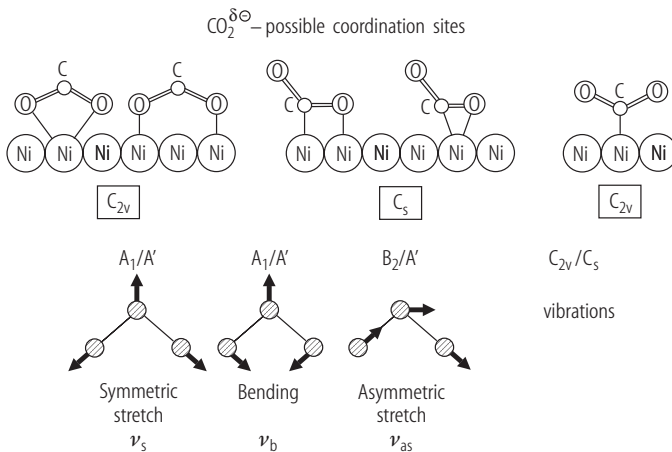


**Fig. 6.** Schematic representation of the stretching and bending vibrations in bent CO<sub>2</sub> for the three types of CO<sub>2</sub><sup>-</sup> coordination. The irreducible representations of the vibrations are given for the sites of C<sub>2v</sub> and C<sub>s</sub> symmetries [96Fre].

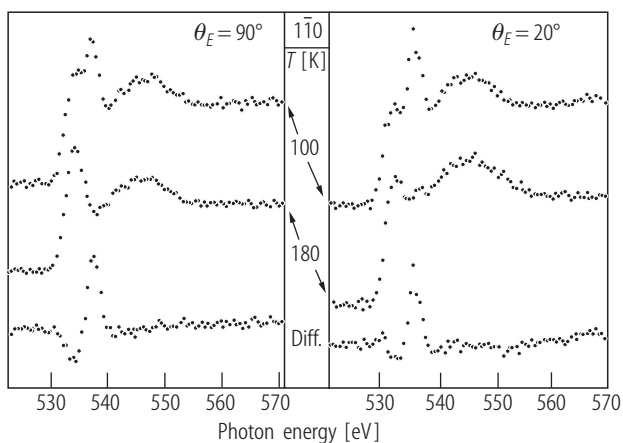


**Fig. 7.** NEXAFS spectra at the oxygen edge. The spectrum at 180 K has been subtracted from that at 100 K.  $\theta_E = 90^\circ$  (left panel),  $\theta_E = 20^\circ$  (right panel) [88III].

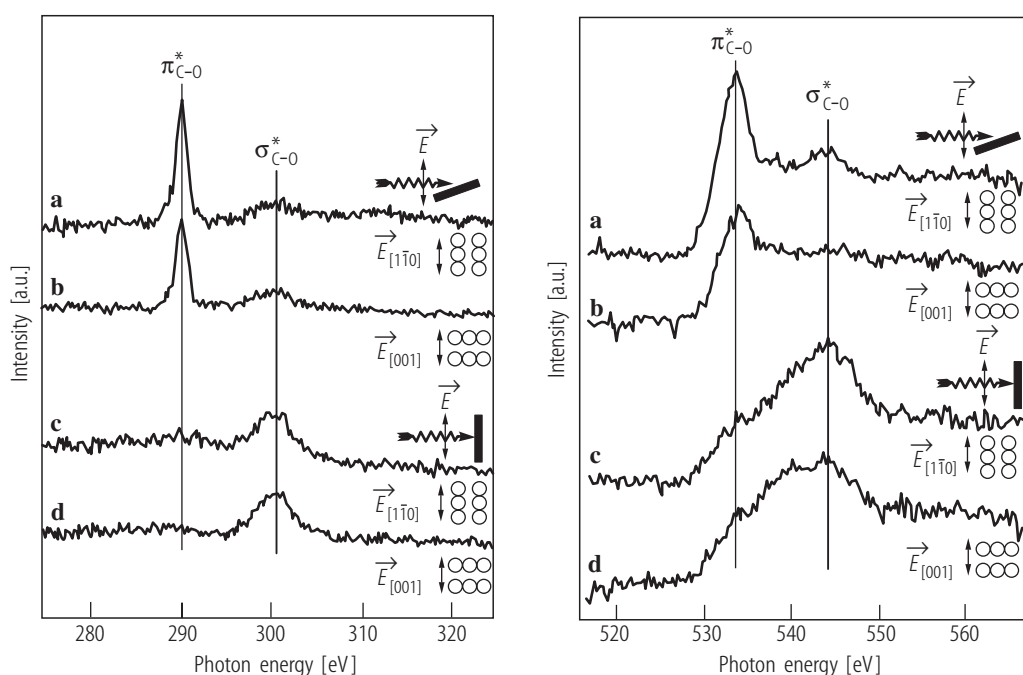


**Fig. 8.** Carbon (left) and oxygen (right) K-edge NEXAFS spectra for surface carbonate on Ag(110) at room temperature are shown as a function of polar and azimuthal orientations. The  $\pi^*$  resonance is predominate at glancing incidence ( $\theta = 20^\circ$ ) and the  $\sigma^*$  resonance is predominate at normal incidence indicating that the C-O bonds of the carbonate species lie in the plane parallel to the surface [88Mad].

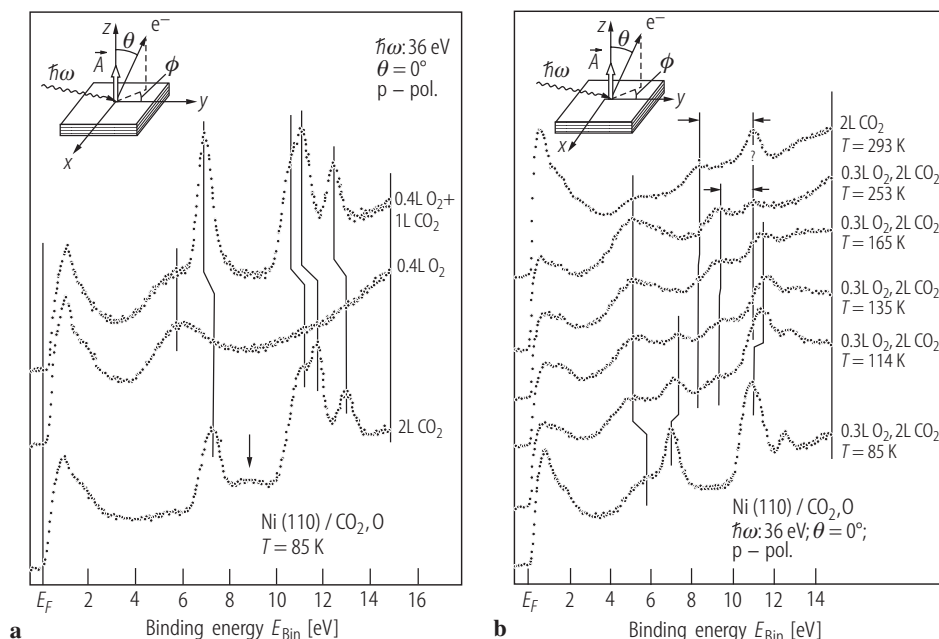


**Fig. 9.** (a) Comparison of a pure Ni(110)/CO<sub>2</sub> adsorbate with a CO<sub>2</sub> adsorbate on an oxygen precovered surface. For reference the spectrum of the oxygen covered surface is shown. (b) Photoelectron spectra recorded at normal emission of the CO<sub>2</sub>, O/Ni(110) coadsorbate as a function of surface temperature. For comparison, the spectrum of a dissociated CO<sub>2</sub>/Ni(110) adsorbate is shown at the top [87Bar1].

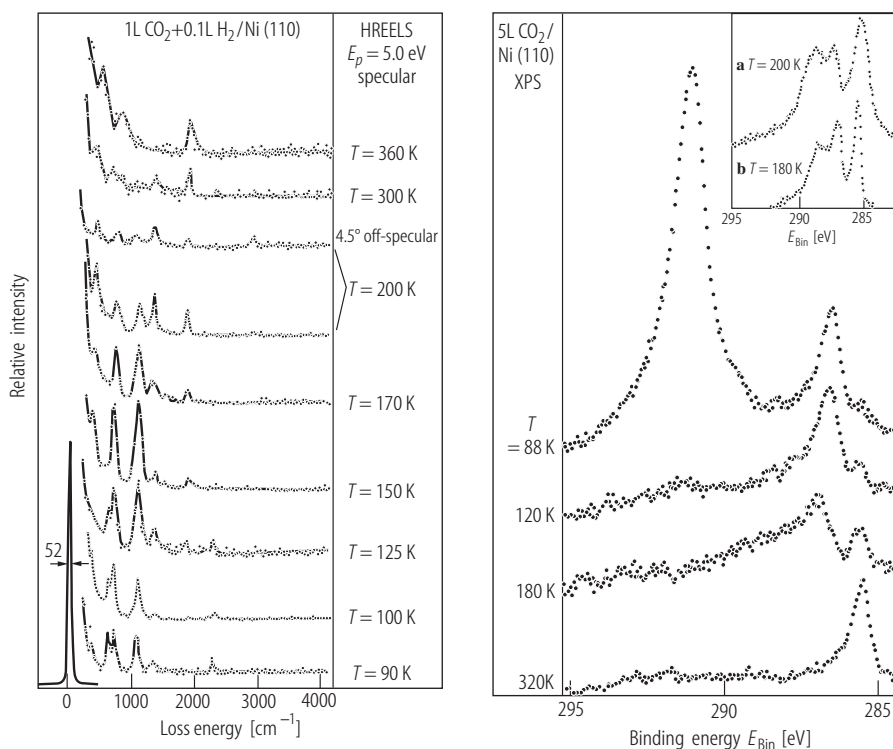


**Fig. 10.** HREELS spectra obtained after heating a Ni(110) surface that had been dosed with 1 L CO<sub>2</sub> + 0.1 L H<sub>2</sub>. The spectrum at T = 200 K was also measured for a 4.5° off-specular scattering geo-metry [91Wam].

**Fig. 11.** High-resolution C(1s) XPS spectra of 5 L CO<sub>2</sub> + H<sub>2</sub>/Ni(110) as a function of temperature. The inset compares formate species formed (a) (in the top spectrum) out of formic acid by heating to 200 K with formic acid as solvent, and (b) after reaction of CO<sub>2</sub> and H<sub>2</sub> at 180 K solvated with readsorbed CO<sub>2</sub> [91Wam].

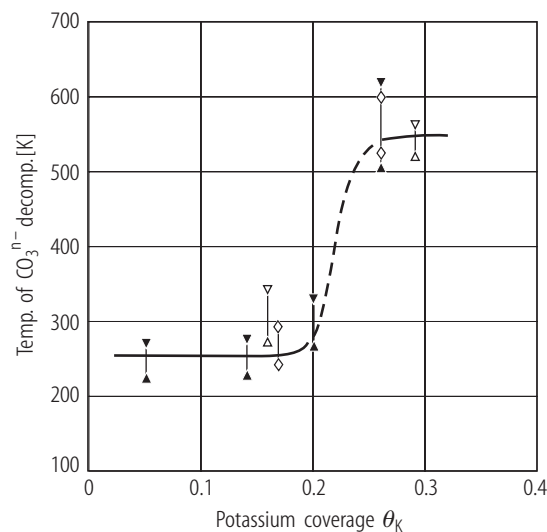
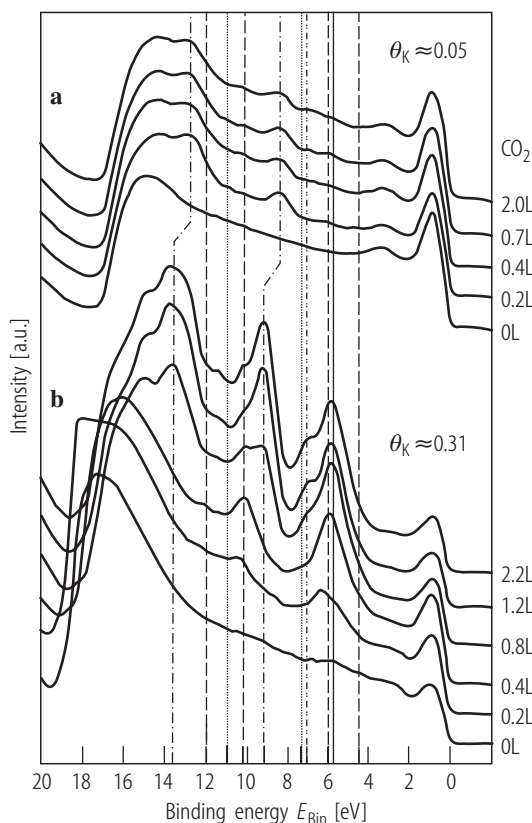


**Fig. 13.** Decomposition temperature of the  $\text{CO}_3^{n-}$  species as a function of potassium coverage. The lower symbols correspond to the temperature just before, the upper symbols to the temperature after complete decomposition (( $\Delta$ ): HeI UPS; ( $\diamond$ ): HeII UPS; ( $\blacktriangle$ ): XPS) [94Mey2].

← **Fig. 12.** Hel UPS spectra of a K-covered Fe(110) surface at 85 K for (a)  $\theta_K \approx 0.05$  and (b)  $\theta_K \approx 0.31$  after subsequent exposures to  $\text{CO}_2$  as indicated. In (a) vertical lines denote positions of molecular orbital levels of different adsorbed species: ( $\cdot - \cdot - \cdot - \cdot$ ):  $\text{CO}_2$ ; ( $\cdots$ ):  $\text{CO}$ ; ( $- - -$ ):  $\text{CO}_3^{n-}$ ; ( $\cdot - \cdot - \cdot - \cdot$ ): species A (see text); ( $-$ ):  $\text{O}_{\text{ox}}$  [94Mey1].

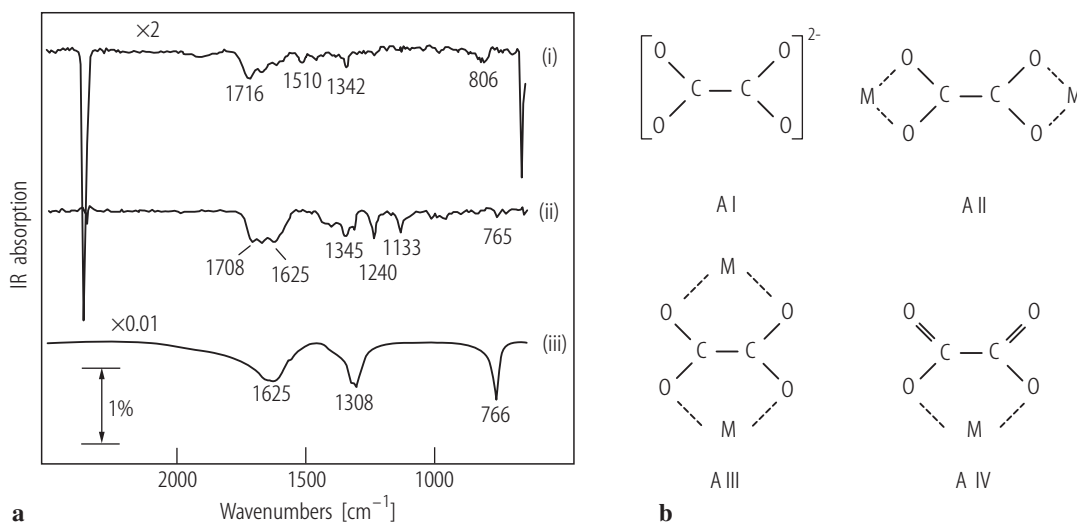


**Fig. 14.** (a) Vibrational spectra of oxalate species: (i)  $(\sqrt{3} \times \sqrt{3})\text{R}30^\circ\text{-K-Ru}(0001)$ ; (ii) K-multilayer; (iii) bulk  $\text{K}_2\text{C}_2\text{O}_4$ . (b) Schematic representation of oxalate structures. [94Hof]

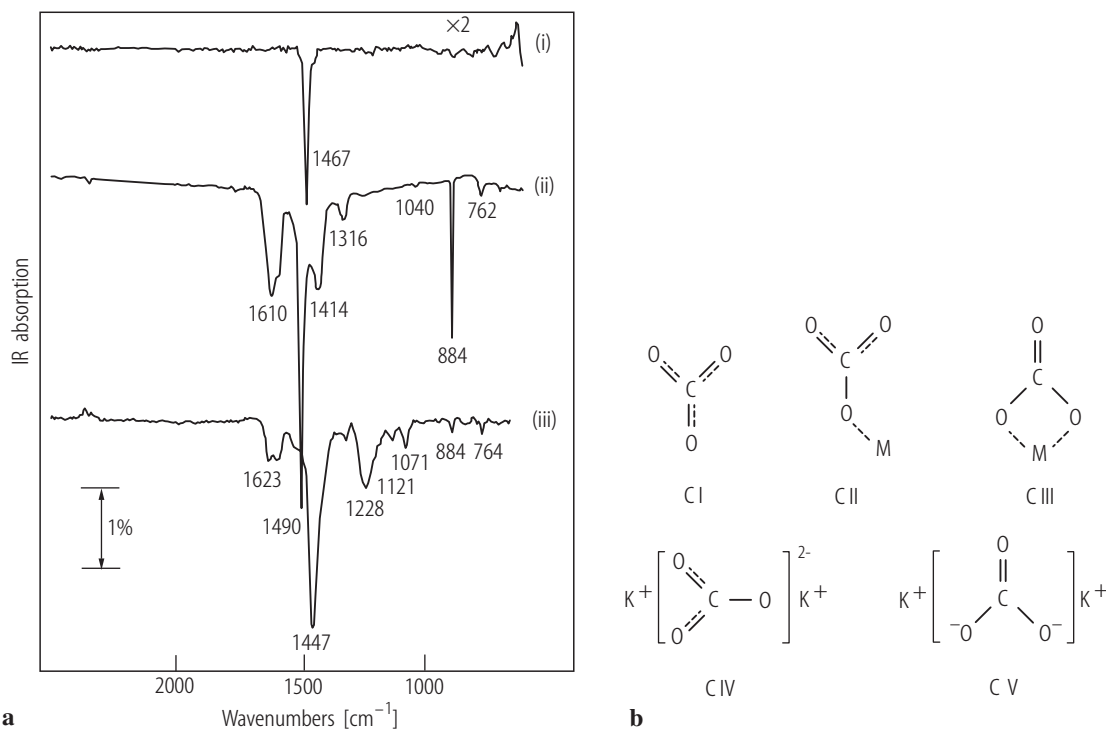


**Fig. 15.** (a) Vibrational spectra of carbonate species: (i) (√3×√3)R30°-K-Ru(0001); (ii) K-bilayer; (iii) K-multilayer. (b) Schematic representation of carbonate structures. [94Hof]

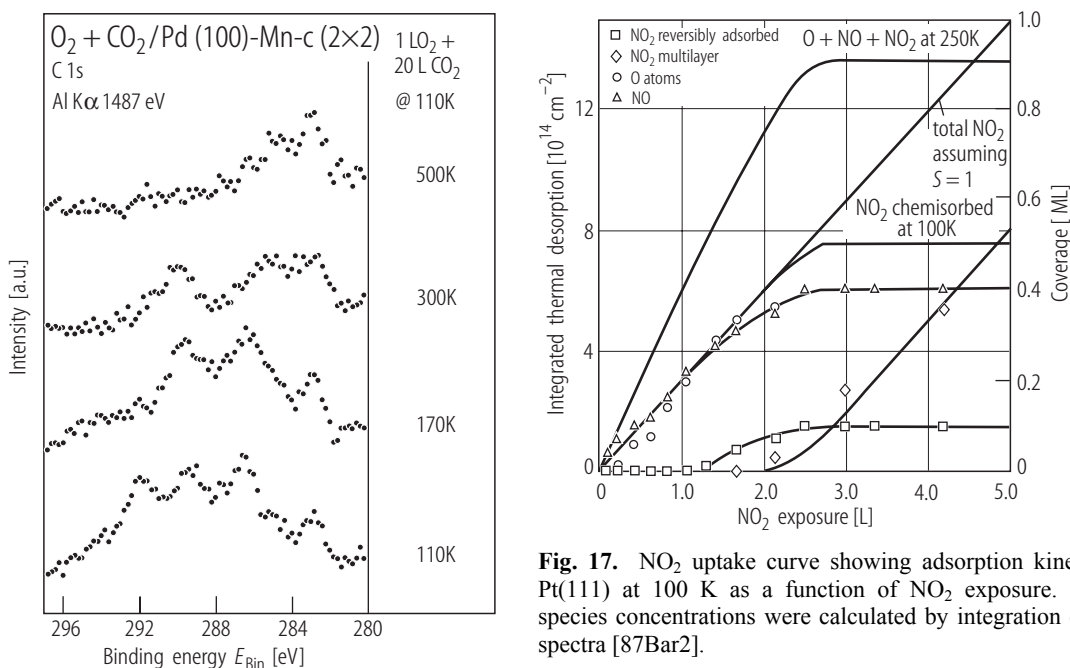


**Fig. 16.** C (1s) XPS spectra for CO<sub>2</sub> on a O<sub>2</sub>-pretreated Pd(100)-Mn-c(2×2) surface alloy before and after subsequent heating [99San].

**Fig. 17.** NO<sub>2</sub> uptake curve showing adsorption kinetics on Pt(111) at 100 K as a function of NO<sub>2</sub> exposure. Surface species concentrations were calculated by integration of TPD spectra [87Bar2].

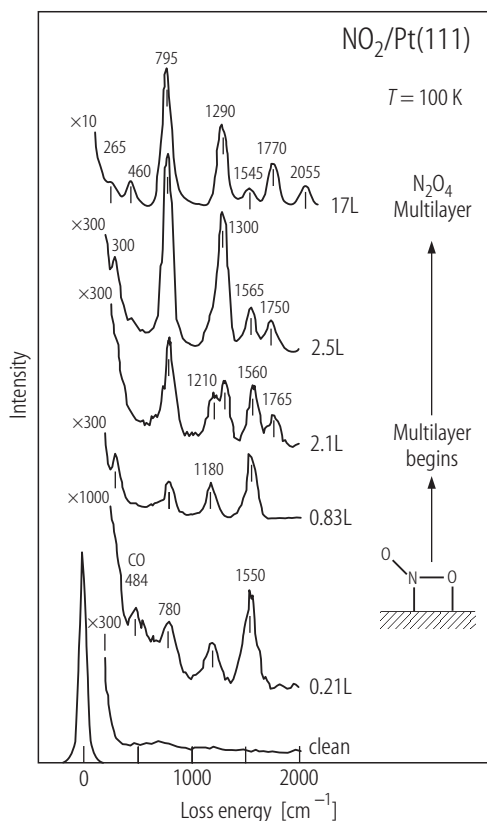


**Fig. 18.** HREELS spectra for increasing NO<sub>2</sub> exposures on Pt(111) at 100 K [87Bar2].

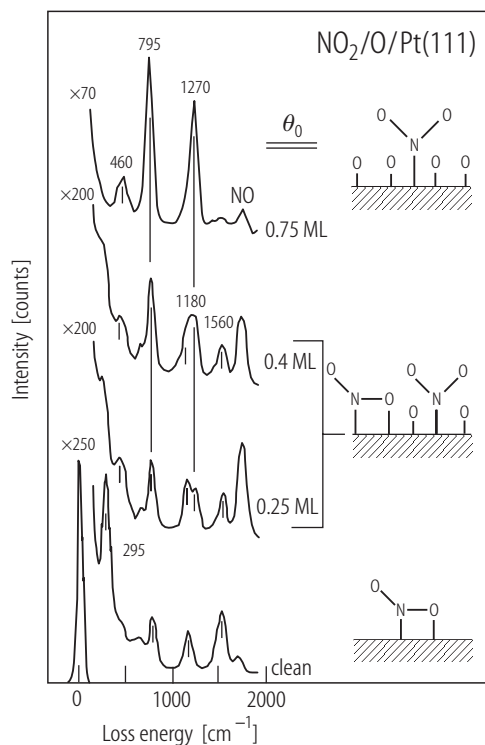


**Fig. 19.** HREELS spectra for NO<sub>2</sub> adsorbed with increasing amounts of preadsorbed O adatoms on Pt(111) at 170 K [88Bar].

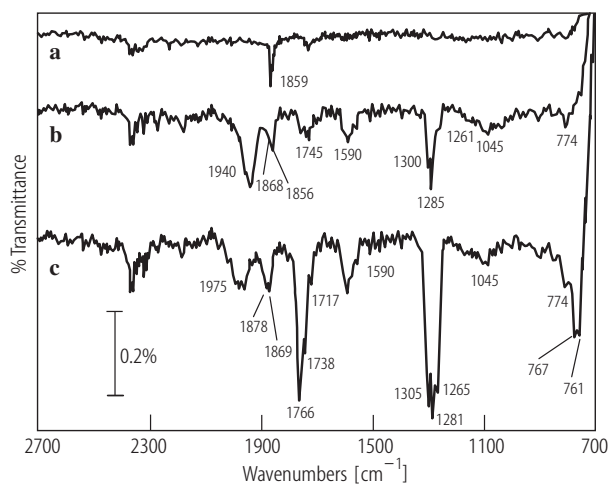


**Fig. 20.** IRAS spectra following the adsorption of NO<sub>2</sub> on Ag(111) at 86 K. The exposures for the spectra are (a) 0.5, (b) 1 and (c) 2 L [95Bro1].

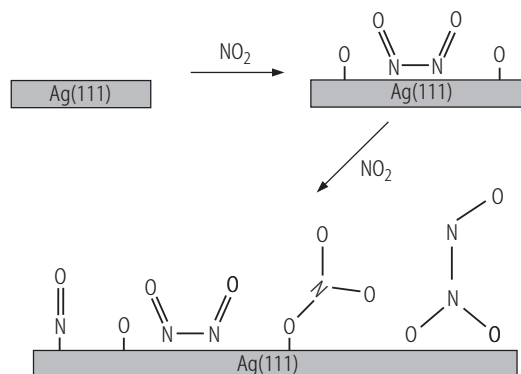


**Fig. 21.** A reaction scheme for adsorption of NO<sub>2</sub> on Ag(111) at 86 K. Initial adsorption is dissociative and subsequent adsorption leads to formation of NO<sub>3</sub> and N<sub>2</sub>O<sub>3</sub>. Further adsorption leads to multilayers of N<sub>2</sub>O<sub>4</sub> [95Bro1].

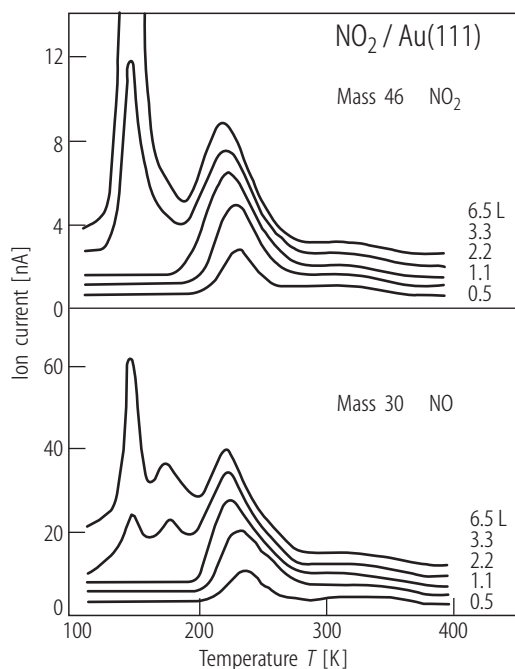


**Fig. 22.** Desorption spectra after NO<sub>2</sub> exposures on Au(111) at 100 K. Except for a peak at 170 K, the NO signal followed the NO<sub>2</sub> signal with the expected cracking ratio [89Bar].

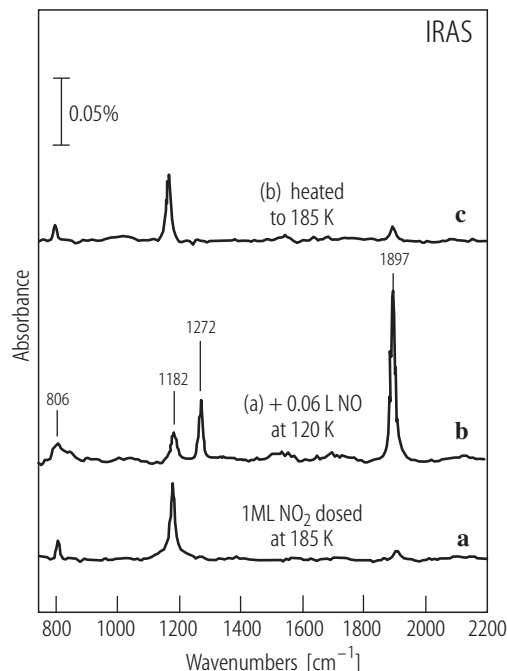


**Fig. 23.** IRAS spectra obtained after (a) NO<sub>2</sub> dosed on Au(111) at 185 K to give a pure monolayer of chelating, chemisorbed NO<sub>2</sub>, (b) NO exposure on a chelating NO<sub>2</sub> monolayer on Au(111) at 120 K to form a pure N<sub>2</sub>O<sub>3</sub> monolayer and (c) annealing the surface in (b) to 185 K for 30 s. All of the spectra were collected at 86 K [98Wan1].

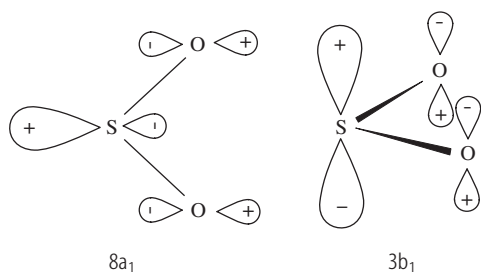


**Fig. 24.** Schematic drawings of the HOMO ( $8a_1$ ) and LUMO ( $3b_1$ ) for SO<sub>2</sub> [81Rya].

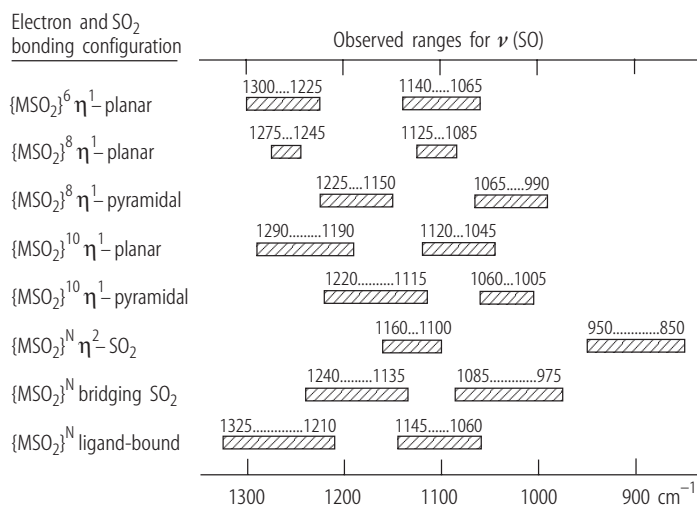


**Fig. 25.** Diagnostic features of SO<sub>2</sub> coordination geometries [81Rya]

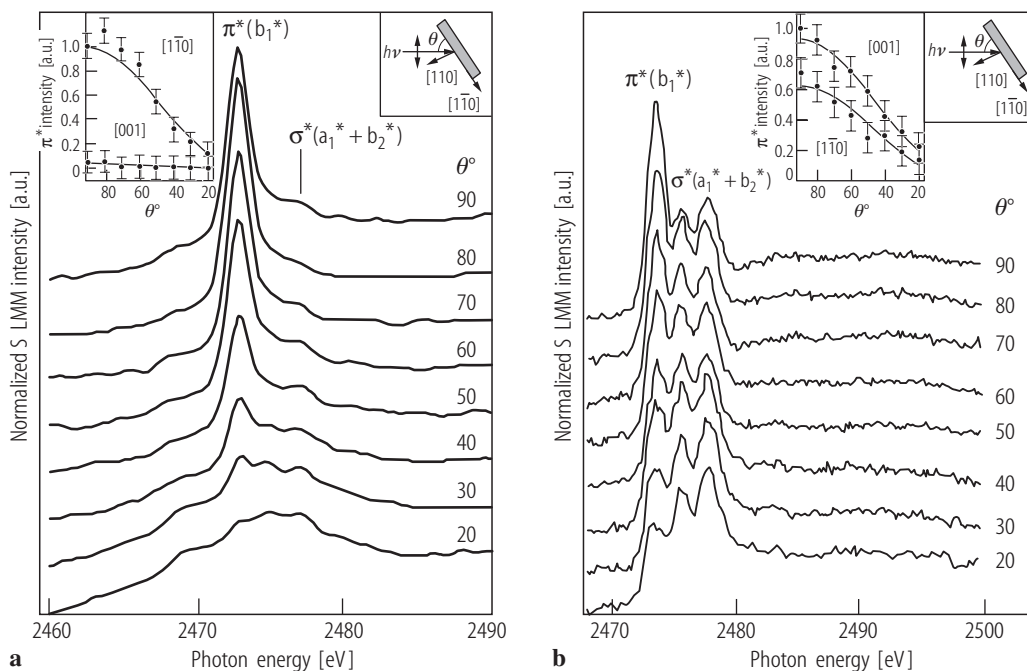


**Fig. 26.** Sulfur K-edge NEXAFS spectra of Ag(110) (a) after exposure to 500 L SO<sub>2</sub> at 95 K to form a multilayer and subsequent heating to the measurement temperature of 180 K, yielding a coverage of  $0.3 \pm 0.1$  ML and (b) then recooling the sample to 100 K and readsorbing SO<sub>2</sub> to give a coverage of  $0.6 \pm 0.1$  ML. The X-ray  $E$  vector is along the  $[1\bar{1}0]$  azimuth. The inset shows the absorption-edge-step normalized Gaussian area of the  $\pi^*$  resonance recorded in the two azimuths. The best fit to the data points is for (a)  $\alpha = 88 \pm 5^\circ$ ,  $\phi = 0 \pm 5^\circ$  and (b)  $\alpha = 77 \pm 5^\circ$ ,  $\phi = 55 \pm 5^\circ$ , for the  $[1\bar{1}0]$  azimuth data in the function  $I \propto (\cos^2 \theta \cos^2 \alpha + \sin^2 \alpha \cos^2 \theta)$ , where  $\theta$  is the angle of incidence,  $\alpha$  is the angle between the molecular plane and the surface, and  $\phi$  is the angle between the molecular plane normal and the measurement azimuth [96Gut2].

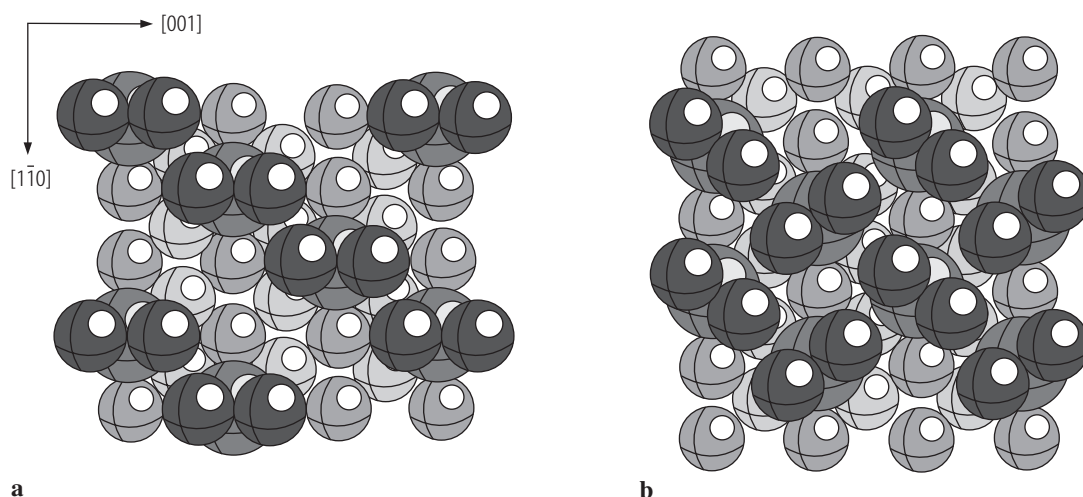


**Fig. 27.** Models of the Ag(110) surface with the suggested bond geometries of SO<sub>2</sub> at coverages of (a) 1/3 ML and (b) 1/2 ML. S and O atoms are shown as dark circles and are scaled to the Van der Waals radii. The gas-phase geometry of SO<sub>2</sub> has been assumed [96Gut2].



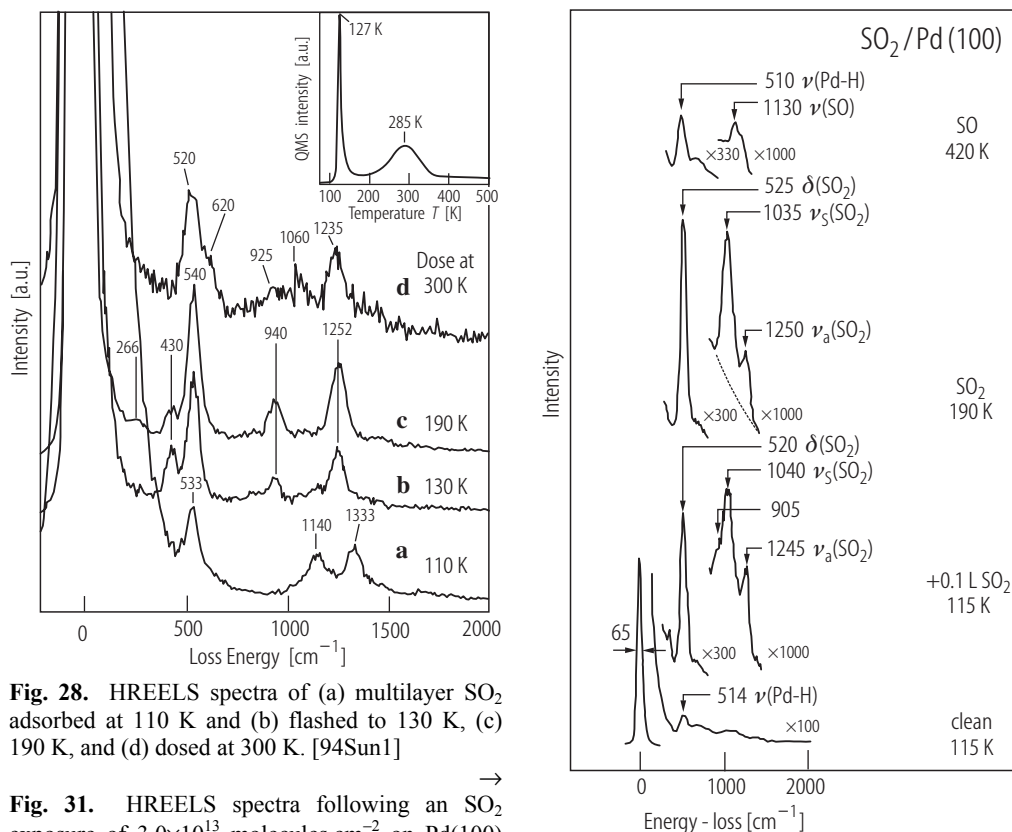


**Fig. 28.** HREELS spectra of (a) multilayer SO<sub>2</sub> adsorbed at 110 K and (b) flashed to 130 K, (c) 190 K, and (d) dosed at 300 K. [94Sun1]

**Fig. 31.** HREELS spectra following an SO<sub>2</sub> exposure of 3.0×10<sup>13</sup> molecules·cm<sup>-2</sup> on Pd(100) at 115 K. The dotted line denotes the baseline subtracted to find loss intensities [88Bur1].

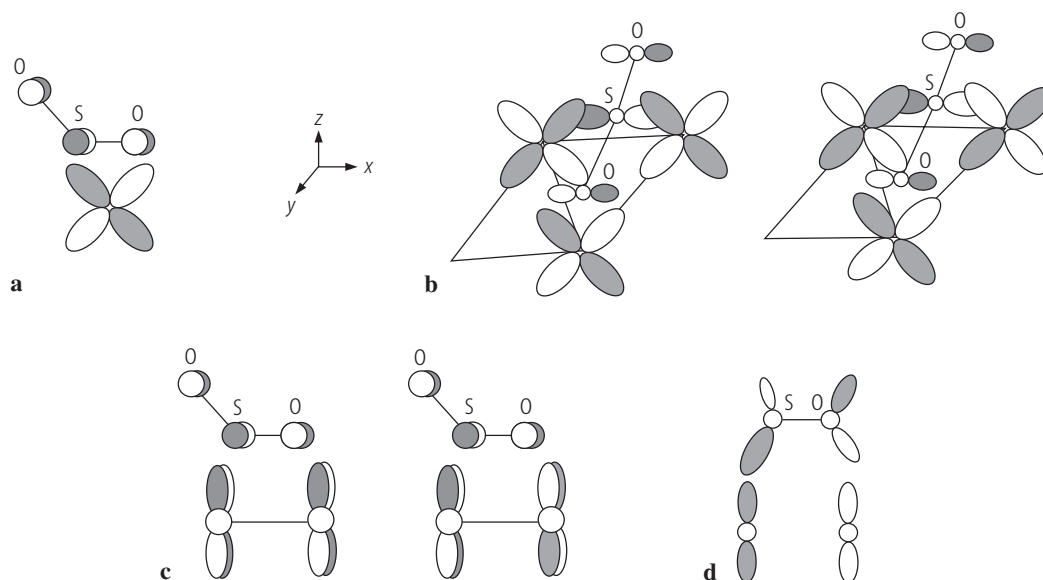


**Fig. 29.** SO<sub>2</sub> bonding configurations on Pt(111). (a) SO<sub>2</sub> on an atop site with its HOMO interacting with a d<sub>xz</sub> or d<sub>yz</sub> orbital, (b) SO<sub>2</sub> in a three-fold site with its HOMO interacting with the d<sub>xz</sub> bonding combination (left) and antibonding combination (right), (c) SO<sub>2</sub> on a two-fold site with its HOMO interacting with the d<sub>xz</sub> bonding combination (left) and antibonding combination (right) and (d) SO<sub>2</sub> on a two-fold site with its LUMO to d<sub>x<sup>2</sup>-y<sup>2</sup></sub> antibonding combination [94Sun1].

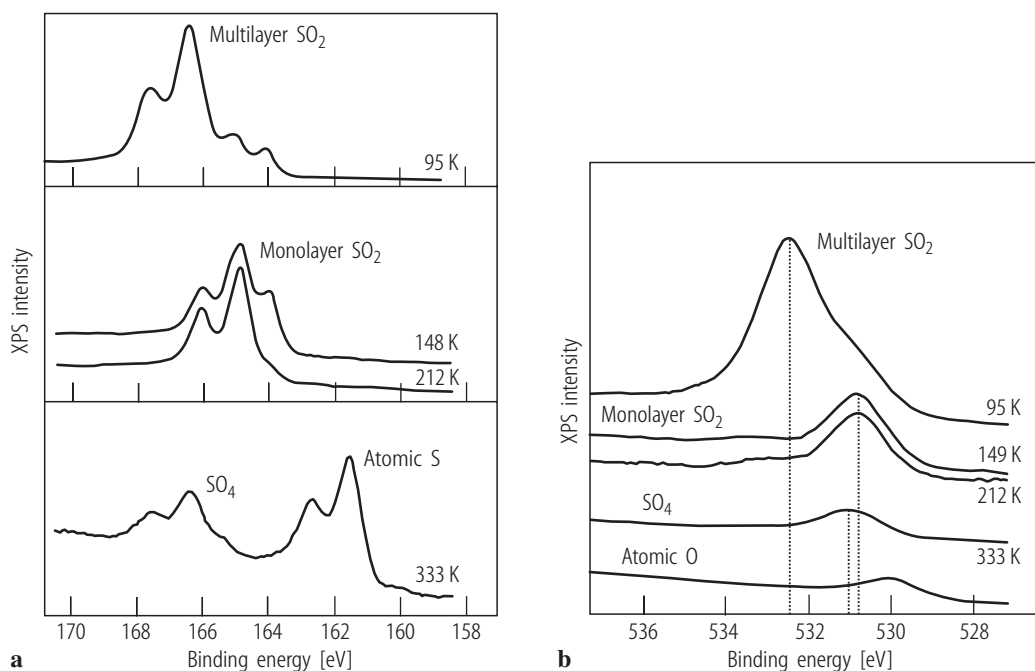


**Fig. 30.** (a) S (2p) data for an SO<sub>2</sub> multilayer (top), two-monolayer phase (middle) formed from SO<sub>2</sub> adsorption at 148 K and subsequent heating to 212 K, respectively, and a phase formed on heating a multilayer to 333 K (bottom). (b) O (1s) data corresponding to the S (2p) spectra of (a). For comparison, the O (1s) spectrum of Pt(111)-(2×2)-O (bottom) is also shown [97Pol].

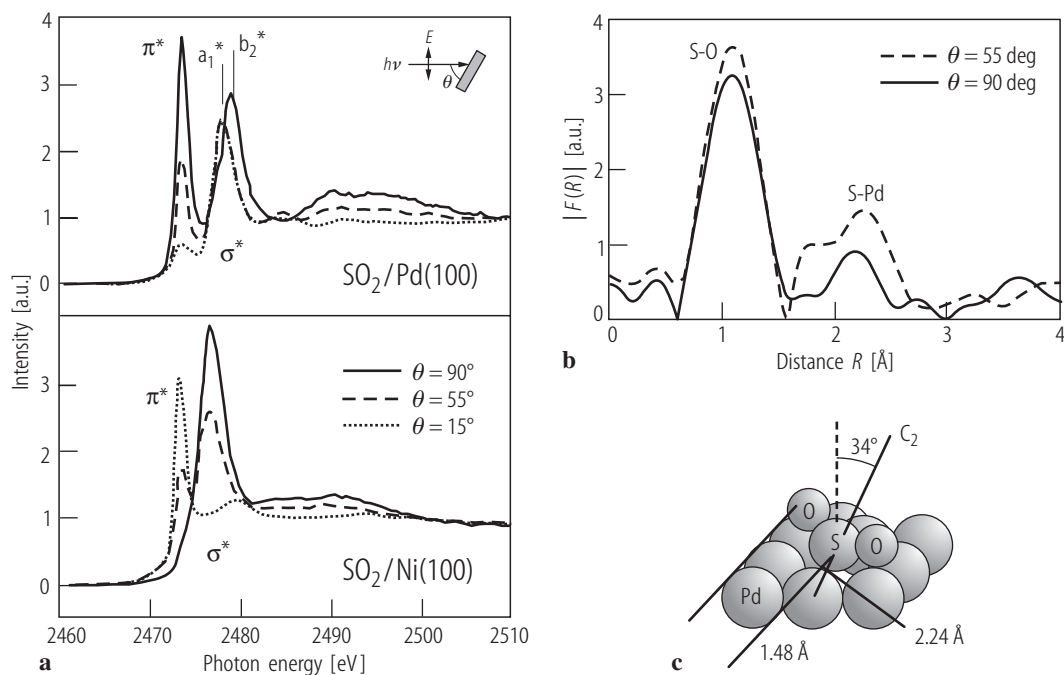


**Fig. 32.** (a) Sulfur K-edge NEXAFS spectra of SO<sub>2</sub>/Pd(100) (top) and SO<sub>2</sub>/Ni(100) (bottom). (b) Fourier transforms of the sulfur K-edge EXAFS functions  $k^2\chi(k)$  of SO<sub>2</sub>/Pd(100). (c) Schematic view of the surface structure of SO<sub>2</sub>/Pd(100) [97Ter].

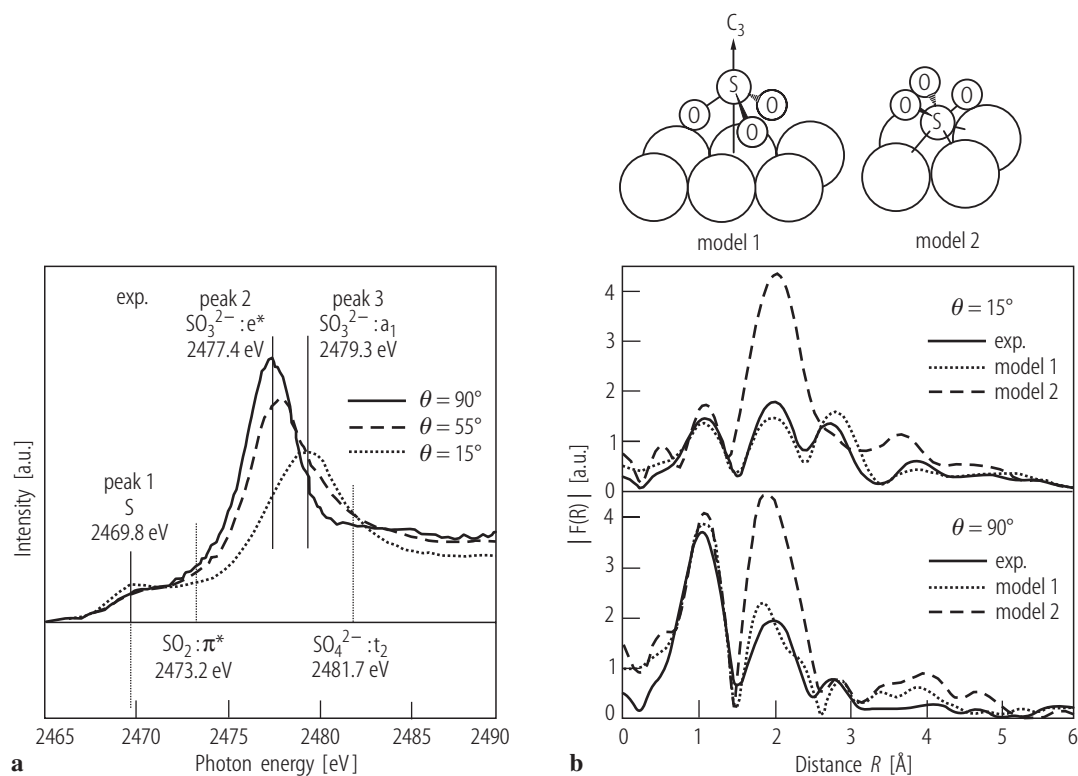


**Fig. 33.** (a) S K-edge NEXAFS spectra after 5 L SO<sub>2</sub> on Cu(100), compared with those of some references. (b) Fourier transforms of the SEXAFS spectra at  $\theta = 15^\circ$  and  $90^\circ$ , compared with the FEFF6-simulated curves for models 1 and 2 [97Nak1].

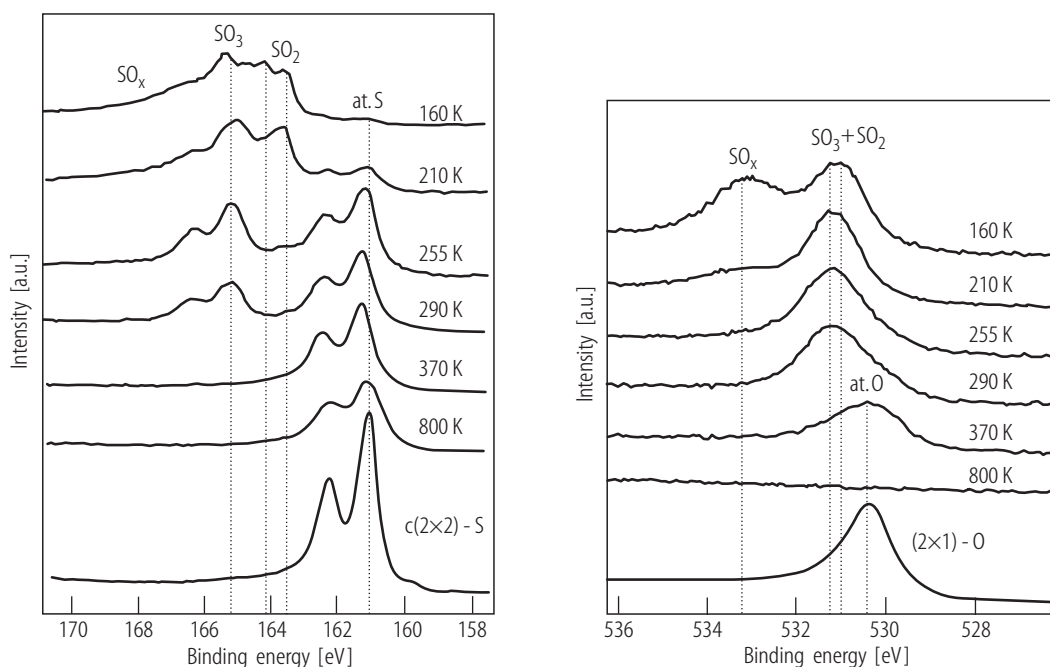


**Fig. 34.** S(2p) (left) and O(1s) (right) core-level photoemission data for Ni(110)-SO<sub>2</sub> with the sample temperature as a parameter during continuous heating ( $\sim 0.1$  K/s). For comparison, corresponding spectra of reference structures are included [98Wil].

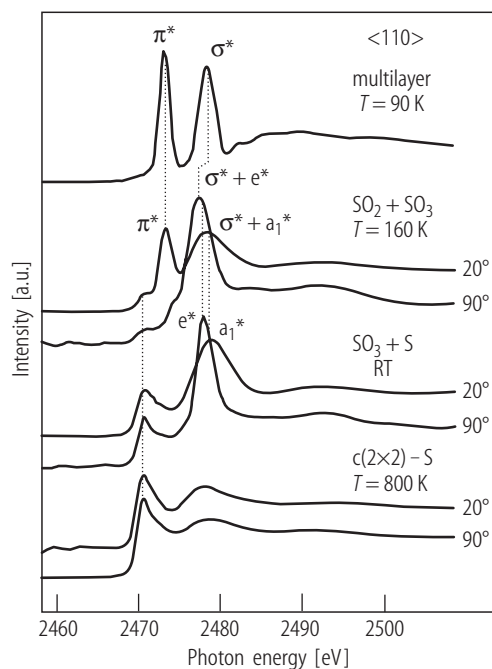


**Fig. 35.** S K-edge NEXAFS spectra of SO<sub>2</sub> condensed on Ni(110) (top), adsorbed at 160 K (second from top) and subsequently heated to room temperature (second from bottom) and 800 K (bottom) taken along the <110> azimuth at polar angles of 20° and 90° [98Wil].

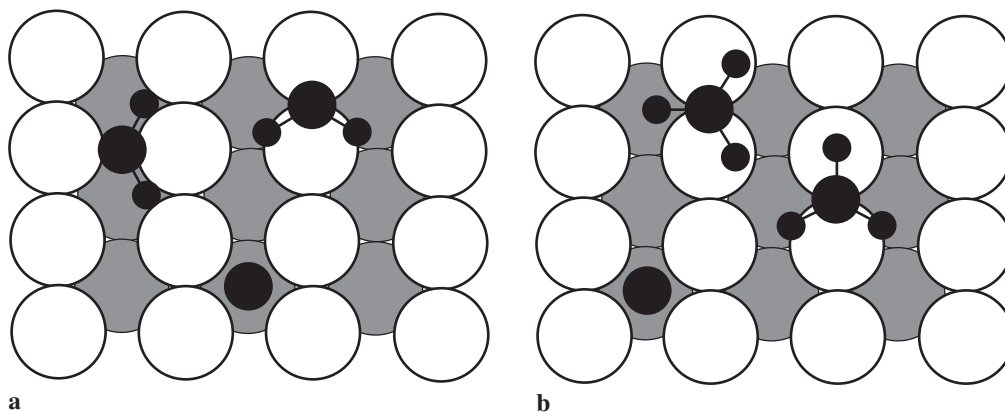


**Fig. 36.** (a) Suggested local SO<sub>2</sub> structures with S atoms in long-bridge and short-bridge sites and atomic S in hollow sites as determined with SEXAFS. (b) Suggested local SO<sub>3</sub><sup>-</sup> structures with S atoms in short-bridge sites and atomic S in hollow sites as determined with SEXAFS [98Wil].

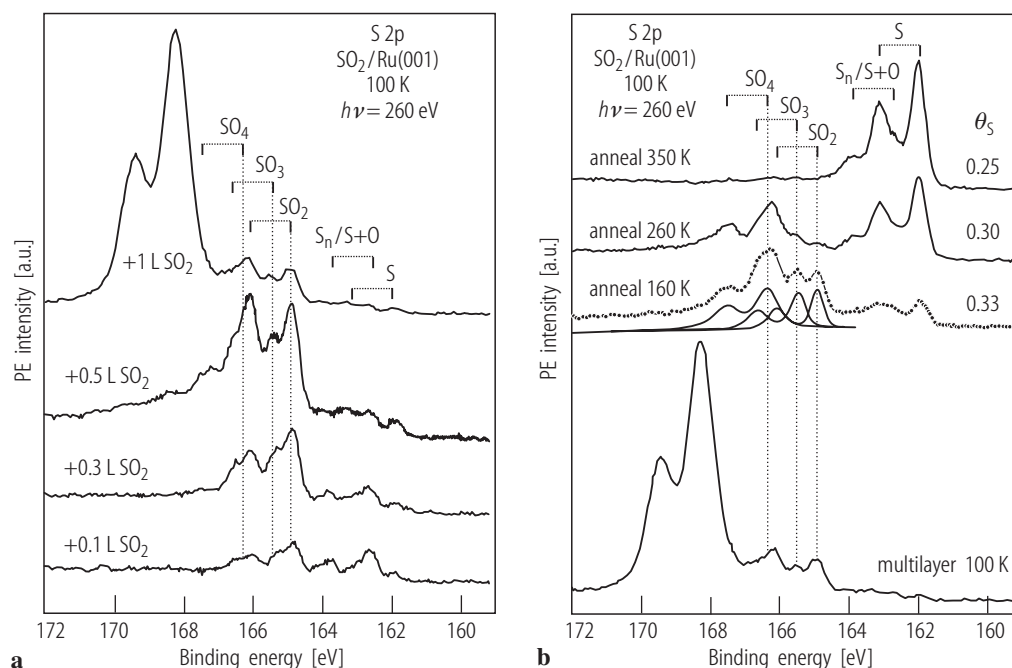


**Fig. 37.** (a) S(2p) photoelectron spectra for different amounts of SO<sub>2</sub> adsorbed on clean Ru(0001) at 100 K (b) S(2p) photoelectron spectra taken after annealing a Ru(0001) surface saturated with SO<sub>2</sub> from 100 to 350 K [98Jir].

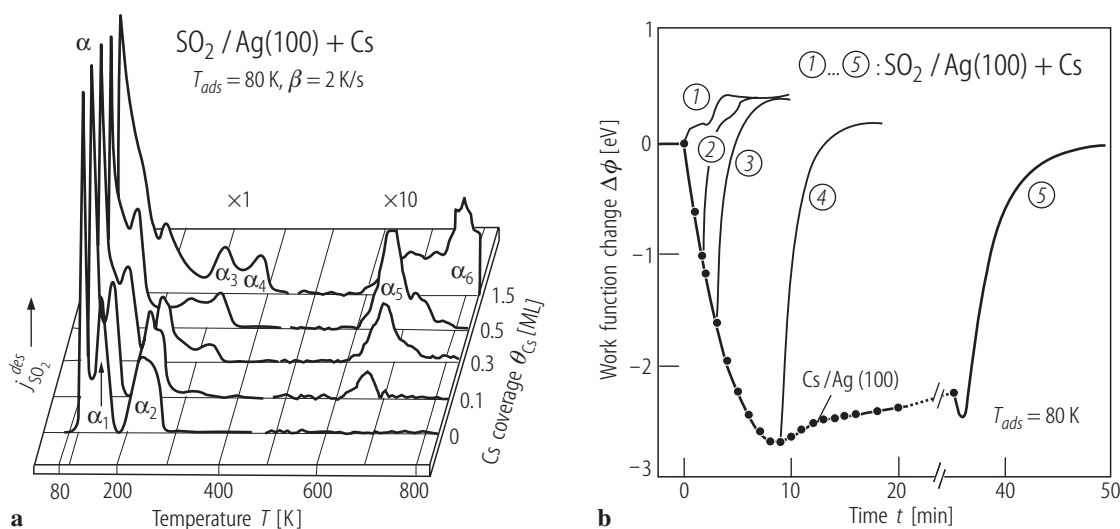


**Fig. 38.** (a) TPD spectra of SO<sub>2</sub> adsorbed on clean and Cs-precovered Ag(100) at 80 K with  $\theta_{\text{Cs}}$  as a parameter. The desorption signal is magnified by a factor of 10 on the right side of the curves. SO<sub>2</sub> was always exposed until the beginning of condensation, indicated by the saturation of  $\Delta\phi(t)$  (see below). (b) Change of the work function  $\Delta\phi$  during Cs exposure on the clean Ag(100) surface (bold curve with points) and during SO<sub>2</sub> exposures of clean (1) and Cs-precovered (2-5) Ag(100) at 80 K. Cs precoverages for curves (2)-(5) are 0.07, 0.13, 0.38 and 1.5 ML, respectively [92Höf].

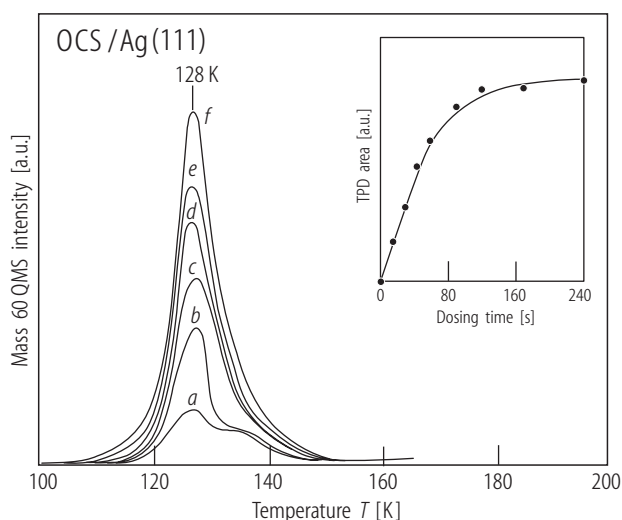


**Fig. 39.** TPD spectra of OCS after dosing at 100 K for (a) 15, (b) 30, (c) 50, (d) 75, (e) 100 and (f) 240 s. The inset shows the OCS TPD area versus dosing time. The temperature ramp rate was 2.5 K/s [90Zho].

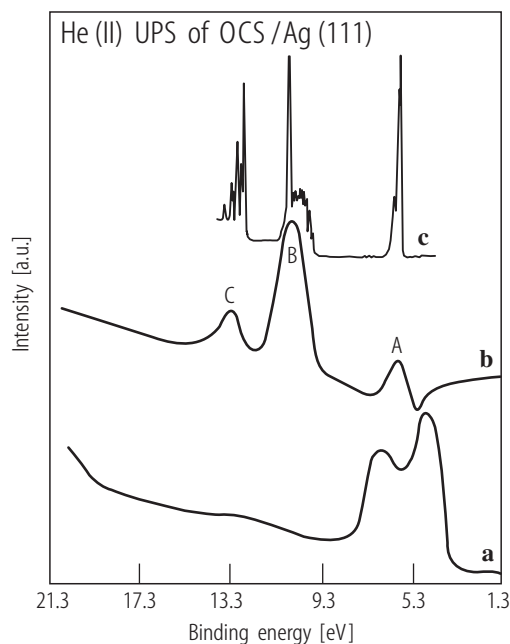


**Fig. 40.** He(II) UPS spectra at 100 K of (a) clean Ag(111), (b) saturation OCS-covered Ag(111) with the clean Ag(111) spectrum subtracted and (c) gas-phase OCS [90Zho].

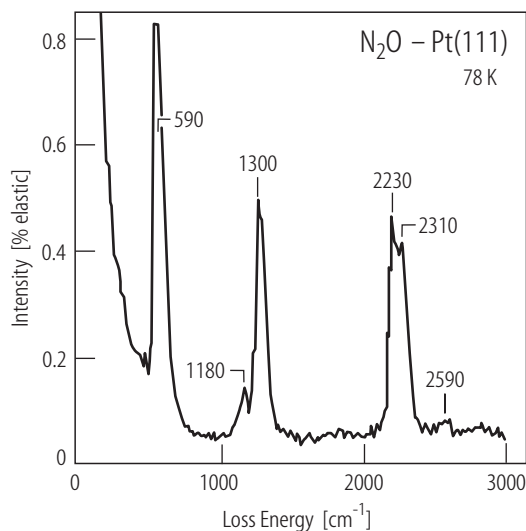
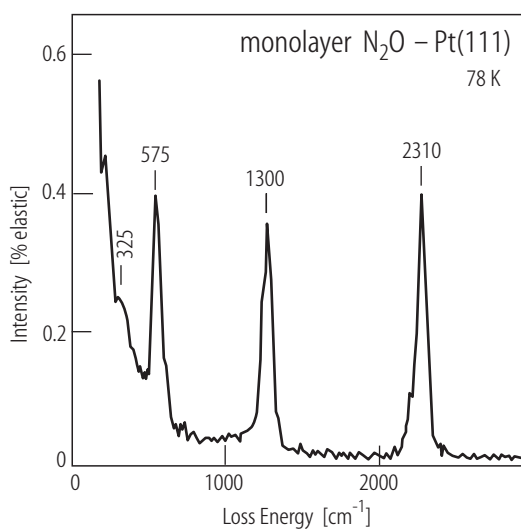


**Fig. 41.** HREELS spectrum (left) of a saturated monolayer of N<sub>2</sub>O on Pt(111) at 78 K and (right) after an N<sub>2</sub>O exposure on Pt(111) at 78 K that produced a multilayer that did not quite screen the monolayer spectrum. The beam energy was 4.1 eV and angle of incidence (to the surface normal) ~60° [83Ave].

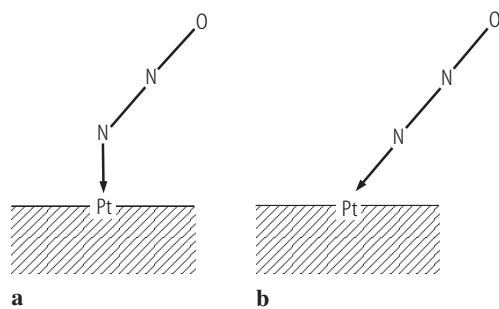


**Fig. 42.** Bond configurations of inclined N<sub>2</sub>O on Pt(111) in (a) bent configuration and (b) linear configuration [83Ave].

**Fig. 43.** N(1s) and O(1s) XPS spectra from W(110) at 100 K after the pretreatments with N<sub>2</sub>O given in the figure (the temporal sequence runs from bottom to top) [79Fug].

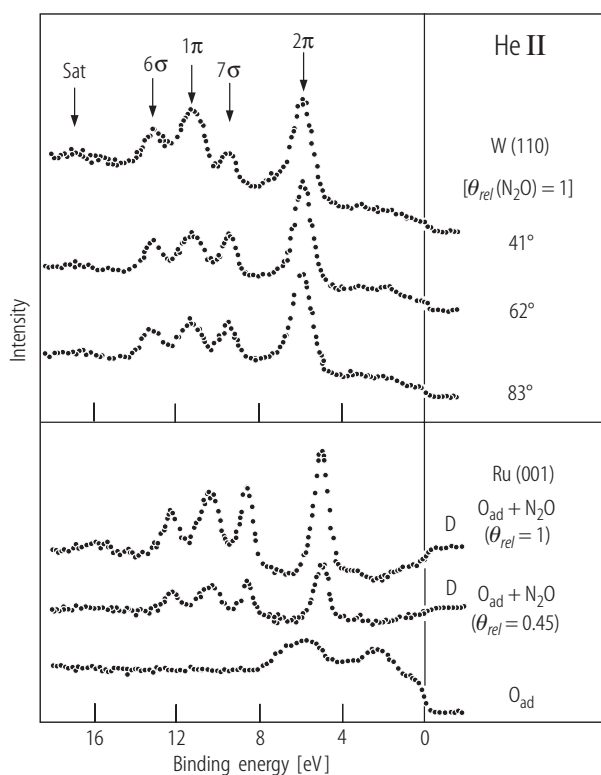
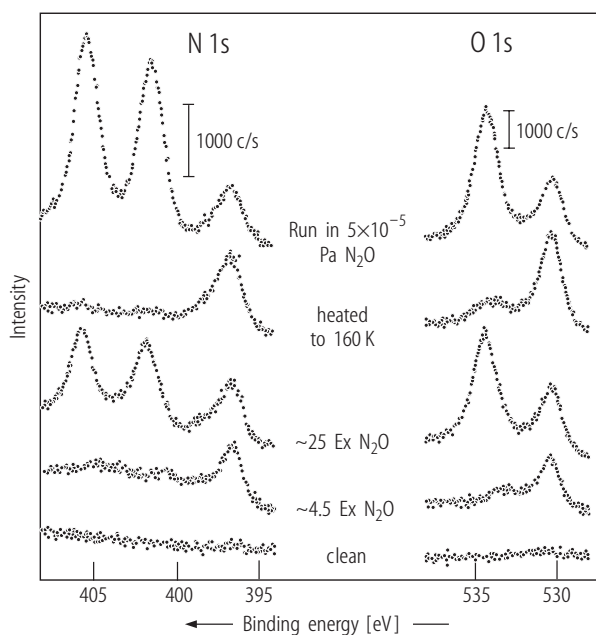


**Fig. 44.** He(II) UPS spectra of molecular N<sub>2</sub>O coadsorbed with dissociated O and N adatoms on W(110) (upper part) and readsorbed on an O-predosed Ru(0001) surface (lower part). The upper spectra are direct curves taken at saturation coverage and at different polar angles as indicated. The lower part contains difference spectra (labeled D) at one-half and full coverages obtained by subtraction of the direct spectrum after oxygen exposure [81Umb].

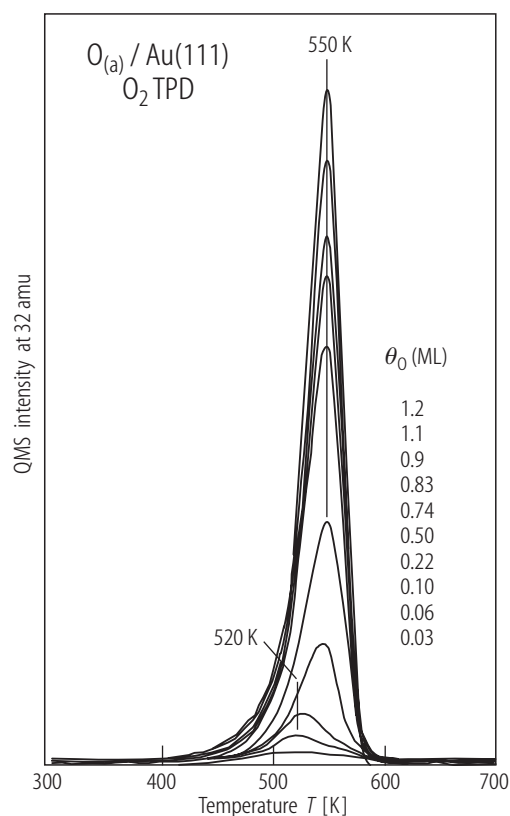


**Fig. 45.** O<sub>2</sub> TPD curves following increasing exposures of O<sub>3</sub> on Au(111) at 300 K. The oxygen coverages indicated were determined from the ratio of the integrated area under the peaks to that of the largest curve for which  $\theta_{\text{O}} = 1.2$  ML [98Sal].

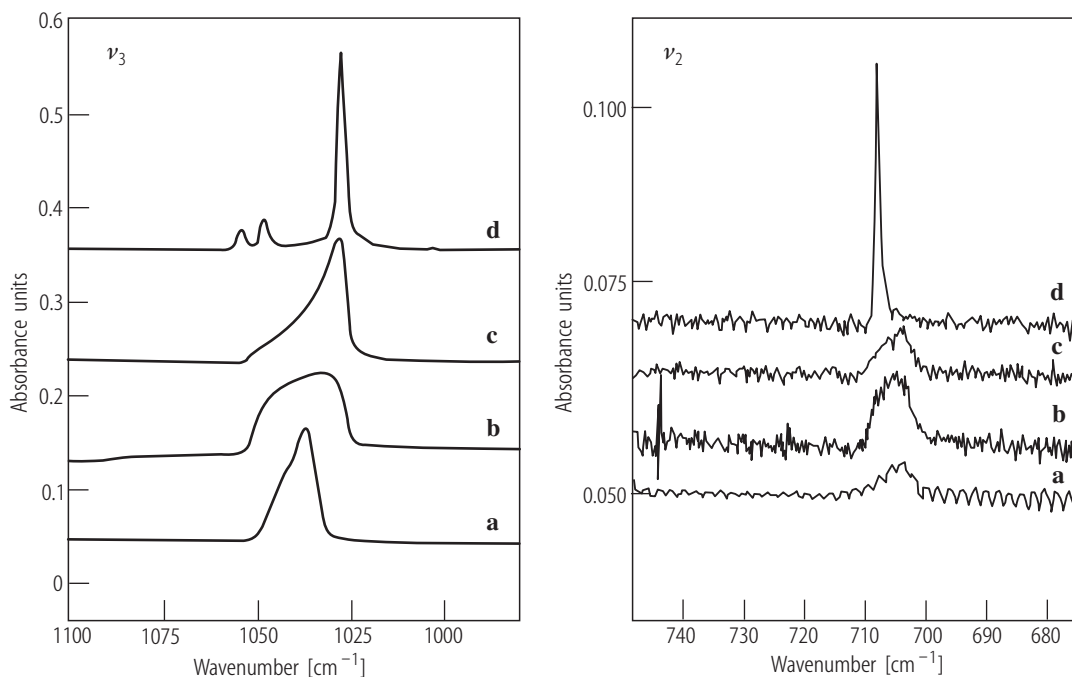


**Fig. 46.** IRAS spectra in the  $\nu_{\text{as}}$  ( $\nu_3$ ) stretching and  $\delta$  ( $\nu_2$ ) bending regions of condensed ozone on a gold cube. Spectra were taken after (a) Ozone deposition at 11 K, (b) O<sub>3</sub>/Ar deposition at the ratio of O<sub>3</sub>:Ar = 1:50 at 20 K and annealing to 40 K to evaporate Ar, (c) O<sub>3</sub>/He deposition at 30 K at the ratio of O<sub>3</sub>:He = 1:20 and (d) ozone deposition at 55 K [00Cha1].

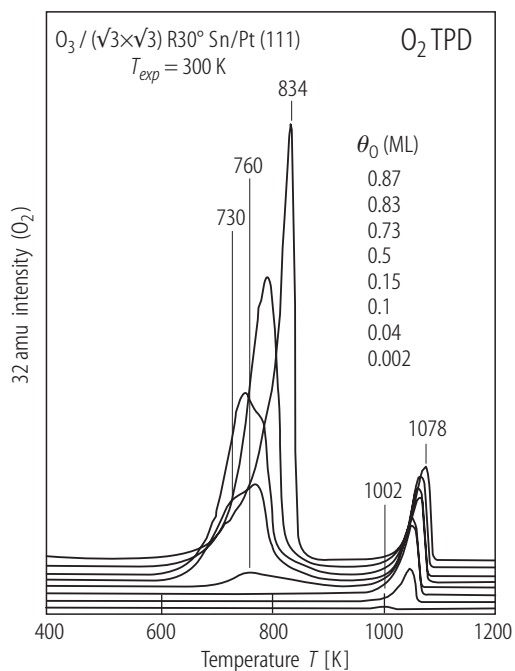


**Fig. 47.** O<sub>2</sub> TPD curves following O<sub>3</sub> exposures on the (√3×√3)R30°-Sn/Pt(111) alloy at 300 K [99Sal2].



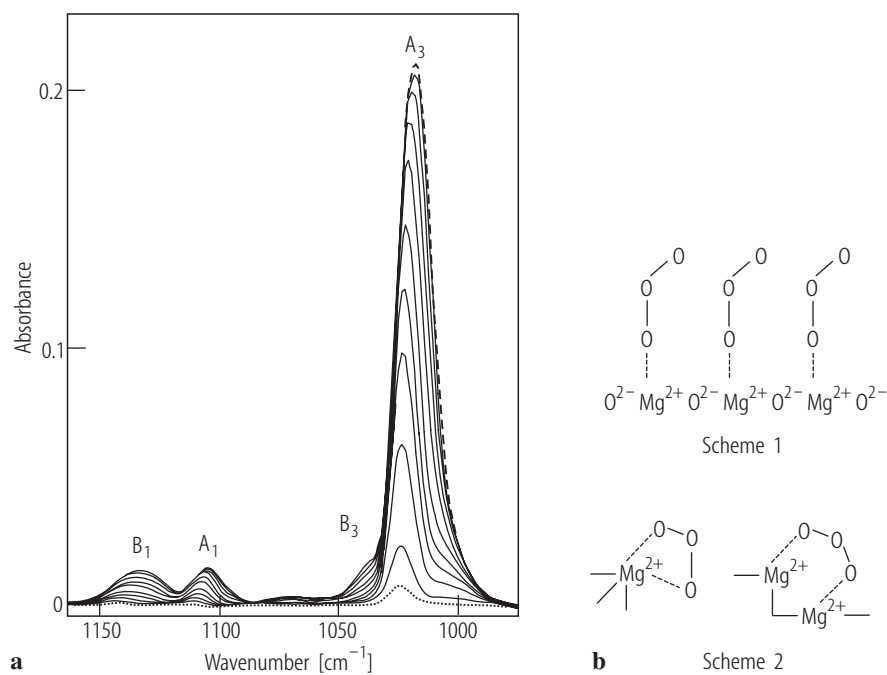


**Fig. 48.** (a) FTIR spectra of ozone adsorbed at 77 K on polycrystalline MgO. Spectra were taken between  $P_{\text{O}_3} = 5$  Torr (dashed line, top) and  $P_{\text{O}_3} = 10^{-3}$  Torr (dotted line, bottom). (b) Schematic drawings of ozone adsorbed on MgO [02Ber].

**3.8.4.10 References for 3.8.4**

- 54Pol Polo, S.R., Wilson, M.K.: *J. Chem. Phys.* **22** (1954) 900.  
57Eis Eischens, R.P., Pliskin, W.A.: *Adv. Catal.* **12** (1957) 662.  
58Har Harvey, K.B., Bass, A.M.: *J. Mol. Spec.* **2** (1958) 405.  
64Yam Yamada, H., Person, W.B.: *J. Chem. Phys.* **41** (1964) 2478.  
65StL St. Louis, R.V., Crawford, B.L.: *J. Chem. Phys.* **42** (1965) 857.  
66Her Herzberg, G.: *Electronic spectra of polyatomic molecules*, New York: Van Nostrand, 1966.  
66Sid Sidhu, K.S., Csizmadia, I.G., Strausz, O.P., Gunning, H.E.: *J. Am. Chem. Soc.* **88** (1966) 2412.  
68Mac MacCaa, D.J., Shaw, J.H.: *J. Mol. Spec.* **25** (1968) 374.  
70Tur Turner, D.W., Baker, A.D., Baker, C., Brundle, C.R.: *Molecular photoelectron spectroscopy*, London: Wiley and Sons, 1970.  
71Roo Roos, B., Siegbahn, P.: *Theor. Chim. Acta* **21** (1971) 368.  
72All Allan, C.J., Gelius, U., Allison, D.A., Johansson, G., Siegbahn, H., Siegbahn, K.: *J. Electron Spectrosc. Relat. Phenom.* **1** (1972/73) 131.  
72And Andrews, L. Spiker, Jr. R.C.: *J. Phys. Chem.* **76** (1972) 3208.  
72Bot Bottomley, F., Crawford, J.R.: *J. Am. Chem. Soc.* **94** (1972) 9092.  
72Goo Goodsel, A.J., Blyholder, G.: *J. Catal.* **26** (1972) 11.  
72Las Lassiter, W.S.: *J. Phys. Chem.* **76** (1972) 1289.  
72Shi Shimanouchi, T., *Tables of molecular vibrational frequencies consolidated*, Volume I, Washington: National Bureau of Standards, 1972, p. 1 - 160.  
72Wes West, L.A., Somorjai, G.A.: *J. Vac. Sci. Technol.* **9** (1972) 668.  
73McC McCarty, I., Falconer, J., Madix, R.J.: *J. Catal.* **30** (1973) 235.  
73Wei Weinberg, W.H.: *J. Catal.* **28** (1973) 459.  
74Ang Angoletta, M., Bellon, P.L., Manasero, M., Sansoni, M.: *J. Organomet. Chem.* **81** (1974) C40.  
74Dia Diamantis, A.A., Sparrow, G.J.: *J. Colloid Interface Sci.* **47** (1974) 455.  
74Nor Norton, P.R.: *Surf. Sci.* **44** (1974) 624.  
74Rob *Handbook of Spectroscopy*, Vol. 1: Robinson, J.W. (ed.), CRC Press, Cleveland 1974.  
75Bru Brundle, C.R., Carley, A.F.: *Faraday Discuss. Chem. Soc.* **60** (1975) 51.  
75Nor Norton, P.R., Richard, P.J.: *Surf. Sci.* **49** (1975) 567.  
76Bru Brundle, C.R.: *J. Vac. Sci. Technol.* **13** (1976) 301.  
76Nor Norton, P.R., Tapping, R.L.: *Chem. Phys. Lett.* **38** (1976) 207.  
76Sin Sinfelt, J.H., Lam, Y.L., Cusumano, J.A., Barnett, A.E.: *J. Catal.* **42** (1976) 227.  
77Are Aresta, M., Nobile, C.F.: *J. Chem. Soc. Dalton Trans.* **7** (1977) 708.  
77Bot Bottomley, F., Brooks, W.V.F.: *Inorg. Chem.* **16** (1977) 501.  
77Sex Sexton, B.A., Somorjai, G.A.: *J. Catal.* **46** (1977) 167.  
77Shi Shimanouchi, T.: *Tables of Molecular Vibrational Frequencies Consolidated Volume II*, *J. Phys. Chem. Rev. Data* **6(3)** (1977) 993.  
78Cas Castner, D.G., Sexton, B.A., Somorjai, G.A.: *Surf. Sci.* **71** (1978) 519.  
78Ele Eley, D.D., Moore, P.B.: *Surf. Sci.* **76** (1978) L599.  
78Fur Furuyama, M., Kishi, K., Ikeda, S.: *J. Electron Spectrosc. Relat. Phenom.* **13** (1978) 59.  
78Min Mingos, D.M.P.: *Transition Met. Chem. (London)* **3** (1978) 1.  
79Ben Benziger, J.B., Madix, R.J.: *Surf. Sci.* **79** (1979) 394.  
79Cas Castner, D.G., Somorjai, G.A.: *Surf. Sci.* **83** (1979) 60.  
79Dub Dubois, L.H., Somorjai, G.A.: *Surf. Sci.* **88** (1979) L13.  
79Fug Fuggle, J.C., Menzel, D.: *Surf. Sci.* **79** (1979) 1.  
79Joh Johnson, D.W., Matloob, M.H., Roberts, M.W.: *J. Chem. Soc. Faraday Trans.* **75** (1979) 2143.  
79Kub Kubas, G.J.: *Inorg. Chem.* **18** (1979) 182.  
80Cam Campbell, C.T., Ertl, G., Kuipers, H., Segner, J.: *J. Chem. Phys.* **73** (1980) 5862.  
80Del Delwiche, J., Hubin-Franskin, M.-J., Caprace, G., Natalis, P.: *J. Electron. Spectrosc. Relat. Phenom.* **21** (1980) 205.  
80Dub Dubois, L.H., Somorjai, G.A.: *Surf. Sci.* **91** (1980) 514.

- 80Kle Klein, R., Siegel, R.: *Surf. Sci.* **92** (1980) 337.
- 80Leg LeGaré, P., Hilaire, L., Sotto, M., Maire, G.: *Surf. Sci.* **91** (1980) 175.
- 81Bar Barteau, M.A., Madix, R.J.: *J. Chem. Phys.* **74** (1981) 4144.
- 81Dan Daniel, W.M., Kim, Y., Peebles, H.C., White, J.M.: *Surf. Sci.* **111** (1981) 189.
- 81Ku Ku, R.C., Wynblatt, P.: *Appl. Surf. Sci.* **8** (1981) 250.
- 81Rov Rovida, R., Pratesi, F.: *Surf. Sci.* **104** (1981) 609.
- 81Rya Ryan, R.R., Kubas, G.J., Moody, D.C., Eller, P.G.: *Struct. Bonding (Berlin)* **46** (1981) 47.
- 81Sal Sales, B.C., Turner, J.E., Maple, M.B.: *Surf. Sci.* **112** (1981) 272.
- 81Sau Sau, R., Hudson, J.B.: *J. Vac. Sci. Technol.* **18** (1981) 607.
- 81Shi Shi, S.-K., Lee, H.-I., White, J.M.: *Surf. Sci.* **102** (1981) 56.
- 81Umb Umbach, E., Menzel, D.: *Chem. Phys. Lett.* **84** (1981) 491.
- 82Ast Astegger, St., Bechtold, E.: *Surf. Sci.* **122** (1982) 491.
- 82Dah Dahlgren, D., Hemminger, J.C.: *Surf. Sci.* **123** (1982) L739.
- 82Hit Hitchman, M.A., Rowbottom, G.L.: *Coord. Chem. Rev.* **42** (1982) 55.
- 82Kat Katekaru, R.C., Garwood, G.A., Hershberger, J.F., Hubbard, A.T.: *Surf. Sci.* **121** (1982) 396.
- 82Kim Kim, Y., Schreifels, J.A., White, J.M.: *Surf. Sci.* **114** (1982) 349.
- 82Köh Köhler, U., Wassmuth, H.-W.: *Surf. Sci.* **117** (1982) 668.
- 82Nor Norton, P.R., Davies, J.A., Jackman, T.E.: *Surf. Sci.* **122** (1982) L593.
- 82Seg Segner, J., Vielhaber, W., Ertl, G.: *Isr. J. Chem.* **22** (1982) 375.
- 82Stu Stuve, E.M., Madix, R.J., Sexton, B.A.: *Chem. Phys. Lett.* **89** (1982) 48.
- 83Ave Avery, N.R.: *Surf. Sci.* **131** (1983) 501.
- 83Bac Backx, C., De Groot, C.P.M., Biloen, P., Sachtler, W.M.H.: *Surf. Sci.* **128** (1983) 81.
- 83Bar Barteau, M.A., Madix, R.J.: *J. Electron Spectrosc. Relat. Phenom.* **31** (1983) 101.
- 83Beh Behm, R.J., Brundle, C.R.: *J. Vac. Sci. Technol. A* **1** (1983) 1223.
- 83Cal Calabrese, J.C., Herskovitz, T., Kinney, J.B.: *J. Am. Chem. Soc.* **105** (1983) 5914.
- 83Gai Gainey, T.C., Hopkins, B.J.: *J. Phys. C* **16** (1983) 975.
- 83Köh Köhler, U., Wassmuth, H.-W.: *Surf. Sci.* **126** (1983) 448.
- 83Mad Madey, T.E., Avery, N.R., Anton, A.B., Toby, B.H., Weinberg, W.H.: *J. Vac. Sci. Technol. A* **1** (1983) 1220.
- 83Wei Weinberg, W.H.: *Surf. Sci.* **128** (1983) L224.
- 84Can Canning, N.D.S., Outka, D., Madix, R.J.: *Surf. Sci.* **141** (1984) 240.
- 84Foc Fock, J.-H., Lau, H.-J., Koch, E.E.: *Chem. Phys.* **83** (1984) 377.
- 84Out Outka, D.A., Madix, R.J.: *Surf. Sci.* **137** (1984) 242.
- 84Pir Pireaux, J.J., Chtaib, M., Delrue, J.P., Thiry, P.A., Liehr, M., Caudano, R.: *Surf. Sci.* **141** (1984) 211.
- 84Seg Segner, J., Campbell, C.T., Doyen, G., Ertl, G.: *Surf. Sci.* **138** (1984) 505.
- 84Sol Solymosi, F., Kiss, J.: *Chem. Phys. Lett.* **110** (1984) 639.
- 84Spi Spitzer, A., Lüth, H.: *Phys. Rev. B* **30** (1984) 3098.
- 85Beh Behner, H., Wedler, G.: *Surf. Sci.* **160** (1985) 271.
- 85Köl Kölzer, J.G., Wassmuth, H.-W.: *Ann. Phys. (Leipzig)* **42** (1985) 265.
- 85Sak Sakaki, S., Sato, H., Imai, Y., Morokuma, K., Ohbuko, K.: *Inorg. Chem.* **24** (1985) 4538.
- 85Sal Saleh, J.M., Nasser, F.A.K.: *J. Phys. Chem.* **89** (1985) 3392.
- 85Sch Schwalke, U., Niehus, H., Comsa, G.: *Surf. Sci.* **152/153** (1985) 596.
- 85Sol Solymosi, F., Kiss, J.: *Surf. Sci.* **149** (1985) 17.
- 86Beh Behner, H., Spiess, W., Wedler, G., Borgmann, D.: *Surf. Sci.* **175** (1986) 276.
- 86Ber Berkó, A., Solymosi, F.: *Surf. Sci.* **171** (1986) L498.
- 86Cam Campbell, S., Hollins, P., McCash, E., Roberts, M.W.: *J. Electron Spectrosc. Relat. Phenom.* **39** (1986) 145.
- 86Ega Egawa, C., Doi, I., Naito, S., Tamaru, K.: *Surf. Sci.* **176** (1986) 491.
- 86Fre Freund, H.-J., Messmer, R.P.: *Surf. Sci.* **172** (1986) 1.
- 86Out1 Outka, D.A., Madix, R.J.: *Langmuir* **2** (1986) 406.
- 86Out2 Outka, D.A., Madix, R.J., Fisher, G.B., DiMaggio, C.: *J. Phys. Chem.* **90** (1986) 4051.
- 86Sau Sault, A.G., Madix, R.J.: *Surf. Sci.* **169** (1986) 347.
- 86Sch1 Schwalke, U., Parmeter, J.E., Weinberg, W.H.: *J. Chem. Phys.* **84** (1986) 4036.

- 86Sch2 Schwalke, U., Parmeter, J.E., Weinberg, W.H.: *Surf. Sci.* **178** (1986) 625.  
86Sol Solymosi, F., Berkó, A.: *J. Catal.* **101** (1986) 458.  
86Zom Zomack, M., Baberschke, K.: *Surf. Sci.* **178** (1986) 618.  
87Alb Albert, M.R., Yates, J.T.: *The surface scientist's guide to organometallic chemistry*, Washington, DC: ACS, 1987.  
87Bab Baberschke, K., Farle, M., Zomack, M.: *Appl. Phys. A* **44** (1987) 13.  
87Bar1 Bartos, B., Freund, H.-J., Kühlenbeck, H., Neumann, M., Lindner, H., Müller, K.: *Surf. Sci.* **179** (1987) 59.  
87Bar2 Bartram, M.E., Windham, R.G., Koel, B.E.: *Surf. Sci.* **184** (1987) 57.  
87Bau Bauer, R., Behner, H., Borgmann, D., Pirner, M., Spiess, W., Wedler, G.: *J. Vac. Sci. Technol. A* **5** (1987) 1110.  
87Beh Behner, H., Spiess, W., Wedler, G., Borgmann, D., Freund, H.-J.: *Surf. Sci.* **184** (1987) 335.  
87Car Carley, A.F., Gallagher, D.E., Roberts, M.W.: *Surf. Sci.* **183** (1987) L263.  
87Col Collman, J.P., Hegedus, L.S., Norton, J.R., Finke, R.G.: *Principles and applications of organotransition metal chemistry*, University Science Books, Mill Valley, CA, 1987.  
87Fre Freund, H.-J., Behner, H., Bartos, B., Wedler, G., Kühlenbeck, H., Neumann, M.: *Surf. Sci.* **180** (1987) 550.  
87Hof Hoffman, D., Hudson, J.B.: *Surf. Sci.* **180** (1987) 77.  
87Lin Lindner, H., Rupprecht, D., Hammer, L., Müller, K.: *J. Electron Spectrosc. Relat. Phenom.* **44** (1987) 141.  
87Mat Matsushima, T.: *J. Phys. Chem.* **91** (1987) 6192.  
87Out Outka, D.A., Madix, R.J., Fisher, G.B., Dimaggio, C.: *Surf. Sci.* **179** (1987) 1.  
87Pel Peled, H., Asscher, M.: *Surf. Sci.* **183** (1987) 201.  
87Pir Pirner, M., Bauer, R., Borgmann, D., Wedler, G.: *Surf. Sci.* **189/190** (1987) 147.  
87Sak Sakurai, M., Okano, T., Tuzi, Y.: *J. Vac. Sci. Technol. A* **5** (1987) 431.  
87Sol Solymosi, F., Bugyi, L.: *J. Chem. Soc. Faraday Trans. I* **83** (1987) 2015.  
87Zom Zomack, M., Baberschke, K.: *Phys. Rev. B* **36** (1987) 5756.  
88Ass Asscher, M., Kao, C.-T., Somorjai, G.A.: *J. Phys. Chem.* **92** (1988) 2711.  
88Bar Bartram, M.E., Windham, R.G., Koel, B.E.: *Langmuir* **4** (1988) 240.  
88Beh Behr, A.: *Angew. Chem.* **27** (1988) 661.  
88Bur1 Burke, M.L., Madix, R.J.: *Surf. Sci.* **194** (1988) 223.  
88Bur2 Burke, M.L., Madix, R.J.: *J. Vac. Sci. Technol. A* **6** (1988) 789.  
88Cop Copperthwaite, R.G., Davies, P.R., Morris, M.A., Roberts, M.W., Ryder, R.A.: *Catal. Lett.* **1** (1988) 11.  
88Hor Horsley, J.A., in: *Chemistry and physics of solid surfaces VII*, Springer Series in Surface Science 10, Vanselow, R., Howe, R.F. (eds.), Berlin: Springer-Verlag, 1988.  
88Ill Illing, G., Heskett, D., Plummer, E.W., Freund, H.-J., Somers, J., Lindner, T., Bradshaw, A.M., Buskotte, U., Neumann, M., Starke, U., Heinz, K., deAnders, P.L., Saldin, D., Pendry, J.B.: *Surf. Sci.* **206** (1988) 1.  
88Kis Kiss, J., Révész, K., Solymosi, F.: *Surf. Sci.* **207** (1988) 36.  
88Mad Madix, R.J., Solomon, J.L., Stöhr, J.: *Surf. Sci.* **197** (1988) L253.  
88Sas Sass, C.S., Rabalais, J.W.: *Surf. Sci. Lett.* **194** (1988) L95.  
89Bar Bartram, M.E., Koel, B.E.: *Surf. Sci.* **213** (1989) 137.  
89Leu Leung, K.T., Zhang, X.S., Shirley, D.A.: *J. Phys. Chem.* **93** (1989) 6164.  
89Liu Liu, Z.M., Zhou, Y., Solymosi, F., White, J.M.: *J. Phys. Chem.* **93** (1989) 4383.  
89Par Parker, D.H., Bartram, M.E., Koel, B.E.: *Surf. Sci.* **217** (1989) 489.  
89Pas Pashutski, A., Folman, M.: *Surf. Sci.* **216** (1989) 395.  
89Pau Paul, J.: *Surf. Sci.* **224** (1989) 348.  
89Rob Roberts, M.W.: *Chem. Soc. Rev.* **18** (1989) 451.  
89Rod Rodriguez, J.A., Clendening, W.D., Campbell, C.T.: *J. Phys. Chem.* **93** (1989) 5238.  
89Wam Wambach, J., Odörfer, G., Freund, H.-J., Kühlenbeck, H., Neumann, M.: *Surf. Sci.* **209** (1989) 159.  
89Woh Wohlrab, S., Ehrlich, D., Wambach, J., Kühlenbeck, H., Freund, H.-J.: *Surf. Sci.* **220** (1989) 243.

- 90Ahn Ahner, J., Effendy, A., Vajen, K., Wassmuth, H.-W.: *Vacuum* **41** (1990) 98.  
90Ban Banse, B.A., Koel, B.E.: *Surf. Sci.* **232** (1990) 275.  
90Cor Cornish, J.C.L., Avery, N.R.: *Surf. Sci.* **235** (1990) 209.  
90Dix Dixon-Warren, St.J., Leggett, K., Matyjasczyk, M.S., Polanyi, J.C., Young, P.A.: *J. Chem. Phys.* **93** (1990) 3659.  
90Ehr Ehrlich, D., Wohlrab, S., Wambach, J., Kuhlenbeck, H., Freund, H.-J.: *Vacuum* **41** (1990) 157.  
90Gri Grimblot, J., Alnot, P., Behm, R.J., Brundle, C.R.: *J. Electron Spectrosc. Relat. Phenom.* **52** (1990) 175.  
90Höf Höfer, M., Hilling, S., Wassmuth, H.-W.: *Vacuum* **41** (1990) 102.  
90Leg Leggett, K., Polanyi, J.C., Young, P.A.: *J. Chem. Phys.* **93** (1990) 3645.  
90May Maynard, K.J., Moskovitz, M.: *Surf. Sci.* **225** (1990) 40.  
90Par Parker, D.H., Koel, B.E.: *J. Vac. Sci. Technol. A* **8** (1990) 2585.  
90Pol1 Polzonetti, G., Alnot, P., Brundle, C.R.: *Surf. Sci.* **238** (1990) 226.  
90Pol2 Polzonetti, G., Alnot, P., Brundle, C.R.: *Surf. Sci.* **238** (1990) 237.  
90Pol3 Polanyi, J.C., Young, P.A.: *J. Chem. Phys.* **93** (1990) 3673.  
90Rod Rodriguez, J.A.: *Surf. Sci.* **226** (1990) 101.  
90Sjö Sjövall, P., So, S.K., Kasemo, B., Franchy, R., Ho, W.: *Chem. Phys. Lett.* **171** (1990) 125.  
90vom vom Felde, A., Kern, K., Higashi, G.S., Chabal, Y.J., Christman, S.B., Bahr, C.C., Cardillo, M.J.: *Phys. Rev. B* **42** (1990) 5240.  
90Zho Zhou, X.-L., White, J.M.: *Surf. Sci.* **235** (1990) 259.  
91Aln Alnaji, O., Dartiguenave, M., Dartiguenave, Y., Simard, M., Beauchamp, A.L.: *Inorg. Chim. Acta* **187** (1991) 31.  
91Beh Behm, R.J., Brundle, C.R.: *Surf. Sci.* **255** (1991) 327.  
91Bro Browne, V.M., Carley, A.F., Copperthwaite, R.G., Davies, P.R., Moser, E.M., Roberts, M.W.: *Appl. Surf. Sci.* **47** (1991) 375.  
91Cas Castro, M.E., White, J.M.: *J. Chem. Phys.* **95** (1991) 6057.  
91Kis Kiss, J., Lennon, D., Jo, S.K., White, J.M.: *J. Phys. Chem.* **95** (1991) 8054.  
91Liu Liu, Z.M., Zhou, Y., Solymosi, F., White, J.M.: *Surf. Sci.* **245** (1991) 289.  
91Mal Malik, I.J., Hrbek, J.: *J. Phys. Chem.* **95** (1991) 10188.  
91Rod Rodriguez, J.A., Campbell, R.A., Goodman, D.W.: *Surf. Sci.* **244** (1991) 211.  
91Sol1 Solymosi, F.: *J. Mol. Catal.* **65** (1991) 337.  
91Sol2 Solomon, J.L., Madix, R.J., Wurth, W., Stöhr, J.: *J. Phys. Chem.* **95** (1991) 3687.  
91Wam Wambach, J., Illing, G., Freund, H.-J.: *Chem. Phys. Lett.* **184** (1991) 239.  
91Wic Wickham, D.T., Banse, B.A., Koel, B.E.: *Surf. Sci.* **243** (1991) 83.  
91Zit Zittel, P.F.: *J. Phys. Chem.* **95** (1991) 6802.  
92Ahn Ahner, J., Effendy, A., Wassmuth, H.-W.: *Surf. Sci.* **269/270** (1992) 372.  
92Höf Höfer, M., Stolz, H., Wassmuth, H.-W.: *Surf. Sci.* **272** (1992) 342.  
92Mal Malik, I.J., Hrbek, J.: *J. Vac. Sci. Technol. A* **10** (1992) 2565.  
92Saw Sawabe, K., Matsumoto, Y.: *Chem. Phys. Lett.* **194** (1992) 45.  
93Ahn Ahner, J., Wassmuth, H.-W.: *Surf. Sci.* **287/288** (1993) 125.  
93Bec Beckendorf, M., Katter, U.J., Schlienz, H., Freund, H.-J.: *J. Phys. Condens. Matter* **5** (1993) 5471.  
93Bro Brosset, P., Dahoo, R., Gauthier-Roy, B., Abouaf-Marguin, L.: *Chem. Phys.* **172** (1993) 315.  
93Höf Höfer, M., Stolz, H., Wassmuth, H.-W.: *Surf. Sci.* **287/288** (1993) 130.  
93Nas Nassir, M.H., Dwyer, D.J.: *J. Vac. Sci. Technol. A* **11** (1993) 2104.  
93Pan Pangher, N., Köppe, H.M., Feldhaus, J., Haase, J.: *Phys. Rev. Lett.* **71** (1993) 4365.  
93Pre Pressley, L.A., Kiss, J., White, J.M., Castro, M.E.: *J. Phys. Chem.* **97** (1993) 902.  
93Rod Rodriguez, J.A.: *J. Phys. Chem.* **97** (1993) 6509.  
93Was Wassmuth, H.W., Ahner, J., Höfer, M., Stolz, H.: *Prog. Surf. Sci.* **42** (1993) 257.  
93Zeb Zebisch, P., Weinelt, M., Steinrück, H.-P.: *Surf. Sci.* **295** (1993) 295.  
94Bul Bulanin, K.M., Alexeev, A.V., Bystrov, D.S., Lavalley, J.C., Tsyganenko, A.A.: *J. Phys. Chem.* **98** (1994) 5100.  
94Car Carley, A.F., Roberts, M.W., Strutt, A.J.: *J. Phys. Chem.* **98** (1994) 9175.

- 94Hof Hoffmann, F.M., Weisel, M.D., Paul, J.: *Surf. Sci.* **316** (1994) 277.
- 94Mey1 Meyer, G., Reinhart, E., Borgmann, D., Wedler, G.: *Surf. Sci.* **320** (1994) 110.
- 94Mey2 Meyer, G., Borgmann, D., Wedler, G.: *Surf. Sci.* **320** (1994) 123.
- 94Rod Rodriguez, J.A., Hrbek, J.: *J. Vac. Sci. Technol. A* **10** (1994) 2140.
- 94Sol Solymosi, F., Klivényi, G.: *Surf. Sci.* **315** (1994) 255.
- 94Sun1 Sun, Y.-M., Sloan, D., Alberas, D.J., Kovar, M., Sun, Z.-J., White, J.M.: *Surf. Sci.* **319** (1994) 34.
- 94Sun2 Sun, Z.-J., White, J.M.: *J. Phys. Chem.* **98** (1994) 4641.
- 95Bar Bare, S.R., Griffiths, K., Lennard, W.N., Tang, H.T.: *Surf. Sci.* **342** (1995) 185.
- 95Bro1 Brown, W.A., Gardner, P., King, D.A.: *Surf. Sci.* **330** (1995) 41.
- 95Bro2 Brown, W.A., Gardner, P., King, D.A.: *J. Phys. Chem.* **99** (1995) 7065.
- 95Bul Bulanin, K.M., Lavalley, J.C., Tsyganenko, A.A.: *J. Phys. Chem.* **99** (1995) 10294.
- 95Har Hardacre, C., Roe, G.M., Lambert, R.M.: *Surf. Sci.* **326** (1995) 1.
- 95Hes Hess, G., Froitzheim, H., Baumgartner, C.: *Surf. Sci.* **331-333** (1995) 138.
- 95Hrb Hrbek, J., van Campen, D.G., Malik, I.J.: *J. Vac. Sci. Technol. A* **13** (1995) 1409.
- 95Ons Onsgaard, J., Storm, J., Christensen, S.V., Nerlov, J., Godowski, P.J., Morgan, P., Batchelor, D.: *Surf. Sci.* **336** (1995) 101.
- 95Pet Peterlinz, K.A., Sibener, S.J.: *J. Phys. Chem.* **99** (1995) 2817.
- 95Ter Terada, S., Imanishi, A., Yokoyama, T., Takenaka, S., Kitajima, Y., Ohta, T.: *Surf. Sci.* **336** (1995) 55.
- 95Tou Tournas, A.D., Potts, A.W.: *J. Electron Spectrosc. Relat. Phenom.* **73** (1995) 231.
- 95Wil Wilson, K., Hardacre, C., Lambert, R.M.: *J. Phys. Chem.* **99** (1995) 13755.
- 95Yok1 Yokoyama, T., Terada, S., Yagi, S., Imanishi, A., Takenaka, S., Kitajima, Y., Ohta, T.: *Surf. Sci.* **324** (1995) 25.
- 95Yok2 Yokoyama, T., Imanishi, A., Terada, S., Namba, S.H., Kitajima, Y., Ohta, T.: *Surf. Sci.* **334** (1995) 88.
- 96Ben Benson, S.W.: *Thermochemical kinetics*, New York: Wiley, 1996.
- 96Bro Brown, W.A., Sharma, R.K., King, D.A., Haq, S.: *J. Phys. Chem.* **100** (1996) 12559.
- 96Doh Dohrmann, J., Glebov, A., Toennies, J.P., Weiss, H.: *Surf. Sci.* **368** (1996) 188.
- 96Fre Freund, H.-J., Roberts, M.W.: *Surf. Sci. Rep.* **25** (1996) 225.
- 96Gle Glebov, A., Toennies, J.P., Weiss, H.: *Surf. Sci.* **351** (1996) 200.
- 96Gut1 Gutiérrez-Sosa, A., Crook, S., Haq, S., Lindsay, R., Ludviksson, A., Parker, S., Campbell, C.T., Thornton, G.: *Faraday Discuss.* **105** (1996) 355.
- 96Gut2 Gutiérrez-sosa, A., Walsh, J.F., Muryn, C.A., Finetti, P., Thornton, G., Robinson, A.W., D'Addato, S., Frigo, S.P.: *Surf. Sci.* **364** (1996) L519.
- 96Hua Huang, H.H., Seet, C.S., Zou, Z., Xu, G.Q.: *Surf. Sci.* **356** (1996) 181.
- 96Kat Kato, H., Sawabe, K., Matsumoto, Y.: *Surf. Sci.* **351** (1996) 43.
- 96Kra Krause, J., Borgmann, D., Wedler, G.: *Surf. Sci.* **347** (1996) 1.
- 96Li Li, Y., Bowker, M.: *Surf. Sci.* **348** (1996) 67.
- 96Mit Mitchell, W.J., Weinberg, W.H.: *J. Chem. Phys.* **104** (1996) 9127.
- 96Mor Moreh, R., Finkelstein, Y., Shechter, H.: *Phys. Rev. B* **53** (1996) 16006.
- 96Pol Polcik, M., Wilde, L., Haase, J., Brena, B., Cocco, D., Comelli, G., Paolucci, G.: *Phys. Rev. B* **53** (1996) 13720.
- 96Sch1 Schwaner, A.L., Mahmood, W., White, J.M.: *Surf. Sci.* **351** (1996) 228.
- 96Sch2 Schriver-Mazzuoli, L., Schriver, A., Lugez, C., Perrin, A., Camy-Peyret, C., Flaud, J.M.: *J. Mol. Spectrosc.* **176** (1996) 85.
- 96Yok Yokoyama, T., Terada, S., Imanishi, A., Kitajima, Y., Kosugi, N., Ohta, T.: *J. Electron Spectrosc. Relat. Phenom.* **80** (1996) 161.
- 97Bul Bulanin, K.M., Lavalley, J.C., Tsyganenko, A.A.: *J. Phys. Chem. B* **101** (1997) 2917.
- 97Haa Haase, J.: *J. Phys. Condens. Matter* **9** (1997) 3647.
- 97He He, P., Jacobi, K.: *Phys. Rev. B* **55** (1997) 4751.
- 97Hua Huang, H.H., Zou, Z., Jiang, X., Chan, W.Y., Xu, G.Q.: *J. Phys. Chem. B* **101** (1997) 8164.
- 97Jac Jackson, G.J., Lüdecke, J., Driver, S.M., Woodruff, D.P., Jones, R.J., Chan, A., Cowie, B.C.C.: *Surf. Sci.* **389** (1997) 223.

- 97Kos Kostov, K.L., Gsell, M., Jakob, P., Moritz, T., Widdra, W., Menzel, D.: *Surf. Sci.* **394** (1997) L138.
- 97Kub Kubo, T., Ema, T., Atli, A., Aruga, T., Takagi, N., Nishijima, M.: *Surf. Sci.* **382** (1997) 214.
- 97Luo Luo, M.-F., Zhong, Y.-J., Zhu, B., Yuan, X.-X., Zheng, X.-M.: *Appl. Surf. Sci.* **115** (1997) 185.
- 97Nak1 Nakahashi, T., Hamamatsu, H., Terada, S., Sakano, M., Matsui, F., Yokoyama, T., Kitajima, Y., Ohta, T.: *J. Phys. (Paris) IV Colloq.* **7** (1997) C2-679.
- 97Nak2 Nakahashi, T., Terada, S., Yokoyama, T., Hamamatsu, H., Kitajima, Y., Sakano, M., Matsui, F., Ohta, T.: *Surf. Sci.* **373** (1997) 1.
- 97Pan Pangher, N., Wilde, L., Polcik, M., Haase, J.: *Surf. Sci.* **372** (1997) 211.
- 97Pic Picaud, S., Girardet, C., Glebov, A., Toennies, J.P., Dohrmann, J., Weiss, H.: *J. Chem. Phys.* **106** (1997) 5271.
- 97Pol Polcik, M., Wilde, L., Haase, J., Brena, B., Comelli, G., Paolucci, G.: *Surf. Sci.* **381** (1997) L568.
- 97Ter Terada, S., Kitajima, Y., Yokoyama, T., Ohta, T.: *J. Phys. (Paris) IV Colloq.* **7** (1997) C2-703.
- 97Wil Wilson, K., Hardacre, C., Baddeley, C.J., Lüdecke, J., Woodruff, D.P., Lambert, R.M.: *Surf. Sci.* **372** (1997) 279.
- 98Arn Arnold, D.W., Korolik, M., Wittig, C., Reisler, H.: *Chem. Phys. Lett.* **282** (1998) 313.
- 98Bul Bulanin, K.M., Lavalley, J.C., Lamotte, J., Mariey, L., Tsyganenko, N.M., Tsyganenko, A.A.: *J. Phys. Chem. B* **102** (1998) 6809.
- 98Cha Chaturvedi, S., Rodriguez, J.A., Jirsak, T., Hrbek, J.: *J. Phys. Chem. B* **102** (1998) 7033.
- 98Jir Jirsak, T., Rodriguez, J.A., Chaturvedi, S., Hrbek, J.: *Surf. Sci.* **418** (1998) 8.
- 98Li Li, W., Oyama, S.T.: *J. Am. Chem. Soc.* **120** (1998) 9041.
- 98Llo Llorca, J., Homs, N., Araña, J., Sales, J., de la Piscina, P.R.: *Appl. Surf. Sci.* **134** (1998) 217.
- 98Lu Lu, H., Janin, E., Dávila, M.E., Pradier, C.M., Göthelid, M.: *Surf. Sci.* **408** (1998) 326.
- 98Och Ochs, D., Braun, B., Maus-Friedrichs, W., Kempter, V.: *Surf. Sci.* **417** (1998) 406.
- 98Poh Pohl, M., Otto, A.: *Surf. Sci.* **406** (1998) 125.
- 98Pol Polcik, M., Wilde, L., Haase, J.: *Phys. Rev. B* **57** (1998) 1868.
- 98Rod Rodriguez, J.A., Jirsak, T., Chaturvedi, S., Hrbek, J.: *J. Am. Chem. Soc.* **120** (1998) 11149.
- 98Sal Saliba, N., Parker, D.H., Koel, B.E.: *Surf. Sci.* **410** (1998) 270.
- 98Sey Seyller, T., Borgmann, D., Wedler, G.: *Surf. Sci.* **400** (1998) 63.
- 98Wan1 Wang, J., Koel, B.E.: *J. Phys. Chem. A* **102** (1998) 8573.
- 98Wan2 Wang, J., Voss, M.R., Busse, H., Koel, B.E.: *J. Phys. Chem. B* **102** (1998) 4693.
- 98Wil Wilde, L., Polcik, M., Haase, J., Brena, B., Cocco, D., Comelli, G., Paolucci, G.: *Surf. Sci.* **405** (1998) 215.
- 98Zhu Zhuang, G.R., Chen, Y.F., Ross Jr., P.N.: *Surf. Sci.* **418** (1998) 139.
- 99Böt Böttcher, A., Niehus, H.: *J. Chem. Phys.* **110** (1999) 3186.
- 99Jir1 Jirsak, T., Dvorak, J., Rodriguez, J.A.: *Surf. Sci.* **436** (1999) L683.
- 99Jir2 Jirsak, T., Dvorak, J., Rodriguez, J.A., Hrbek, J.: *Surf. Sci.* **426** (1999) 319.
- 99Kid Kidd, R.T., Lennon, D., Meech, S.R.: *J. Phys. Chem. B* **103** (1999) 7480.
- 99Lee Lee, A.F., Wilson, K., Lambert, R.M., Hubbard, C.P., Hurley, R.G., McCabe, R.W., Gandhi, H.S.: *J. Catal.* **184** (1999) 491.
- 99Mat Matsumoto, T., Kubota, J., Kondo, J.N., Hirose, C., Domen, K.: *Langmuir* **15** (1999) 2158.
- 99Rod Rodriguez, J.A., Jirsak, T., Chaturvedi, S.: *J. Chem. Phys.* **110** (1999) 3138.
- 99Sal1 Saliba, N.A., Tsai, Y.-L., Panja, C., Koel, B.E.: *Surf. Sci.* **419** (1999) 79.
- 99Sal2 Saliba, N.A., Tsai, Y.-L., Koel, B.E.: *J. Phys. Chem. B* **103** (1999) 1532.
- 99San Sandell, A., Jaworowski, A.J., Beutler, A., Wiklund, M.: *Surf. Sci.* **421** (1999) 116.
- 99Sei Seiferth, O., Wolter, K., Dillmann, B., Klivenyi, G., Freund, H.-J., Scarano, D., Zecchina, A.: *Surf. Sci.* **421** (1999) 176.
- 99Wan Wang, J., Koel, B.E.: *Surf. Sci.* **436** (1999) 15.
- 00Cha1 Chaabouni, H., Schriver-Mazzuoli, L., Schriver, A.: *J. Phys. Chem. A* **104** (2000) 6962.
- 00Cha2 Chaabouni, H., Schriver-Mazzuoli, L., Schriver, A.: *Low Temp. Phys.* **26** (2000) 712.
- 00Jir Jirsak, T., Kuhn, M., Rodriguez, J.A.: *Surf. Sci.* **457** (2000) 254.

- 
- 00Kid Kidd, R.T., Lennon, D., Meech, S.R.: J. Chem. Phys. **113** (2000) 8276.  
00Oya Oyama, S.T.: Catal. Rev. Sci. Eng. **42** (2000) 279.  
01Bor Borget, F., Chiavassa, T., Allouche, A., Aycard, J.P.: J. Phys. Chem. B **105** (2001) 449.  
01God Godowski, P.J., Onsgaard, J., Hoffmann, S.V., Quist-Sckerl, S.: Vacuum **63** (2001) 257.  
01Wat Waterhouse, G.I.N., Bowmaker, G.A., Metson, J.B.: Appl. Surf. Sci. **183** (2001) 191.  
02Ber Berlier, G., Yamamoto, T., Spoto, G., Lamberti, C., Gribov, E., Zecchina, A.: Phys. Chem. Chem. Phys. **4** (2002) 3872.  
04Vos Voss, M.R., Zhao, H., Koel, B.E.: Surf. Sci. **560** (2004) 235.